Unit 6
Rigid and Semi-Rigid Body Rotation

(a) $H^{octahedral} = BJ^2 + t_0 J^4 + t_4(J_{\bar{1}}^4 + J_{\bar{2}}^4 + J_{\bar{3}}^4)$

(b) $H^{cubic} = BJ^2 + t_0 J^4 + t_{22}(J_{\bar{1}}^2 J_{\bar{2}}^2 + J_{\bar{1}}^2 J_{\bar{3}}^2 + J_{\bar{2}}^2 J_{\bar{3}}^2)$

$J_{\bar{3}}$

$J_{\bar{2}}$

$J_{\bar{1}}$

J(100) affects centrifugal stretch of XY_6

J(111) affects centrifugal bend of XY_6

$x_{\bar{3}}$

$x_{\bar{1}}$

$x_{\bar{2}}$

J

J(111) affects centrifugal stretch of XY_4 or XY_8

J(100) affects centrifugal bend of XY_4 or XY_8

J

Radial bonds resistant

Bend bonds compliant

Radial bonds resistant

*Bend bonds compliant*

J
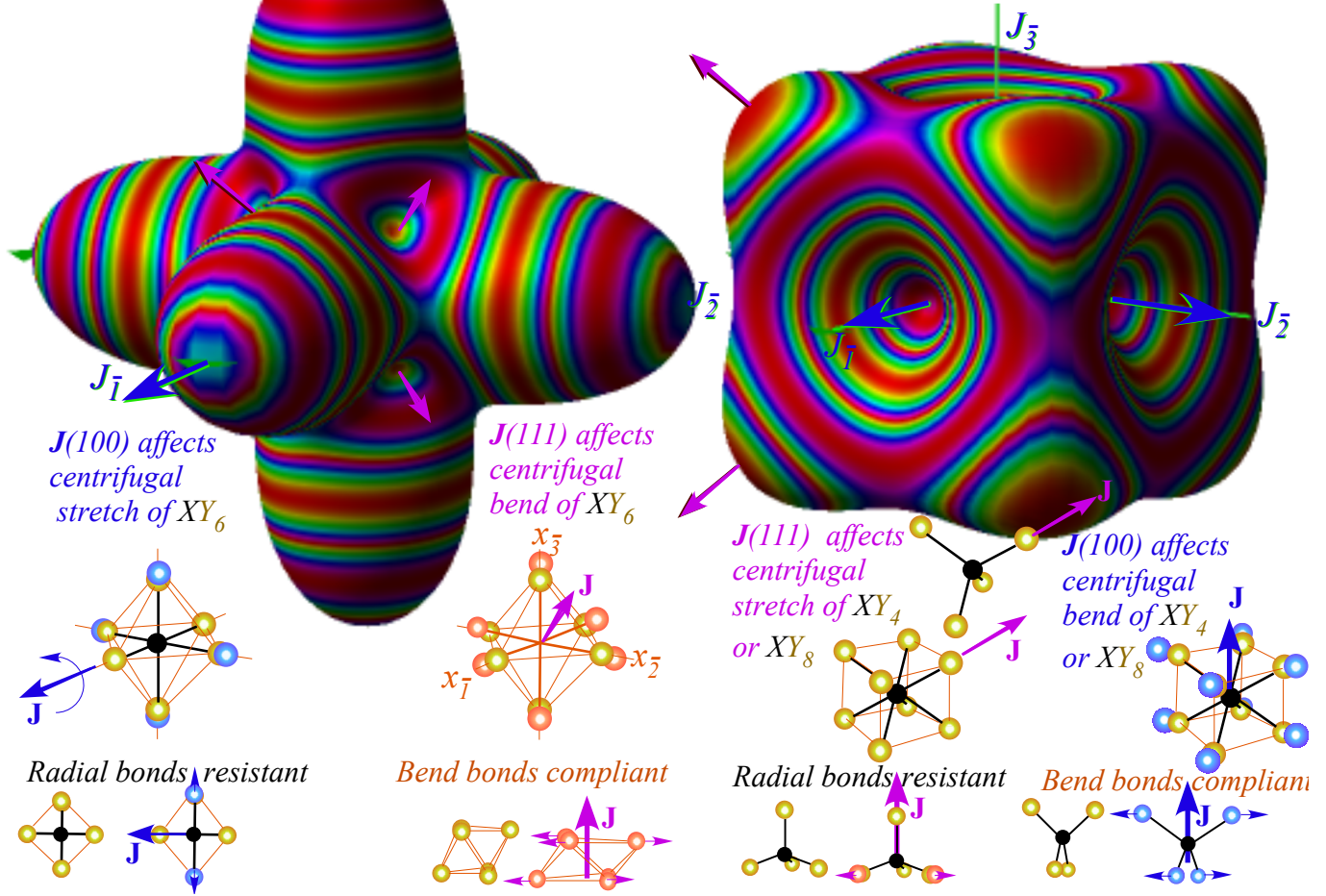
William G. Harter

A lot depends on one's view. Astronomers did not tell rotation from orbit until Copernicus showed that the Earth did both. The Copernican relativity was a jump in conceptual mechanics followed by the relativity of Galileo, Newton, Mach and Einstein. Rotational relativity is introduced here in the simplest classical context beginning with two and three particles then extended to rigid and semi-rigid body rotation and ro-vibration. Euler angles and related rotational coordinates, transformation operations, momentum, and equations of motion are developed.
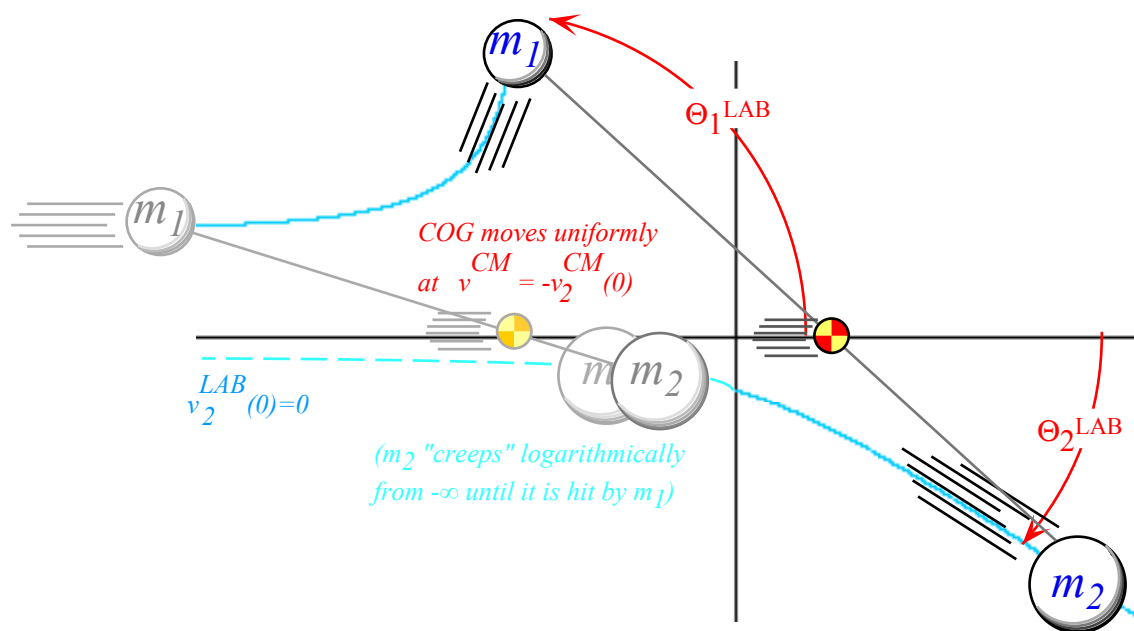
Hyperbolic Rutherford scattering orbits in LAB frame
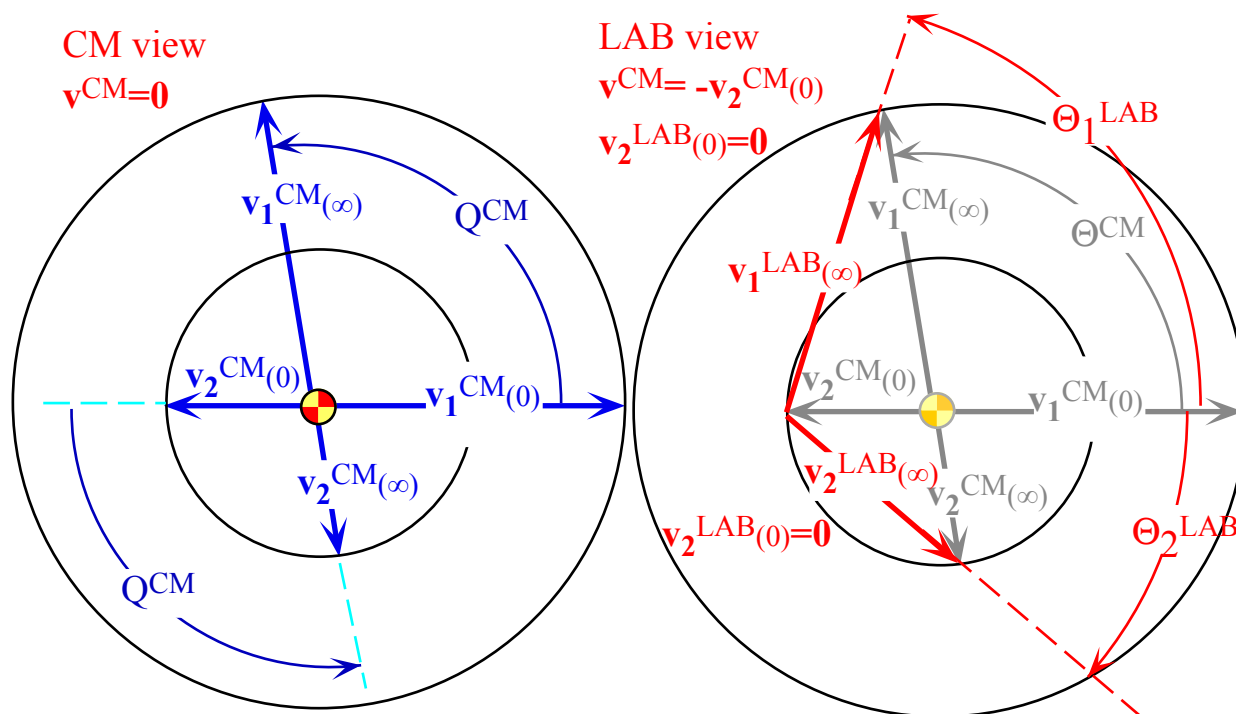
Rutherford scattering orbit momentum in CM frame and in LAB frame

Unit 6. Rigid and Semi-Rigid Body Rotation

Chapter 6.1 Introduction

POP! POP! Pop! Pop! Pop!… Pop! Countless water molecules rotate furiously in tune with microwave radiation quickly turning H_2O liquid to steam to explode corn kernels into delicious popcorn. Tri-atomic asymmetric molecules like ground state H_2O (but not ground state CO_2) are some of the simplest objects to exhibit full 3D rotational body mechanics that is not possible for just a single particle, a pair of particles, or even three particles in a line.

The concept of a single *particle* is a well-known fiction in classical mechanics. Everyone thinks they know what it means; a point of stuff with no life of its own beyond that it has a mass *m* and obeys Newton's equations in their simplest form $\mathbf{F}=m\mathbf{a}$. In fact, all the things we treat this way (with the possible exception of a single electron) appear to made of many and countless particles which themselves seem to be made of smaller particles, and so on.

To begin clarifying the concept of a particle we will consider a system or body consisting of just two particles. Two-particle mechanics is relatively easy to analyze completely. Then the problems associated with three or more particle systems will be discussed. Three-or-more-particle systems, in general, are not solvable outside of a computer. However, with certain constraints and restrictions a many-particle system may be subject to "exact" analysis. This includes so-called *rigid bodies*. It is these objects of thought that we generally have been calling "particles" in preceding discussions. It amounts to a kind of circular or "hoist by bootstraps" logic.

However, rigid bodies have in addition to their Cartesian coordinates of position an elegant set of generalized curvilinear coordinates called *Euler angles* to describe rotational orientation. This development was started in Unit 4 Chapter 4. Here, a full GCC analysis of rotational transformations and angular momentum will be developed. This turns out to be important for analysis of dynamics beyond that of rigid bodies.

One type of non-rigid body of interest to molecular and condensed matter physics is the so-called semi-rigid body, roughly speaking a collection of masses held together by springs. For these objects the centrifugal and Coriolis forces have small but important effects on the vibrational and rotational dynamics. One technique for describing the phase space of semi-rigid body rotation uses an effective *rotational energy (RE)* surface that is analogous to an effective potential energy (PE) surface used many times for translation and oscillation in preceding Units.

Chapter 6.2. Two-particle systems

Two particle theory begins with just two sets of 3-dimensional Cartesian coordinate vectors $\mathbf{r_1} = (x_1, y_1, z_1)$ and $\mathbf{r_2} = (x_2, y_2, z_2)$, as indicated in Fig. 6.2.1. To these we add a second pair of coordinate vectors including the *relative coordinate vector* $\mathbf{r}$ defined by

$$\mathbf{r} = \mathbf{r_1} - \mathbf{r_2} ,\qquad(6.2.1)$$

and the *mass-weighted-average* $\bar{\mathbf{r}}$ or *center-of-mass coordinate vector* $\mathbf{r_{CM}}$ defined by

$$\bar{\mathbf{r}} = \mathbf{r_{CM}} = \frac{m_1\mathbf{r_1} + m_2\mathbf{r_2}}{m_1 + m_2}\qquad(6.2.2)$$

These are shown below with the following inverse coordinate transformation.

$$\mathbf{r_1} = \mathbf{r_{CM}} + \frac{m_2\mathbf{r}}{m_1 + m_2} ,\qquad \mathbf{r_2} = \mathbf{r_{CM}} - \frac{m_1\mathbf{r}}{m_1 + m_2}\qquad(6.2.3)$$
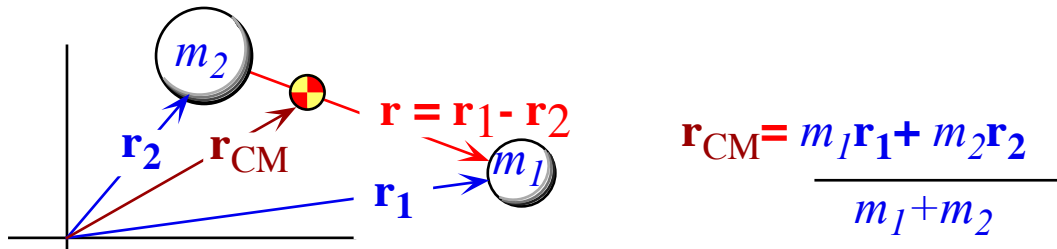
Fig. 6.2.1 Two-particle coordinate vectors

a. Reduced mass: Ptolemetric views

Let radial inter-particle force $\mathbf{F}_{12}$ be on m_1 due to m_2 and $\mathbf{F}_{21} = -\mathbf{F}_{12}$ be on m_2 due to m_1.

$$\mathbf{F}_{12} = \mathbf{F}(r)\mathbf{e_r} = F(r)\hat{\mathbf{r}} = F(r)\frac{\mathbf{r}}{r} = \frac{F(r)}{r}\left(\mathbf{r_1} - \mathbf{r_2}\right) = -\mathbf{F}_{21}\qquad(6.2.4)$$

It acts along relative coordinate vector $\mathbf{r} = \mathbf{r_1} - \mathbf{r_2}$ and depends only upon the relative distance $r = |\,\mathbf{r_1} - \mathbf{r_2}\,|$. Then Newton's equations for the individual coordinates are as follows.

$$\mathbf{F}_{12} = m_1\ddot{\mathbf{r}}_1 = F(r)\hat{\mathbf{r}} = F(r)\frac{\mathbf{r}}{r} = \frac{F(r)}{r}\left(\mathbf{r_1} - \mathbf{r_2}\right)$$
$$\mathbf{F}_{21} = m_2\ddot{\mathbf{r}}_2 = -F(r)\hat{\mathbf{r}} = -F(r)\frac{\mathbf{r}}{r} = -\frac{F(r)}{r}\left(\mathbf{r_1} - \mathbf{r_2}\right)\qquad(6.2.5a)$$

Sum $\mathbf{F}_{12} + \mathbf{F}_{21}$ yields zero because of Newton's 3rd-law action-reaction cancellation.

$$(m_1 + m_2)\ddot{\mathbf{r}}_{\mathbf{CM}} = m_1\ddot{\mathbf{r}}_1 + m_2\ddot{\mathbf{r}}_2 = \mathbf{0}\qquad(6.2.5b)$$

Difference $\mathbf{F}_{12} - \mathbf{F}_{21}$ reduces to $\mu\ddot{\mathbf{r}} = \mathbf{F}(r)$ using *reduced mass*: $\mu = \dfrac{m_2 m_1}{m_1 + m_2}$ since $\ddot{\mathbf{r}}_{\mathbf{CM}} = 0$.

$$[\qquad m_1\ddot{\mathbf{r}}_1 \qquad] - [\qquad m_2\ddot{\mathbf{r}}_2 \qquad] = \frac{2F(r)}{r}\left(\mathbf{r_1} - \mathbf{r_2}\right)$$
$$\left[m_1\ddot{\mathbf{r}}_{\mathbf{CM}} + \frac{m_1 m_2\ddot{\mathbf{r}}}{m_1 + m_2}\right] - \left[m_2\ddot{\mathbf{r}}_{\mathbf{CM}} + \frac{m_2 m_1\ddot{\mathbf{r}}}{m_1 + m_2}\right] = \frac{2F(r)}{r}\left(\mathbf{r_1} - \mathbf{r_2}\right)\qquad(6.2.5c)$$
$$\mu\ddot{\mathbf{r}} = F(r)\hat{\mathbf{r}} = F(r)\mathbf{e_r} = \mathbf{F}(r)\qquad(6.2.5d)$$

According to (6.2.5b), the CM point continues with velocity unchanged by inter particle forces. This holds for any inter-particle force including <u>ani</u>stropic and (for non-relativistic velocity) time dependent ones, too. Meanwhile, the relative radius $\mathbf{r} = \mathbf{r_1} - \mathbf{r_2}$ behaves like the radius vector of *reduced mass* μ going around a force center fixed in an inertial frame. Anyone on mass m_1 will see mass m_2 orbiting at point $-\mathbf{r}$ according to force $\mathbf{F}_{21}$ $= -F(r)\mathbf{r}$ as though they (on mass m_1) were an infinitely massive center of the universe! The same, vice-versa, applies for people on mass m_2 who see a body orbiting at point $+\mathbf{r}$ according to force $\mathbf{F}_{12} = +F(r)\mathbf{r}$ as though they (on mass m_2) were a fixed center. Of course neither m_1 nor m_2 are fixed and so we will call their pictures *Ptolemetric* views after the famous astronomer who pictured the entire solar system geocentrically. (Since planets do not orbit the Earth, a Ptolemetric view of them is even more complicated than the simple two-particle orbits being described here. Fortunately, Copernicus come along to straighten this out.)

Note that the orbiting body in either an m_1-or m_2-Ptolemetric view behaves as though it has the same reduced mass μ given by an inverse sum relation involving both of the masses.

$$\frac{1}{\mu} = \frac{1}{m_1} + \frac{1}{m_2} = \frac{m_1 + m_2}{m_1 m_2} \qquad\qquad (6.2.6)$$

Reduced mass is approximated as follows if the masses are quite different.

$$\mu = \frac{m_1}{1 + \dfrac{m_1}{m_2}} = m_1\left(1 - \frac{m_1}{m_2}...\right) \ (m_2 >> m_1) \ \text{(6.2.7a)} \qquad\qquad \mu = \frac{m_2}{1 + \dfrac{m_2}{m_1}} = m_2\left(1 - \frac{m_2}{m_1}...\right) \ (m_1 >> m_2) \ \text{(6.2.7b)}$$

The μ is called a *reduced* mass because it is the smaller mass (say, m_1) *reduced* by approximately the fraction equal to the mass ratio of smaller over larger (m_1 / m_2). The μ is always *less* than either mass.

b. Re-scaled force: A Copernican view

Instead let us set up a coordinate system with its origin fixed at the center-of-mass so the vector $\mathbf{r_{CM}}$ is identically zero. ($\mathbf{r_{CM}} = \mathbf{0}$) The inverse coordinate transformation (6.2.3) becomes

$$\mathbf{r_1} = \frac{m_2 \mathbf{r}}{m_1 + m_2} = \frac{\mu}{m_1}\mathbf{r} \ , \qquad \mathbf{r_2} = \frac{-m_1 \mathbf{r}}{m_1 + m_2} = \frac{-\mu}{m_2}\mathbf{r} \qquad\qquad (6.2.8)$$

and the relative radius vector is

$$\frac{m_1}{\mu}\mathbf{r_1} = \mathbf{r} = \frac{-m_2}{\mu}\mathbf{r_2} \qquad\qquad (6.2.9)$$

Then Newton's equations for the individual coordinate vectors are

$$\mathbf{F}_{12} = m_1\ddot{\mathbf{r}}_1 = F\left(\frac{m_1}{\mu}r_1\right)\hat{\mathbf{r}}_1 = -\mathbf{F}_{21}$$

$$\mathbf{F}_{21} = m_2\ddot{\mathbf{r}}_2 = F\left(\frac{m_2}{\mu}r_2\right)\hat{\mathbf{r}}_2 = -\mathbf{F}_{12} \qquad\qquad (6.2.10)$$

In the inertial CM frame each orbiting particle maintains it original mass m_1 or m_2, but each experiences an individual *coordinate-re-scaled force field F(m_1 r_1 / μ) or F(m_2 r_2 / μ)* field, respectively.

Each *radial re-scaling factor m_1 / μ or m_2 / μ* is always greater than one. It will either reduce force or increase it depending on the functional form of $F(r)$. A Coulomb force $F(r)=-k/r^2$ is scaled down so the effective Coulomb constants k_1 or k_2 for mass m_1 or m_2 are both reduced.

$$F(r) = \frac{k}{r^2} \text{ becomes: } F(\frac{m_1}{\mu}r_1) = \frac{\mu^2}{m_1^2}\frac{k}{r_1^2} \; , \tag{6.2.11}$$

$$k \rightarrow k_1 = k\,\mu^2 / m_1^2 \; , \quad k \rightarrow k_2 = k\,\mu^2 / m_2^2$$

However, a harmonic oscillator force coupling $F(r)=-kr$ has both its constants increased.

$$F(r) = -k\,r \text{ becomes: } F(\frac{m_1}{\mu}r_1) = -\frac{m_1}{\mu}k\,r_1 \; , \tag{6.2.12}$$

$$k \rightarrow k_1 = k\,m_1 / \mu \; , \quad k \rightarrow k_2 = k\,m_2 / \mu$$

Examples of Coulomb and harmonic oscillator 2-particle orbits are shown in Fig. 6.2.2. The two particles must remain in synchronous motion balanced by their fixed CM origin. So their orbit periods are identical to each other and to the period of the Ptolemetric orbit. The two Copernican orbits must be mass-scaled copies with equal aspect ratio (a/b), eccentricity, and orientation. They differ only in size of axes (a_1, b_1) and (a_2, b_2) and placement of their center (for the Coulomb case) or foci (for the oscillator). The Cartesian axis dimensions are in inverse proportion to their mass values, and this applies as well to the Ptolometric orbit axes (a, b).

$$a_1 m_1 = a_2 m_2 = a\mu \; , \quad \text{and: } b_1 m_1 = b_2 m_2 = b\mu \tag{6.2.13}$$

The relation between polar parameters follows from (5.2.25). Radii scale but ratio ε does not.

$$\lambda_1 m_1 = \lambda_2 m_2 = \lambda\mu \; , \quad \text{and: } \varepsilon_1 = \varepsilon_2 = \varepsilon \tag{6.2.14}$$
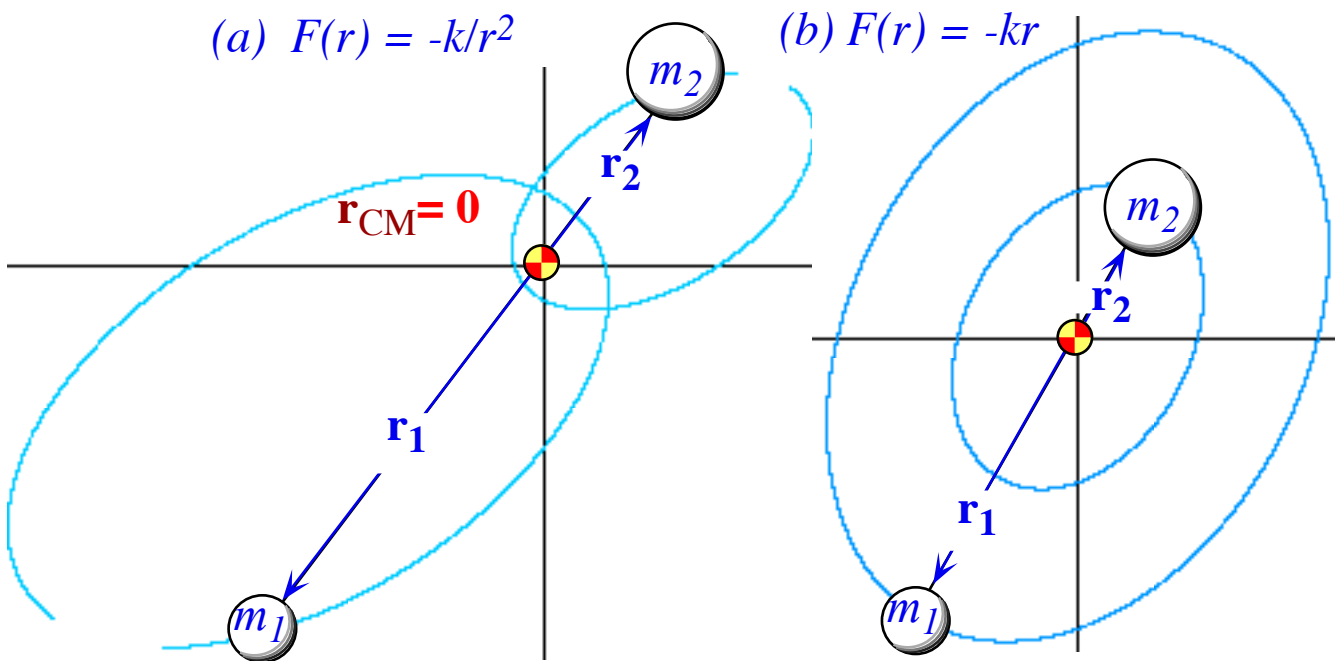
Fig. 6.2.2 Two-particle orbits ($m_2 = 2m_1$) (a) Coulomb coupling force, (b) Linear H.O. coupling

The following three harmonic oscillator orbit periods (Recall (5.2.8-11).) must then match.

$$T = 2\pi\sqrt{\frac{\mu}{k}} = 2\pi\sqrt{\frac{m_1}{k_1}} = 2\pi\sqrt{\frac{m_2}{k_2}} \qquad (6.2.15a)$$

Indeed, they do by (6.2.12). The three Coulomb periods based on (5.2.35) match, too.

$$T = 2\pi\sqrt{\frac{\mu a^3}{k}} = 2\pi\sqrt{\frac{m_1 a_1^3}{k_1}} = 2\pi\sqrt{\frac{m_2 a_2^3}{k_2}} \qquad (6.2.15b)$$

The three Coulomb orbit energy values satisfy the same proportion relation as their axes (6.2.13).

$$E_1 m_1 = E_2 m_2 = E\mu , \quad \text{where:} \quad |E_1| = \frac{|k_1|}{2a_1} , \quad |E_2| = \frac{|k_2|}{2a_2} , \quad |E| = \frac{|k|}{2a} . \qquad (6.2.16a)$$

In fact the three energy values and the three axes satisfy the same sum relation.

$$E_1 + E_2 = \frac{m_1}{\mu} E + \frac{m_2}{\mu} E = E , \quad \text{and:} \quad a_1 + a_2 = \frac{m_1}{\mu} a + \frac{m_2}{\mu} a = a \qquad (6.2.16b)$$

The preceding relations apply as well to the harmonic oscillator, indeed they are general ones based on the fundamental geometry. In particular, you should check that the dimensions of the two Copernican orbits have to sum up to equal those of the single Ptolemetric one.

Chapter 6.3. Two-particle collision dynamics

Two particle collisions benefit also from a comparison of Ptolemetric and Copernican views. Recall that a Ptolemetric view is one in which one of the two particles is seen to be at rest, while the Copernican view is one in which their center of mass is at rest. For interacting particles, only the latter Copernican view is in an inertial frame. The Ptolemetric frame of view is attached to an accelerating particle, and this is a serious handicap for most classical dynamics.

Scattering theory employs quasi-Ptolemetric views using so-called *inertial laboratory (LAB) frames* in which one of the particles is *initially* at rest before the collision takes place. Since laboratory frames must be inertial frames their favored particle is usually knocked away by the collision.

Scattering theory also relaxes the Copernican view by using so-called *center of momentum (COM) frames* in which the total momentum sums to zero. The Copernican frame is a special case of a COM frame in which the origin is exactly at the center of mass, or using an older jargon, it is a *center of gravity (COG) frame*. A COM frame is one with origin fixed at some point in the COG frame. A COG frame is a COM frame that is convenient for doing classical orbit geometry.

a. Center of momentum view of collision dynamics

The Unit 5 construction of Fig. 5.3.1 for a single particle Coulomb -Rutherford scattering orbit is also applicable to 2-particle scattering in a COG frame. An example drawn in Fig. 6.3.1 has mass m_2 is twice that of m_1. Given a total energy E, we distribute it onto the separate particle energies E_1 and E_2 inversely according to their mass by (6.2.16). (Here, mass m_1 gets twice the energy of m_2.) The same applies to the semi-major and semi-minor axes by (6.2.13) which are the hyperbolic radii and impact parameters. (Here, radius a_1 is twice a_2, and impact parameter b_1 is twice b_2.)

The scattering angle, eccentricity, and angular dynamics are similar for each particle, but the orbit of the lighter and higher energy particle is *(m_2/m_1)*-times as big (twice as big here) as the heavier particle and has *(m_2/m_1)*-times as much total energy. The lighter particle also has this many times as much angular momentum, but with the ±sign reversed, and conserved by each. However, the two always have the same amount of linear momentum, again with ±sign reversed so their total is a zero vector (**p_1+p_2 = 0**) even as both exchange momentum while colliding in the COM frame.

b. LAB view of collision dynamics and kinematics

The COG or COM (abbreviated to CM) frame view of Coulomb scattering is geometrically precise and constructable as shown in Fig. 6.3.1. The LAB frame is not so easy to construct or visualize. In fact, the coordinate LAB frame does not even exist at all! The picture shown in Fig. 6.3.2 is more of a cartoon, though the paths are valid computer plots of an approximate LAB picture. By demanding that one particle (m_2 in this case) be a stationary (**$v_2^{LAB}(0)= 0$**) "target" particle we run afoul of the logarithmic time behavior discussed after equation (5.3.5).
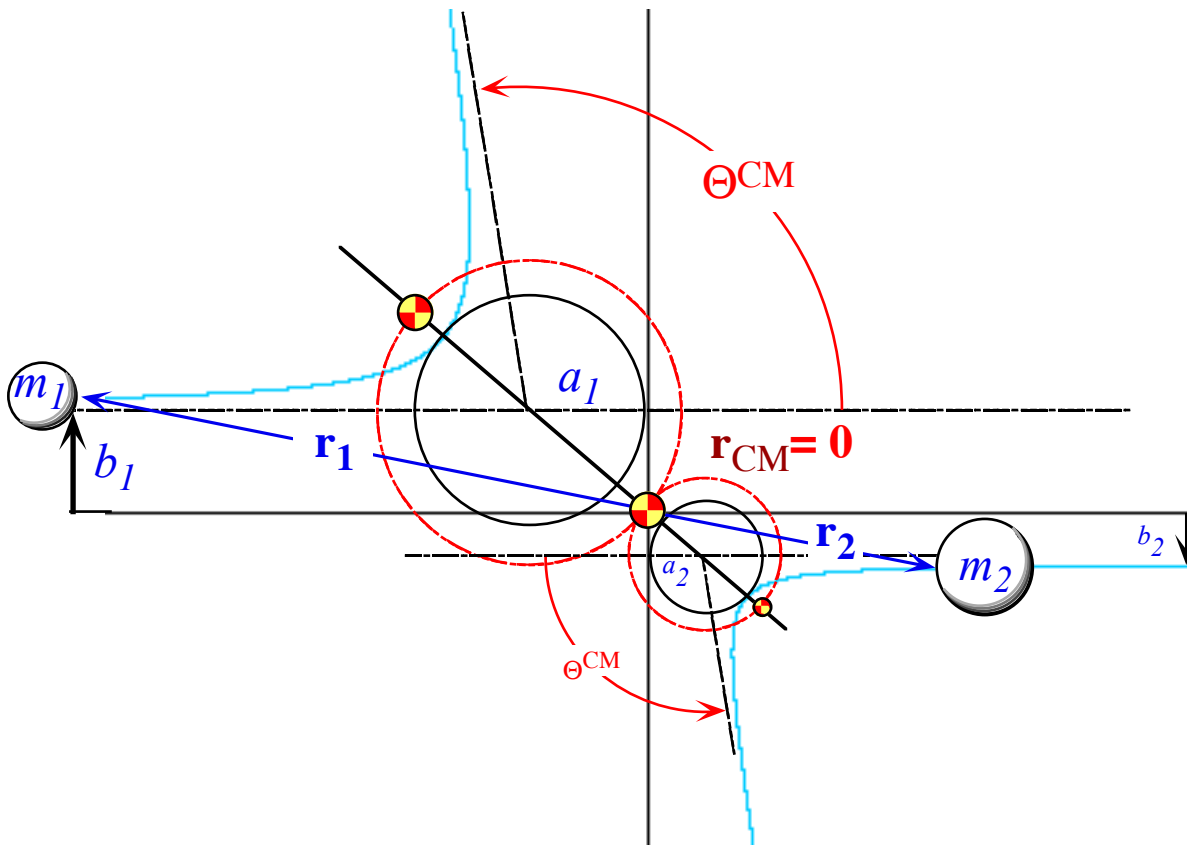
Fig. 6.3.1 Two-particle Coulomb scattering ($m_2 = 2m_1$) viewed in the COG frame

The final LAB velocities $v_1{}^{LAB}(\infty)$ and $v_2{}^{LAB}(\infty)$ and LAB scattering angles $\Theta_1{}^{LAB}$ and $\Theta_2{}^{LAB}$ are easily constructed for both the "projectile" particle m_1 and the "stationary target" particle m_2 as shown in Fig. 6.3.3. First the CM angle Θ^{CM} constructed in Fig. 6.3.1 is used to graph the final CM velocities $v_1{}^{CM}(\infty)$ and $v_2{}^{CM}(\infty)$ on the left hand side of Fig. 6.3.3. Then these are re drawn on the right hand side of the figure relative to an origin shifted by velocity $v_2{}^{CM}(0)$ that makes the m_2 target initially stationary. This is the *kinematic* (velocity) part of the problem.

The *dynamic* (space-time) part of the problem is impossible. Neither the initial target starting point nor the final asymptotes for either particle exist. Supposing it only takes m_1 a few seconds for m_1 to cross Fig. 6.3.1 or 2, it will take m_2 literally years to "creep" logarithmically up to the scattering origin where it gets kicked off to the lower right very quickly. Then the tangent lines for both particles begin their "logarithmic creep" to the right hand side of Fig. 6.3.2. It will take these "LAB asymptotes" several years to creep off the page, and they will keep on moving ever so slowly, forever and ever.
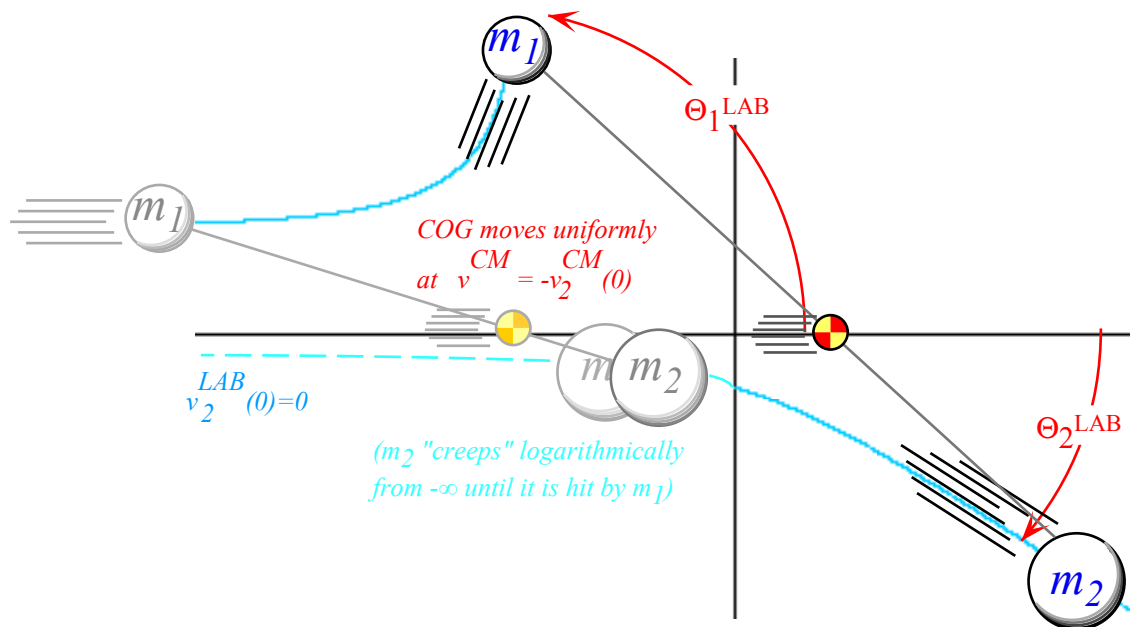
Fig. 6.3.2 Two-particle scattering ($m_2 = 2m_1$) viewed in the LAB frame
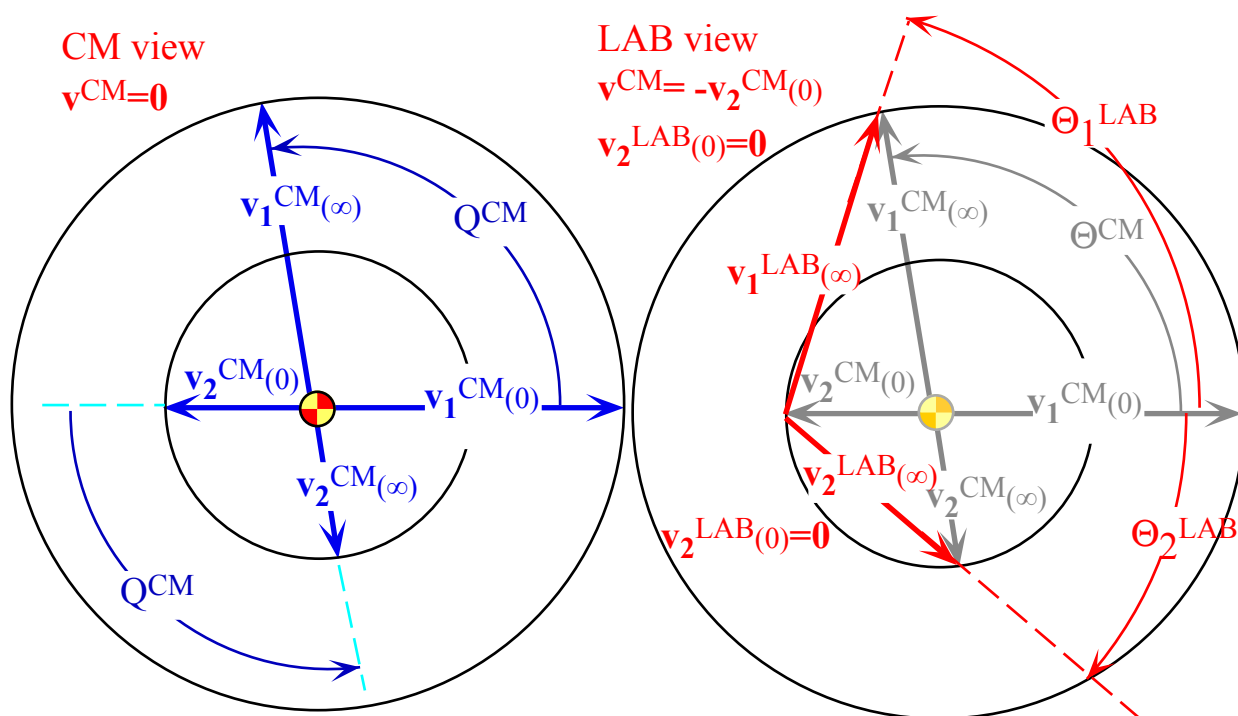
Fig. 6.3.3 Two-particle scattering ($m_2 = 2m_1$) velocities viewed in the CM and LAB frames.

c. Ideal pool shot

No mechanics book is complete without showing the simplest, yet surprising, analysis of the common pool or billiards shot. By adapting the general construction in the previous Figs. 6.3.2 and 6.3.3 to a pair of equal masses ($m_2 = m_1$) it should be noticed in Fig. 6.3.4 that the particles always come out at *exactly 90°* to each other at speeds which vary with the CM angle. To avoid sinking the white ("cue") ball while aiming the other requires this mechanics knowledge. Clearly, this analysis ignores ball spin or "English" that will be discussed later.
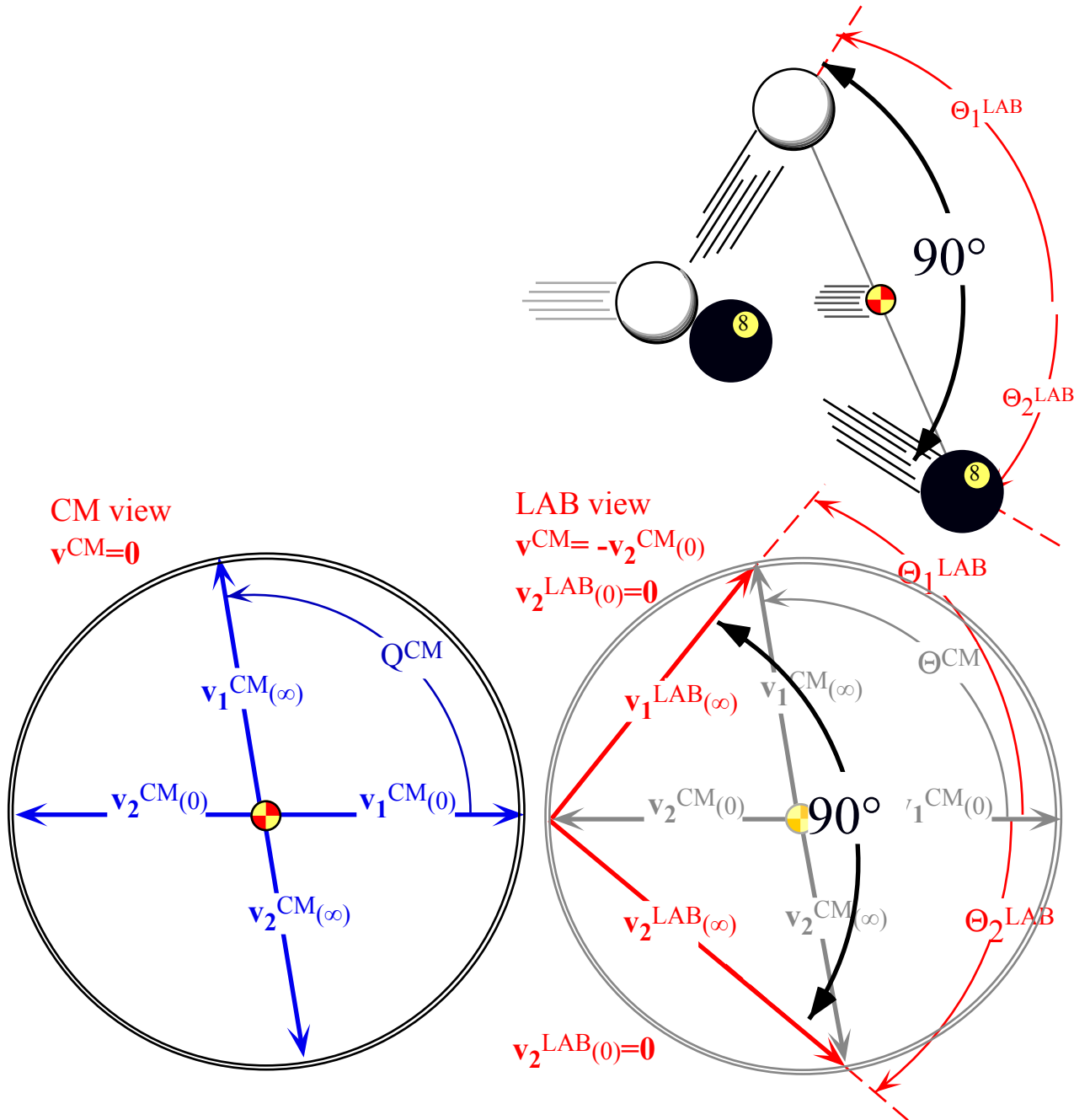
Fig. 6.3.4 Magic 90° pool ball scattering ($m_2 = m_1$) velocities viewed in the LAB frame.

d. Super-elastic bounce

A discussion of *super-elastic bounce (SEB)* was given in Unit 1 using a plot of vertical velocity of one ball against the other as in Fig. 6.3.5. (Recall Fig. 1.4.1 thru Fig. 1.5.1 in Unit 1.)
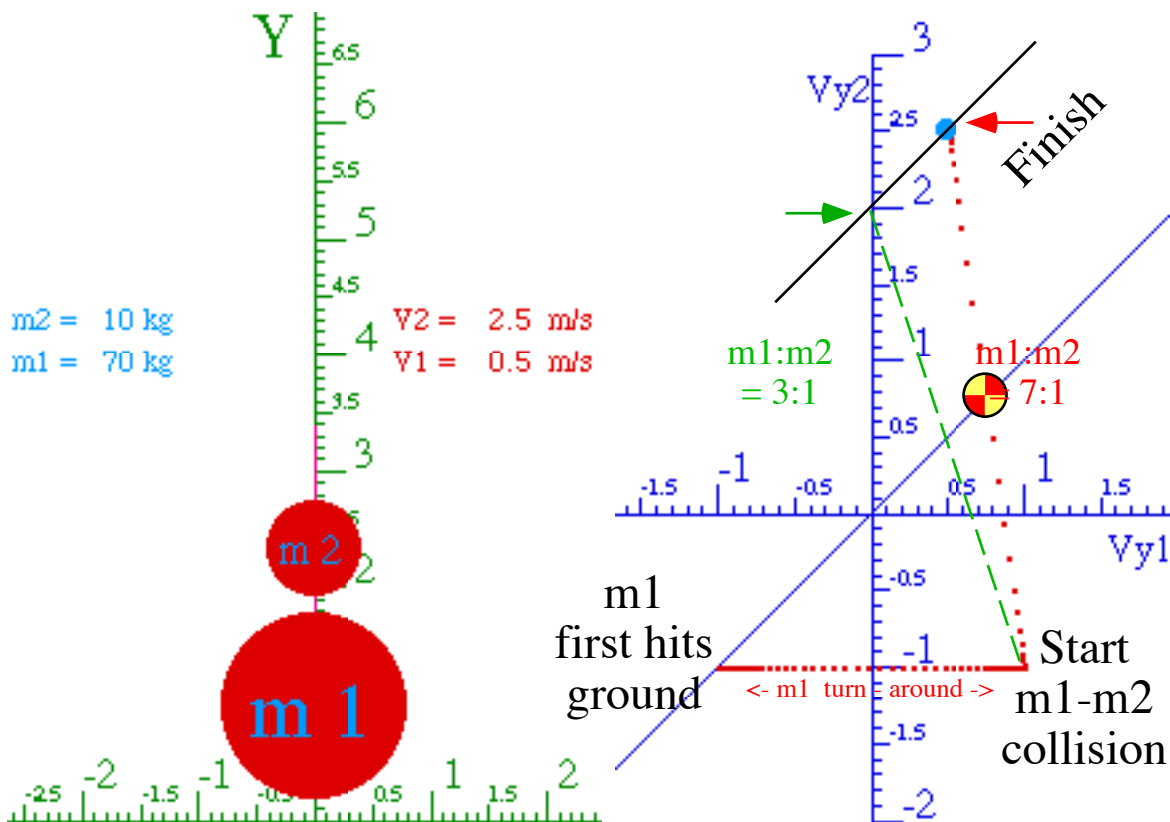
Fig. 6.3.5 Super-elastic bounce and momentum analysis.

The conservation of momentum for the m_1-m_2 collision requires $m_1v_1+m_2v_2=const.$ and results in a straight line of slope equal the negative of the mass ratio m_1 / m_2. (The collision indicated by dots in Fig. 6.3.5 has mass ratio $m_1:m_2 =7:1$.) A *45°* line (slope 1:1) intersects the momentum conservation line at exactly the point that is the final velocity in the event of *totally inelastic* collision with two masses stuck together into one mass $m_1 + m_2$. This intersection is the *center of momentum (COM)* point for that collision. For a *totally elastic* collision the initial and final velocities (These are labeled "Start" and "Finish" in the Fig. 6.3.4) must balance on the COM point. It is a simple (but little-known) geometric construction for solving 1-dimensional elastic collisions introduced at the beginning of review Unit 1.

A ratio $m_1:m_2 =3:1$ stands out. As seen from the dashed line in the figure, this ratio gives 100% energy transfer from m_1 to m_2. It is also the limit SEB ratio of 3:1 as $m_1:m_2$ approaches ∞. Using more balls as discussed in Ch. 1.8 (Unit 1) leads to SEB ratios well above 3:1 as shown in Fig. 1.8.1.

Chapter 6.4. Multi-particle systems

Most of the techniques needed to discus multiparticle systems can be developed using just three particles. In fact, as we will see, a rigid three-particle system has enough mechanical structure to mimic perfectly any rigid body whatsoever.

a. A 3-particle system

A three-particle system is sketched in Fig. 6.4.1.
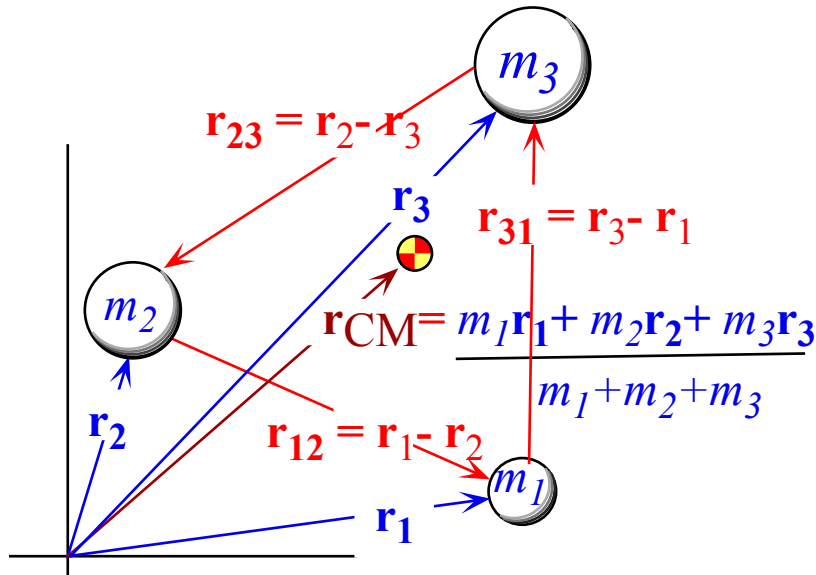
Fig. 6.4.1 Three-particle coordinate vectors

There are nine Cartesian coordinates, three for each of three position vectors

$$\mathbf{r_1} = (x_1, y_1, z_1),\ \mathbf{r_2} = (x_2, y_2, z_2),\ \text{and}\ \mathbf{r_3} = (x_3, y_3, z_3), \qquad (6.4.1)$$

shown in Fig. 6.4.1. If the three inter particle vectors

$$\mathbf{r_{12}} = (x_{12}, y_{12}, z_{12}),\ \mathbf{r_{23}} = (x_{23}, y_{23}, z_{23}),\ \text{and}\ \mathbf{r_{31}} = (x_{31}, y_{31}, z_{31}), \qquad (6.4.2)$$
$$= \mathbf{r_1} - \mathbf{r_2} \qquad\qquad = \mathbf{r_2} - \mathbf{r_3} \qquad\qquad = \mathbf{r_3} - \mathbf{r_1}$$

have constant lengths or magnitudes

$$|\mathbf{r_{12}}|^2 = (x_{12}^2 + y_{12}^2 + z_{12}^2) = const.$$
$$|\mathbf{r_{23}}|^2 = (x_{23}^2 + y_{23}^2 + z_{23}^2) = const. \qquad (6.4.3)$$
$$|\mathbf{r_{31}}|^2 = (x_{31}^2 + y_{31}^2 + z_{31}^2) = const.$$

then the object is called a *rigid body*. The three equations leave only six free coordinates left, of which three could be the *center of mass* coordinates

$$\mathbf{r_{CM}} = (x_{CM}, y_{CM}, z_{CM}) = \frac{\sum\limits_{j=1}^{3} m_j \mathbf{r_j}}{\sum\limits_{j=1}^{3} m_j} \qquad (6.4.4)$$

and three more could be orientation angles such as Euler angles (α, β, γ) to be described later. A general rigid body with any number of particles will have only these same six coordinates.

b. 3-particle force relations

In order to deal with multiple Newton's equations (one for each particle-j)

$$\mathbf{F}_j^{total} = m_j \, \ddot{x}_j = \dot{\mathbf{p}}_j \qquad (6.4.5a)$$

it is convenient to break the total force into a sum of external applied and internal constraint forces.

$$\mathbf{F}_j^{total} = \mathbf{F}_j^{applied} + \mathbf{F}_j^{constraint}$$

$$= \mathbf{F}_j^{applied} + \sum_{k=1(k \neq j)}^{3} \mathbf{F}_{jk}^{constraint} \qquad (6.4.5b)$$

where $\mathbf{F}_{jk}$ is the force on particle-j due to particle-k where, by Newton's (3-rd) action-reaction law

$$\mathbf{F}_{jk} = -\mathbf{F}_{kj} \qquad (6.4.5c)$$

as pictured in Fig. 6.4.2.
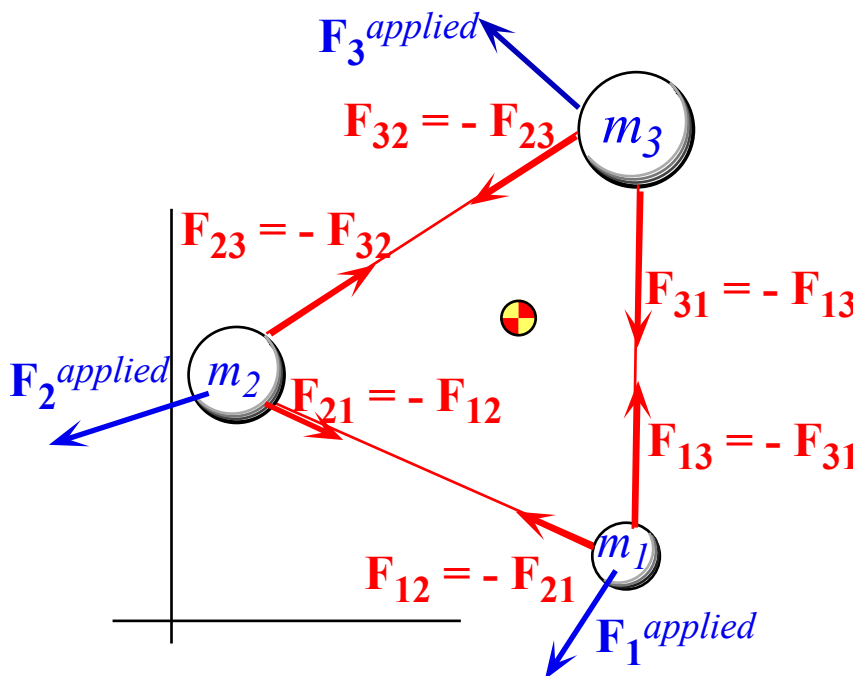
Fig. 6.4.2 Three-particle force vectors

The sum of all the Newton's equations eliminates the internal forces from consideration of the motion of the CM point. Only the total applied force affects $\mathbf{r}_{CM}$.

$$\frac{d}{dt}\left(\sum_{j=1}^{3} m_j \, \ddot{x}_j \right) = \sum_{j=1}^{3} \mathbf{F}_j^{total} = \sum_{j=1}^{3} \mathbf{F}_j^{applied} + \sum_{j=1}^{3} \sum_{k=1(k \neq j)}^{3} \mathbf{F}_{jk}^{constraint}$$

$$M \, \ddot{\mathbf{r}}_{CM} = \sum_{j=1}^{3} \mathbf{F}_j^{applied} + \mathbf{0}, \quad \text{where: } M = \sum_{j=1}^{3} m_j \qquad (6.4.6)$$

This reduces the CM motion of this object to that of a single "particle" of the same total mass.

$$\dot{\mathbf{P}}^{total} \equiv M \, \ddot{\mathbf{r}}_{CM} = \mathbf{F}^{total\ applied} \qquad (6.4.7)$$

c. Angular force and momentum relations: Torque

The three coordinates of translation follow the usual Newton's laws for $\mathbf{r}_{CM}$ of (6.4.7). The next three coordinates (and for a rigid body, the <u>last</u> three free coordinates) are rotational coordinates of some kind. Here we will put off defining Euler angles and just deal with the rotational *kinematics*, that is, the angular *velocity vector* $\boldsymbol{\omega}$ and the *angular momentum vector* $\mathbf{L}$. Let us assume a Copernican view by placing the origin at the center of mass. ($\mathbf{r}_{CM}=\mathbf{0}$)

　　　　Angular velocity vector $\boldsymbol{\omega}$ is a rotation axis that determines linear velocity $\mathbf{v}^{rotation}$ of any mass at $\mathbf{r}$ due just to rotation at angular rate $\omega = |\boldsymbol{\omega}|$ by its perpendicular distance ("lever-arm") from the axis $\boldsymbol{\omega}$ by *Darboux rotational cross-product relations* (3.7.19) to (3.7.23) in Unit 3. (A detailed dynamics discussion is taken up around (6.7.5). This kinematics discussion mostly ignores rotational coordinates.)

$$\mathbf{v}^{rotation} = \boldsymbol{\omega} \times \mathbf{r} \ , \quad \dot{\mathbf{r}} \equiv \mathbf{v}^{total} = \left.\frac{d\mathbf{r}}{dt}\right|_{LAB} = \left.\frac{d\mathbf{r}}{dt}\right|_{Body} + \boldsymbol{\omega} \times \mathbf{r} \tag{6.4.8}$$

The particle's total velocity is the sum of rotational velocity $\mathbf{v}^{rotation}$ and a body's internal "vibrational" velocity $\left.\dfrac{d\mathbf{r}}{dt}\right|_{Body}$ due to $\mathbf{r}_{jk}$ motion. (The latter is zero ($\dot{\mathbf{r}}_{jk} = \mathbf{0}$) for a rigid body.)

　　　　Angular momentum vector $\mathbf{L}_j$ of a mass m_j is determined by its linear momentum $\mathbf{p}_j$ times its lever arm as given by the *angular momentum cross-product relation*

$$\mathbf{L}_j = \mathbf{r}_j \times m_j \dot{\mathbf{r}}_j \equiv \mathbf{r}_j \times \mathbf{p}_j \tag{6.4.9a}$$

The sum-total angular momentum is

$$\mathbf{L} = \mathbf{L}^{total} = \sum_{j=1}^{3} \mathbf{L}_j = \sum_{j=1}^{3} \mathbf{r}_j \times m_j \dot{\mathbf{r}}_j \tag{6.4.9b}$$

It is from the derivative of $\mathbf{L}$ that we get a "second" Newton's equation, one that connnects rotational momentum $\mathbf{r} \times \mathbf{p}$ and rotational force or *torque* $\mathbf{r} \times \mathbf{F}$.

$$\frac{d\mathbf{L}}{dt} = \sum_{j=1}^{3} \mathbf{r}_j \times m_j \ddot{\mathbf{r}}_j = \sum_{j=1}^{3} \mathbf{r}_j \times \mathbf{F}_j^{total}$$

$$= \sum_{j=1}^{3} \mathbf{r}_j \times \mathbf{F}_j^{applied} + \sum_{j=1}^{3} \mathbf{r}_j \times \left(\sum_{k=1(k \neq j)}^{3} \mathbf{F}_{jk}^{constraint} \right)$$

The internal constraint or coupling force terms (6.4.5b) appear at first, to be a nuisance.

$$\sum_{j=1}^{3} \sum_{k=1(k \neq j)}^{3} \mathbf{r}_j \times \mathbf{F}_{jk}^{constraint} = \mathbf{r}_1 \times \left(\mathbf{F}_{12} + \mathbf{F}_{13}^{constraint} \right) + \mathbf{r}_2 \times \left(\mathbf{F}_{21} + \mathbf{F}_{23}^{constraint} \right) + \mathbf{r}_3 \times \left(\mathbf{F}_{31} + \mathbf{F}_{32}^{constraint} \right)$$

$$= \left(\mathbf{r}_1 - \mathbf{r}_2 \right) \times \mathbf{F}_{12}^{constraint} + \left(\mathbf{r}_1 - \mathbf{r}_3 \right) \times \mathbf{F}_{13}^{constraint} + \left(\mathbf{r}_2 - \mathbf{r}_3 \right) \times \mathbf{F}_{23}^{constraint} = \mathbf{0}$$

However, they are clearly zero if the coupling forces act along the lines connecting the masses.

　　　　In fact the sum must vanish even if the individual terms do not, as long as we assume the constraints cannot spin up the whole body. The result is the purely *rotational Newton's equation*.

$$\frac{d\mathbf{L}}{dt} = \mathbf{N} \ , \text{ where: } \mathbf{N} = \sum_{j=1}^{3} \mathbf{N}_j \quad \text{and: } \mathbf{N}_j = \sum_{j=1}^{3} \mathbf{r}_j \times \mathbf{F}_j^{applied} \tag{6.4.10a}$$

These are taken together with the linear or purely *translational Newton's equation*

$$\frac{d\mathbf{P}}{dt} = \mathbf{F} \ , \quad \text{where: } \mathbf{F} = \sum_{j=1}^{3} \mathbf{F}_j^{applied} \quad . \tag{6.4.10b}$$

This is the complete description of rigid body mechanics and the first six equations for the mechanics of any body. The remainder of the equations will be normal mode or GCC forms of some kind.

d. Percussion centers: "Sweet spots"

While the two equations (6.4.10a -b) are translational and rotational versions derived from a single set (6.4.5a) of Newton's equation, they are to be viewed and applied <u>independently</u>. To see an example of this, imagine a vertical mass M stick of length 2ℓ sitting motionless until it receives an impulse Π from a hammer-hit at a distance h from its center of mass (CM) as shown in Fig. 6.4.3. The time integral of force

$$\Pi = \mathbf{P}(\tau) - \mathbf{P}(0) = \int_0^{\tau} \mathbf{F}^{applied} \, dt \tag{6.4.11}$$

is the *momentum impulse* Π . If the initial momentum $\mathbf{P}(0)$ is zero them Π is the new momentum of the stick and the new CM velocity $\mathbf{V}_{CM} = \dot{\mathbf{r}}_{\mathbf{CM}}$ is Π divided by its mass M.

$$\mathbf{V}_{CM} = \dot{\mathbf{r}}_{\mathbf{CM}} = \Pi / M \tag{6.4.12}$$

This is true *no matter what* the distance h between the CM and the hammer-hit.

However, the <u>angular</u> momentum $\mathbf{L}=\Lambda$ the hammer gives to the stick <u>does</u> depend upon the location h of the hammer-hit relative to the CM according to (6.4.10a).

$$\Lambda = \mathbf{L}(\tau) - \mathbf{L}(0) = \int_0^{\tau} \mathbf{r} \times \mathbf{F}^{applied} \, dt \tag{6.4.13}$$

In this case the magnitude Λ of Λ is simply distance h times the linear momentum magnitude Π.

$$\Lambda = h \, \Pi \tag{6.4.14}$$

Clearly, this is zero if the hammer hits dead-on the CM. ($h=0$)

The final angular velocity ω about the CM is the angular momentum Λ divided by the moment of inertia $I= M \ell^2/3$ of the stick.

$$\omega = \Lambda / I \qquad (= 3 \, \Lambda /(M \, \ell^2) \qquad \text{for stick}) \tag{6.4.15a}$$
$$= h \, \Pi / I \qquad (= 3 \, h\Pi /(M \, \ell^2) \qquad \text{for stick}) \tag{6.4.15b}$$

Again, this depends on the hitting radius h and vanishes when $h=0$.

Π = linear momentum ⟶

Π h = angular momentum about

*Imaginary wheel of radius p rolls on imaginary road
that intersects the Center of Percussion P*
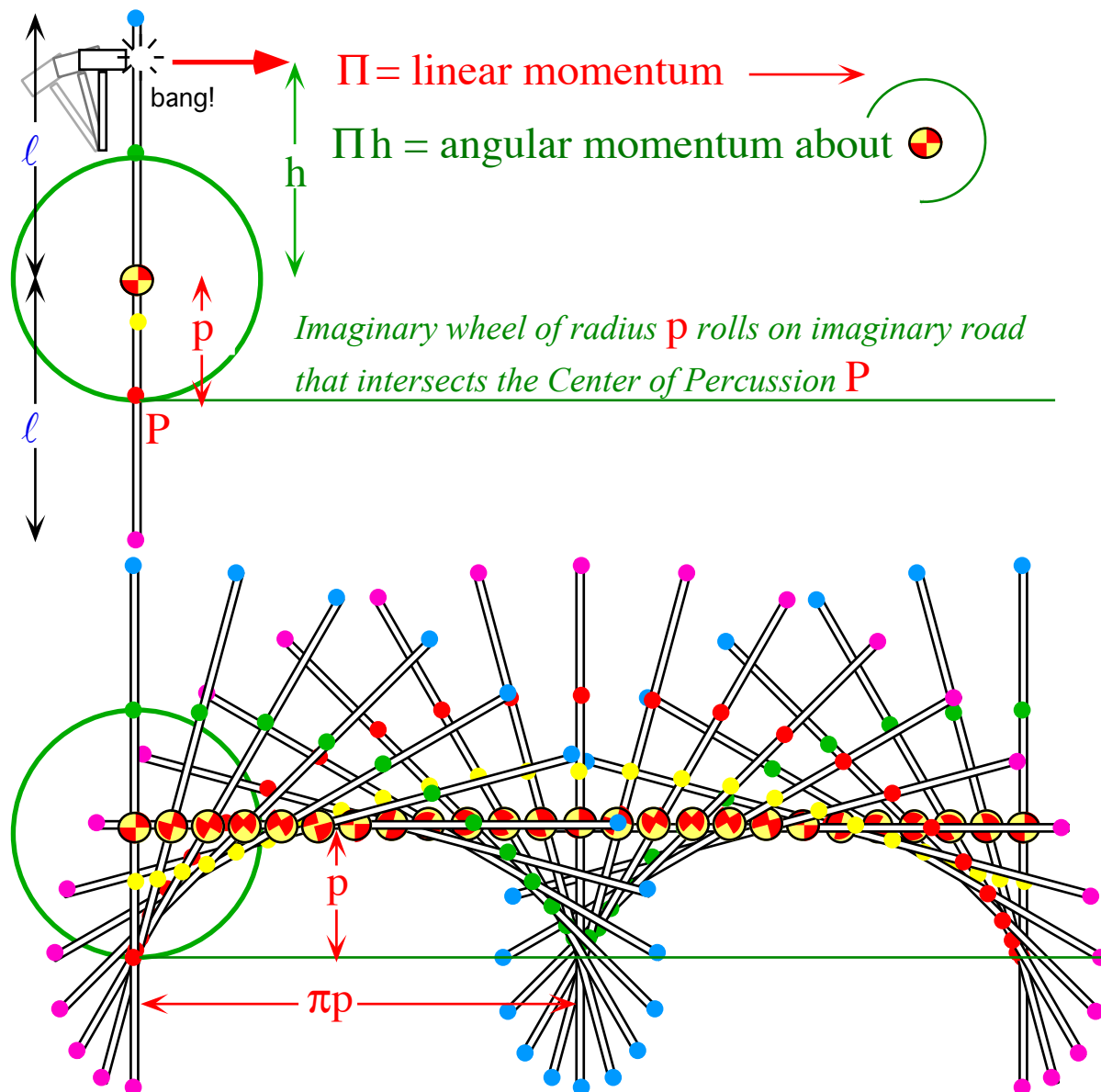
Fig. 6.4.3 The effects of hitting a stationary stick.

The stick proceeds to act like it is a wheel of radius p rolling $2\pi p$ down an imaginary road each time it rotates by 2π as shown in Fig. 6.4.3. The road intersects a point called the *center of percussion* or "sweet spot" that is stationary immediately after the hammer-hit. This is the point on the wheel where the speed $p\omega$ due to rotation just equals the translational speed of the CM.

$$\Pi / M = V_{CM} = p\omega = 3ph\Pi / (M \ell^2) \qquad (6.4.16)$$

Solving gives the *percussion radius p* where you can comfortably grip the stick and hit a ball at h.

$$p = \ell^2/3h \qquad (6.4.17)$$

To hit the ball near one end ($h=\ell$) grip the stick at $r=-p=-\ell/3$, that is, the <u>other</u> end 1/3 of the way from the center. The reverse holds, too. If you grip the end ($p=\ell$) then hit the ball 1/3 of the way from the center to the opposite end To hit a fast ball off the CM, grip it at $p=\infty$, that is, do not hold it at all or it will hurt!

There is a hitting point where the percussion radius p and the hitting radius h are equal. This radius is called the *radius of gyration r^{gyro}*. For the stick of length 2ℓ this is given by

$$r^2 = \ell^2/3 \qquad \text{or:} \qquad r^{gyro} = r = \ell /\sqrt{3} = 0.577\ell \tag{6.4.18}$$

The moment of inertia of any body is its mass times the square of its radius of gyration.

$$I = M\,(r^{gyro}\,)^2\ (= M\ell^2\,/3 \text{ for stick of length } 2\ell) \tag{6.4.19}$$

Hitting a ball outside this radius r^{gyro} means you should hold the body proportionally inside r^{gyro} , (on the other side of the CM, of course!) and vice-versa.

The points at the radius p of percussion on the flying stick in the lower part of Fig. 6.4.3 each generate a cycloid of diameter $2p$. The stick itself generates the tangents of a cycloid of diameter p. Points inside and outside of percussion radii generate, respectively, *prolate* and *curlate* cycloids.
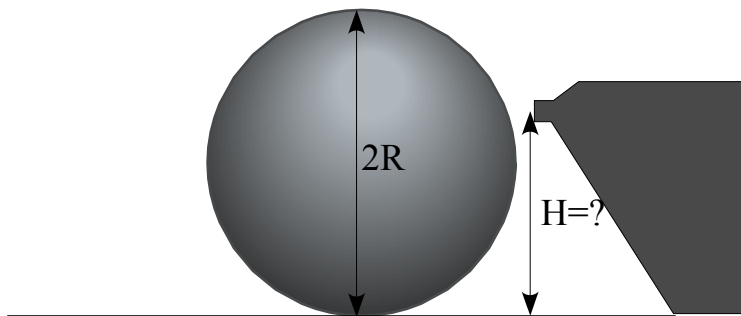
Exercise 6.4.1 Pool clues
Bumpers on pool and billiards tables are set at a height H that is certain fraction of ball diameter $D=2R$ so that the balls bounce without slipping. What is that fraction H/D for three cases listed below?
Case 1 (The usual case.) The ball is a uniform spherical solid.
Case 2 (An unusual case.) The ball is a uniform spherical shell.
Case 3 (A ridiculous case.) The "ball" is a uniform cylindrical shell.
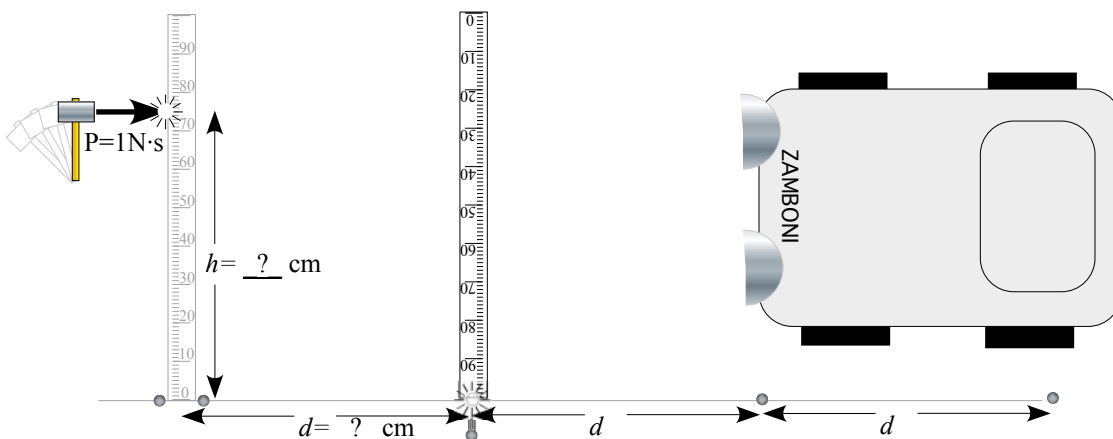
Exercise 6.4.2 Hockey knock
A meter stick is lying flat on an ice rink with two marbles sitting at the lower end on either side of the 0.0cm mark on x-axis. (See figure) A hammer gives impulse $\mathbf{P}=(1\text{N·s})\mathbf{e_x}$ to the stick at the h-cm. mark.
What horizontal distance h is *least* likely to disturb the marbles. At what distances $d, 2d, 3d, \ldots$ along x-axis should the $3^{rd}, 4^{th}, 5^{th},\ldots$ marbles be placed so they are most likely to be knocked below the axis. (See figure above.)

Chapter 6.5. Rigid Body Velocity, Momentum, and Energy

For rigid bodies with no internal motion there are only six coordinates. If we can ignore translation of the CM then there are only three coordinates. The three velocities that go with these coordinates are the components of the angular velocity vector ω introduced in (6.4.8). The three momenta that go with them are the components of the vector **L** introduced in (6.4.9). These are related by a tensor equation that will be discussed now.

a. Inertia tensors

The equations (6.4.8) through (6.4.10) apply to rigid body motion. We rewrite them for the rigid case (no internal vibrational motion) starting with (6.4.8) for Darboux's velocity.

$$\dot{\mathbf{r}}_j = \boldsymbol{\omega} \times \mathbf{r}_j \tag{6.5.1}$$

Putting this into angular momentum relation (6.4.9) gives

$$\mathbf{L} = \sum_{j=1}^{3} \mathbf{r}_j \times m_j \dot{\mathbf{r}}_j = \sum_{j=1}^{3} m_j \mathbf{r}_j \times \left(\boldsymbol{\omega} \times \mathbf{r}_j \right) \tag{6.5.2}$$

We expand using $\mathbf{A} \times (\mathbf{B} \times \mathbf{C}) = (\mathbf{A} \bullet \mathbf{C})\mathbf{B} - (\mathbf{A} \bullet \mathbf{B})\mathbf{C}$ or use Levi-Civita analysis in Appendix 1.A.

$$\mathbf{L} = \sum_{j=1}^{3} m_j \left[\left(\mathbf{r}_j \bullet \mathbf{r}_j \right) \boldsymbol{\omega} - \left(\mathbf{r}_j \bullet \boldsymbol{\omega} \right) \mathbf{r}_j \right] = \sum_{j=1}^{3} m_j \left[\left(\mathbf{r}_j \bullet \mathbf{r}_j \right) \mathbf{1} - \mathbf{r}_j \mathbf{r}_j \right] \bullet \boldsymbol{\omega} = \ddot{\mathbf{I}} \bullet \boldsymbol{\omega} \tag{6.5.3}$$

Now we define the *rotational inertia tensor* **I**. (Compare this **r**-tensor **I** to the ω-tensor in (3.7.23).)

$$\ddot{\mathbf{I}} = \sum_{j=1}^{3} \ddot{\mathbf{I}}_j = \sum_{j=1}^{3} m_j \left[\left(\mathbf{r}_j \bullet \mathbf{r}_j \right) \mathbf{1} - \mathbf{r}_j \mathbf{r}_j \right] \tag{6.5.4}$$

In matrix form the ω-to-**L** relation is

$$\begin{pmatrix} L_x \\ L_y \\ L_z \end{pmatrix} = \sum_{j=1}^{3} m_j \begin{pmatrix} y_j^2 + z_j^2 & -x_j y_j & -x_j z_j \\ -y_j x_j & x_j^2 + z_j^2 & -y_j z_j \\ -z_j x_j & -z_j y_j & x_j^2 + y_j^2 \end{pmatrix} \begin{pmatrix} \omega_x \\ \omega_y \\ \omega_z \end{pmatrix}. \tag{6.5.5a}$$

Here the *inertia matrix* <**I**> is

$$\langle \ddot{\mathbf{I}} \rangle = \sum_{j=1}^{3} \langle \ddot{\mathbf{I}}_j \rangle = \sum_{j=1}^{3} m_j \begin{pmatrix} y_j^2 + z_j^2 & -x_j y_j & -x_j z_j \\ -y_j x_j & x_j^2 + z_j^2 & -y_j z_j \\ -z_j x_j & -z_j y_j & x_j^2 + y_j^2 \end{pmatrix}. \tag{6.5.5b}$$

From this we see that the angular momentum **L** is related through a linear (matrix) transformation to the angular velocity ω, and vice-versa. The two vectors ω and **L** will not point in the same direction unless they are *eigenvectors* of the inertia tensor **I** or matirx <**I**>. Note that the numerical values of the <**I**> matrix components, like components of vectors ω and **L**, depend on the coordinate basis being used. An eigenvector basis gives a diagonal <**I**> matrix.

For example, consider one mass *m* at the end of a bent axle that is rotating around a fixed bearing instantaneously at $\mathbf{r}_m = (x_m, y_m, z_m) = r(\frac{1}{\sqrt{2}}, \frac{1}{\sqrt{2}}, 0)$ as shown in Fig. 6.5.1. The **L**=**I**·ω relation follows.

$$\mathbf{L}=mr^2\begin{pmatrix} -\omega/2 \\ \omega/2 \\ 0 \\ 0 \end{pmatrix}$$

$$\boldsymbol{\omega} = \begin{pmatrix} 0 \\ \omega \\ 0 \end{pmatrix}$$

$$\mathbf{r} = \begin{pmatrix} r/\sqrt{2} \\ r/\sqrt{2} \\ 0 \end{pmatrix}$$
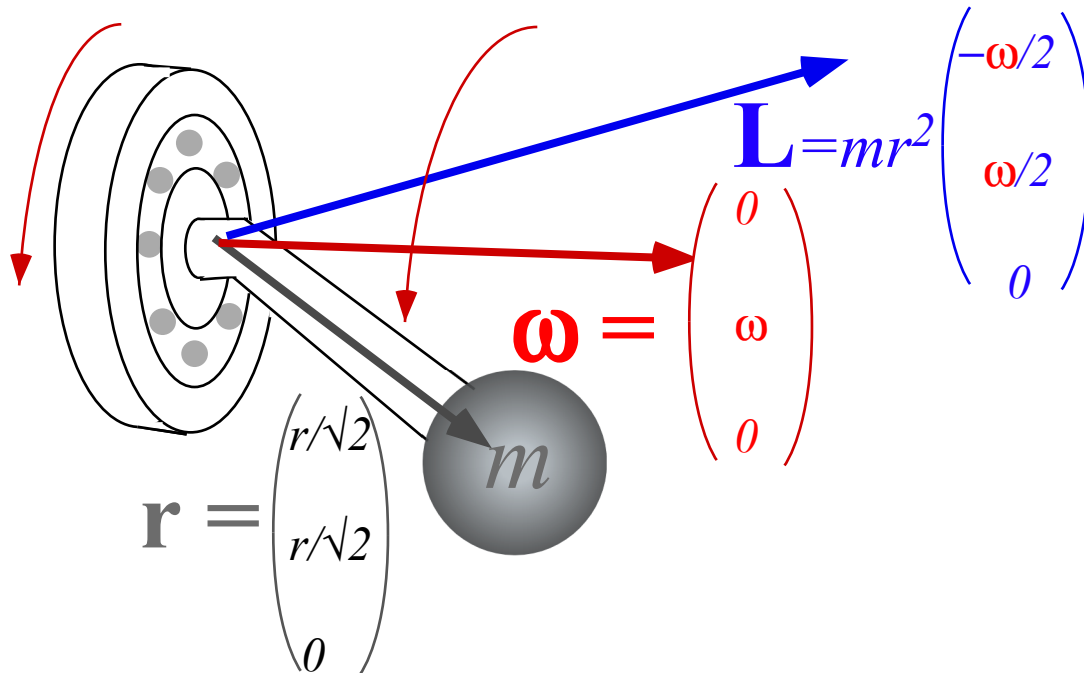
Fig. 6.5.1 Angular momentum for mass rotating on bent axle.

From (6.5.5b) the inertia matrix for the mass at the instant shown (*t=0*) in the Fig. 6.5.1 is

$$\ddot{\mathbf{I}} = mr^2 \begin{pmatrix} \left(1/\sqrt{2}\right)^2 + 0 & -\left(1/\sqrt{2}\right)\left(1/\sqrt{2}\right) & -\left(1/\sqrt{2}\right)0 \\ -\left(1/\sqrt{2}\right)\left(1/\sqrt{2}\right) & \left(1/\sqrt{2}\right)^2 + 0 & -\left(1/\sqrt{2}\right)0 \\ -0\left(1/\sqrt{2}\right) & -0\left(1/\sqrt{2}\right) & \left(1/\sqrt{2}\right)^2 + \left(1/\sqrt{2}\right)^2 \end{pmatrix} = mr^2 \begin{pmatrix} 1/2 & -1/2 & 0 \\ -1/2 & 1/2 & 0 \\ 0 & 0 & 1 \end{pmatrix}$$

Operating on the angular velocity gives the angular momentum shown in the figure.

$$\begin{pmatrix} L_x \\ L_y \\ L_z \end{pmatrix} = mr^2 \begin{pmatrix} 1/2 & -1/2 & 0 \\ -1/2 & 1/2 & 0 \\ 0 & 0 & 1 \end{pmatrix} \begin{pmatrix} 0 \\ \omega \\ 0 \end{pmatrix} = mr^2 \begin{pmatrix} -1/2 \\ 1/2 \\ 0 \end{pmatrix} \omega \qquad (6.5.6)$$

This is a bad thing! The **L**-vector is off the ω-axis so it is rotating around off-center like the mass. So by (6.4.10a) $\dot{\mathbf{L}}=\mathbf{N}$, large ω implies large oscillatory bearing torque **N** and possible catastrophic failure.

b. Kinetic energy in terms of ω

The kinetic energy of a rotating rigid body can be expressed in terms of the inertia matrix, too.

$$T = \frac{1}{2}\sum_{j=1}^{3} m_j \dot{\mathbf{r}}_j \bullet \dot{\mathbf{r}}_j = \frac{1}{2}\sum_{j=1}^{3} m_j \left(\boldsymbol{\omega}\times\mathbf{r}_j\right)\bullet\left(\boldsymbol{\omega}\times\mathbf{r}_j\right) \qquad (6.5.7)$$

We expand using a Levi-Civita identity $\left(\mathbf{A}\times\mathbf{B}\right)\times\left(\mathbf{C}\times\mathbf{D}\right) = \left(\mathbf{A}\bullet\mathbf{C}\right)\left(\mathbf{B}\bullet\mathbf{D}\right) - \left(\mathbf{A}\bullet\mathbf{D}\right)\left(\mathbf{B}\bullet\mathbf{C}\right)$ to get

$$T = \frac{1}{2} \sum_{j=1}^{3} m_j \left[(\boldsymbol{\omega} \bullet \boldsymbol{\omega})(\mathbf{r}_j \bullet \mathbf{r}_j) - (\boldsymbol{\omega} \bullet \mathbf{r}_j)(\mathbf{r}_j \bullet \boldsymbol{\omega}) \right]$$

$$= \frac{1}{2} \boldsymbol{\omega} \bullet \sum_{j=1}^{3} m_j \left[(\mathbf{r}_j \bullet \mathbf{r}_j) \mathbf{1} - (\mathbf{r}_j)(\mathbf{r}_j) \right] \bullet \boldsymbol{\omega} \qquad (6.5.8)$$

$$= \frac{1}{2} \boldsymbol{\omega} \bullet \bar{\bar{\mathbf{I}}} \bullet \boldsymbol{\omega}$$

The kinetic energy is a *quadratic form* like (3.5.2) or else potential (4.3.16). The matrix notation is

$$T = \frac{1}{2} \begin{pmatrix} \omega_x & \omega_y & \omega_y \end{pmatrix} \begin{pmatrix} I_{xx} & I_{xy} & I_{xz} \\ I_{yx} & I_{yy} & I_{yz} \\ I_{zx} & I_{zy} & I_{zz} \end{pmatrix} \begin{pmatrix} \omega_x \\ \omega_y \\ \omega_z \end{pmatrix}$$

$$= \frac{1}{2} \begin{pmatrix} \langle \omega|x \rangle & \langle \omega|y \rangle & \langle \omega|z \rangle \end{pmatrix} \begin{pmatrix} \langle x|\mathbf{I}|x \rangle & \langle x|\mathbf{I}|y \rangle & \langle x|\mathbf{I}|z \rangle \\ \langle y|\mathbf{I}|x \rangle & \langle y|\mathbf{I}|y \rangle & \langle y|\mathbf{I}|z \rangle \\ \langle z|\mathbf{I}|x \rangle & \langle z|\mathbf{I}|y \rangle & \langle z|\mathbf{I}|z \rangle \end{pmatrix} \begin{pmatrix} \langle x|\omega \rangle \\ \langle y|\omega \rangle \\ \langle z|\omega \rangle \end{pmatrix} \text{ (Dirac notation)} \qquad (6.5.9)$$

$$= \frac{1}{2} \begin{pmatrix} \omega_x & \omega_y & \omega_y \end{pmatrix} \sum_{j=1}^{3} m_j \begin{pmatrix} y_j^2 + z_j^2 & -x_j y_j & -x_j z_j \\ -y_j x_j & x_j^2 + z_j^2 & -y_j z_j \\ -z_j x_j & -z_j y_j & x_j^2 + y_j^2 \end{pmatrix} \begin{pmatrix} \omega_x \\ \omega_y \\ \omega_z \end{pmatrix}$$

Since <I> is a symmetric matrix, it will always be possible to find a normal coordinate eigen-basis {*X,Y,Z*} in which the **I**-matrix is diagonal. This basis is called the *principle inertial axes {X,Y,Z}* or *body eigen-axes*. In the body coordinate system the kinetic expression simplifies greatly.

$$T = \frac{1}{2} \begin{pmatrix} \omega_X & \omega_Y & \omega_Z \end{pmatrix} \begin{pmatrix} I_{XX} & I_{XY} & I_{XZ} \\ I_{YX} & I_{YY} & I_{YZ} \\ I_{ZX} & I_{ZY} & I_{ZZ} \end{pmatrix} \begin{pmatrix} \omega_X \\ \omega_Y \\ \omega_Z \end{pmatrix}$$

$$= \frac{1}{2} \begin{pmatrix} \omega_X & \omega_Y & \omega_Z \end{pmatrix} \begin{pmatrix} I_{XX} & 0 & 0 \\ 0 & I_{YY} & 0 \\ 0 & 0 & I_{ZZ} \end{pmatrix} \begin{pmatrix} \omega_X \\ \omega_Y \\ \omega_Z \end{pmatrix} = \frac{I_{XX}\omega_X^2}{2} + \frac{I_{YY}\omega_Y^2}{2} + \frac{I_{ZZ}\omega_Z^2}{2} \qquad (6.5.10)$$

For constant energy *E=T* this is an equation for the *angular velocity or ω-ellipsoid*. The ellipsoid and the principle axes {*X,Y,Z*} are attached to the body and rotate with it.

c. Kinetic energy in terms of L

The ω-**L** relation (6.5.3) usually has an inverse. Recall quadratic form relations around (1.11.10).

$$\mathbf{L} = \bar{\bar{\mathbf{I}}} \bullet \boldsymbol{\omega}, \quad \text{generally implies:} \quad \boldsymbol{\omega} = \bar{\bar{\mathbf{I}}}^{-1} \bullet \mathbf{L}$$

In this way we can rewrite the kinetic energy in terms of either velocity or momentum (or both).

$$T = \frac{1}{2} \boldsymbol{\omega} \bullet \bar{\bar{\mathbf{I}}} \bullet \boldsymbol{\omega} = \frac{1}{2} \boldsymbol{\omega} \bullet \mathbf{L} = \frac{1}{2} \mathbf{L} \bullet \boldsymbol{\omega} = \frac{1}{2} \mathbf{L} \bullet \bar{\bar{\mathbf{I}}}^{-1} \bullet \mathbf{L} \qquad (6.5.11)$$

The latter form is a *Hamiltonian* form while the first is a *Lagrangian* from. (Recall (1.12.8) in Unit 1.) The principle coordinate axes $\{X,Y,Z\}$ are the same for a matrix and its inverse.

$$T = \frac{1}{2}\begin{pmatrix} L_X & L_Y & L_Z \end{pmatrix}\begin{pmatrix} I_{XX} & I_{XY} & I_{XZ} \\ I_{YX} & I_{YY} & I_{YZ} \\ I_{ZX} & I_{ZY} & I_{ZZ} \end{pmatrix}^{-1}\begin{pmatrix} L_X \\ L_Y \\ L_Z \end{pmatrix}$$

$$= \frac{1}{2}\begin{pmatrix} L_X & L_Y & L_Z \end{pmatrix}\begin{pmatrix} 1/I_{XX} & 0 & 0 \\ 0 & 1/I_{YY} & 0 \\ 0 & 0 & 1/I_{ZZ} \end{pmatrix}\begin{pmatrix} L_X \\ L_Y \\ L_Z \end{pmatrix} = \frac{L_X^2}{2I_{XX}} + \frac{L_Y^2}{2I_{YY}} + \frac{L_Z^2}{2I_{ZZ}} \qquad (6.5.12)$$

The Hamiltonian form gives the equation of the *angular momentum or L-ellipsoid*. It is conjugate to the ω-ellipsoid; the major axis of the **L**-ellipsoid becomes a minor axis of the ω-ellipsoid, and vice-versa. The ω-ellipsoid more closely resembles its attached body; where the body is longest there also will be the major axes of the ω-ellipsoid. The **L**-vector has to satisfy two conservation laws in the $\{X,Y,Z\}$ body frame. It's length $|\mathbf{L}|$ must be constant so **L** must lie on a sphere as shown in Fig. 6.5.2. Also $T=E$ must be constant, and so **L** must lie on an intersection of the sphere with the ellipsoid (6.5.12) in the rotating principle axes $\{X,Y,Z\}$ frame.
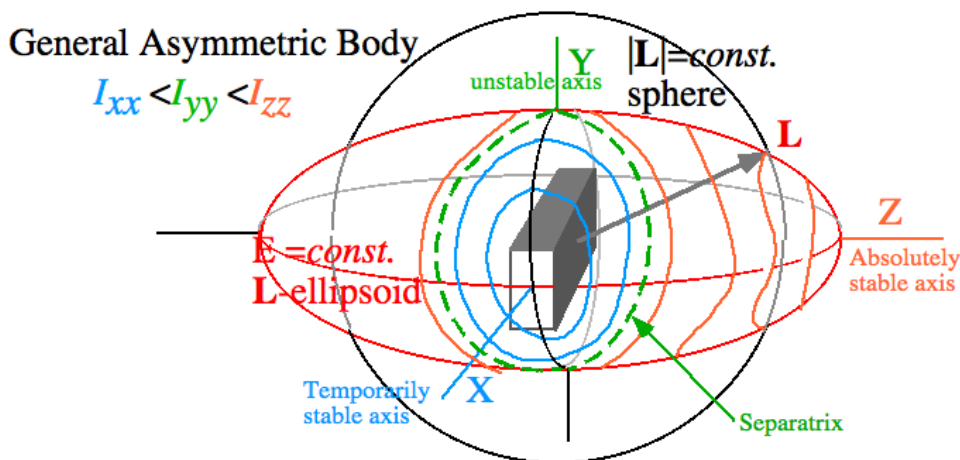
Fig. 6.5.2 Angular momentum ellipsoid for rectangular rigid body in its own or eigen $\{X,Y,Z\}$ frame.

The **L**-vector must then follow the intersection curve which may loop around the Z-axis of greatest inertia I_{ZZ} as shown in Fig. 6.5.2, or if $|\mathbf{L}|$ is smaller or E is greater, it may loop around the X-axis of least inertia I_{XX} as indicated by ovals drawn around the X-axis. However, it may never loop around the Y-axis of intermediate inertia. *Separatrices* intersect at the intermediate axis like the hyperbolic asymptotes on inverted pendulum saddle points in Fig. 1.15.1 on p. 1-25-28.

Motion near a separatrix is very "upsetting" to anyone who might be unfortunate enough to be on board the body. Since vector **L** must remain fixed relative to the stars, the body will turn completely upside down, spin for awhile, and then right itself abruptly, spin, turn over, and so on until it lost energy through creaking joints and sloshing fluids. Then the energy ellipse would shrink quickly, and the body would eventually settle into less wobbly rotation on its Z-axis. The Z-axis of rotation is stable to energy loss; it has the lowest energy for a given magnitude of angular momentum $|\mathbf{L}|$. The X-axis, on the other hand has the highest energy for a given $|\mathbf{L}|$. X-

rotation is stable for a truly rigid body, but not if it loses energy through internal friction! Then it will catastrophically "fall" onto the Z-axis as once happened to a TRW satellite. (That was a multi-million dollar lesson in rotational mechanics!)

While **L** moves on the **L**-ellipsoid in the body frame the ω-vector is moving on its ellipsoid. Since ω is the angular velocity vector, it is the instantaneous rotation axis for motion of every atom in the body relative to the lab or star-fixed frame. ω determines how fast the body moves relative to the in the lab frame **L**-vector, or, in the body frame, how fast the **L**-vector moves (the opposite way) relative to the body. As shown in Fig. 6.5.3, the ω and **L** vectors are normal to each other's ellipsoidal tangent plane and the projection ω •**L** of ω on **L** is constant according to (6.5.11). (Remember that **L** is star-fixed but ω will not be star-stationary unless it lies along **L**.) However, all body points along ω are instantaneously star-stationary since that is, for an instant, the rotation axis. So the ω-ellipsoid rolls without slipping along a star fixed plane normal to **L**. (Recall the geometry of Fig. 1.12.2 in Unit 1.)
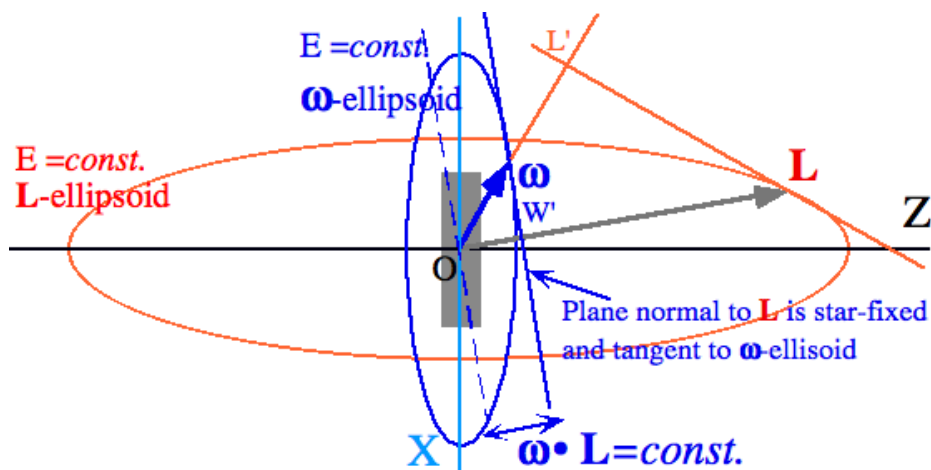
Fig. 6.5.3 Angular momentum and velocity ellipsoids for rectangular rigid body.

You will recall how the gradient ∇V of a potential energy surface points normal to the PE surface and determines the acceleration or "fall-line" in coordinate space. Gradient of a quadratic form in (4.3.16) $\nabla(\mathbf{r} \bullet \mathbf{K} \bullet \mathbf{r}/2) = \mathbf{K} \bullet \mathbf{r}$ is acceleration in (4.3.5). Also, the phase space gradient of a Hamiltonian determines velocity transverse to the fall-line in (2.7.14) of Unit 2.

For rotations the kinetic energy T is the Hamiltonian H or the Lagrangian L in the absence of an applied torque. The canonical momentum $p_\mu = \partial L / \partial \dot{q}^\mu$ from (3.8.1d) is

$$\mathbf{L} = \frac{\partial T}{\partial \boldsymbol{\omega}} = \nabla_\omega T = \frac{\partial}{\partial \boldsymbol{\omega}} \frac{\boldsymbol{\omega} \bullet \mathbf{I} \bullet \boldsymbol{\omega}}{2} = \mathbf{I} \bullet \boldsymbol{\omega} \ . \qquad (6.5.13)$$

That is an ω-gradient of the ω-ellipsoid. Hamilton's 1st equations $\dot{q}^\mu = \partial H / \partial p_\mu$ from (3.8.5d) are as follows.

$$\boldsymbol{\omega} = \frac{\partial H}{\partial \mathbf{L}} = \nabla_L H = \frac{\partial}{\partial \mathbf{L}} \frac{\mathbf{L} \bullet \boldsymbol{\Gamma}^{-1} \bullet \mathbf{L}}{2} = \boldsymbol{\Gamma}^{-1} \bullet \mathbf{L} \qquad (6.5.14a)$$

Angular velocity ω is the **L**-gradient of the **L**-ellipsoid.

Finally, the 2nd Hamiltonian-Lagrange equations $\dot{p}_\mu = -\partial H / \partial q^\mu = \partial L / \partial q^\mu$ from (3.8.5e) are as follows.

$$\dot{\mathbf{L}} = -\frac{\partial H}{\partial \boldsymbol{\theta}} \ (= \mathbf{0} \text{ if no torques applied}) . \tag{6.5.14b}$$

They state the conservation of angular momentum for a freely rotating body.

The rotational motion dictated by the above equations is more like the phase space motion of Fig. 2.7.3 and moves transversely to the gradient around the oval loops and separatrices. This motion is explored in greater detail in Ch. 7 and Ch. 8 of this unit. (See Fig. 6.7.4 and Fig. 6.8.1.)

d. Tensor parallel axis theorem

Consider a mass rotating about some pivot point besides its CM such as in Fig. 6.5.4. Let us express the **I**-tensor around an arbitrary pivot in terms of the one around the CM.
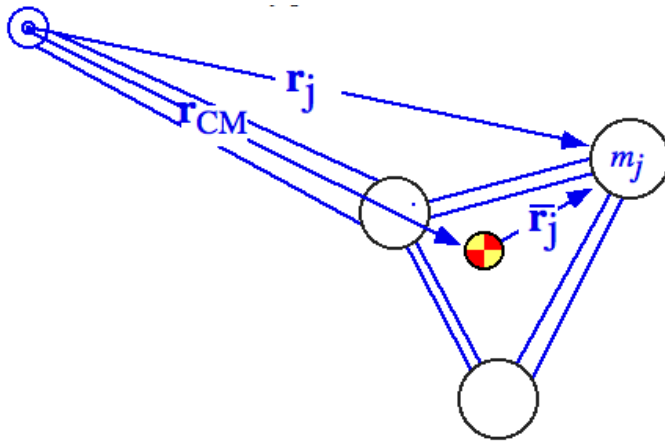
Fig. 6.5.4 Coordinates for off-center rigid body.

Replacing $\mathbf{r}_j$ by the sum $\mathbf{r}_j = \mathbf{r}_{CM} + \bar{\mathbf{r}}_j$ in the inertia tensor (6.5.4) gives an expanded version.

$$\ddot{\mathbf{I}} = \sum_{j=1}^{3} \ddot{\mathbf{I}}_j = \sum_{j=1}^{3} m_j \left[(\mathbf{r}_j \bullet \mathbf{r}_j)\mathbf{1} - \mathbf{r}_j\mathbf{r}_j \right] = \sum_{j=1}^{3} m_j \left[\left((\mathbf{r}_{CM} + \bar{\mathbf{r}}_j) \bullet (\mathbf{r}_{CM} + \bar{\mathbf{r}}_j) \right)\mathbf{1} - (\mathbf{r}_{CM} + \bar{\mathbf{r}}_j)(\mathbf{r}_{CM} + \bar{\mathbf{r}}_j) \right]$$

Multiplying it out gives the following.

$$\ddot{\mathbf{I}} = \left(\sum_{j=1}^{3} m_j \right) \left[(\mathbf{r}_{CM} \bullet \mathbf{r}_{CM})\mathbf{1} - \mathbf{r}_{CM}\mathbf{r}_{CM} \right] + \sum_{j=1}^{3} m_j \left[(\bar{\mathbf{r}}_j \bullet \bar{\mathbf{r}}_j)\mathbf{1} - \bar{\mathbf{r}}_j\bar{\mathbf{r}}_j \right]$$

$$+ 2\left(\sum_{j=1}^{3} m_j \bar{\mathbf{r}}_j \right) \bullet \mathbf{r}_{CM}\mathbf{1} + \left(\sum_{j=1}^{3} m_j \bar{\mathbf{r}}_j \right)\mathbf{r}_{CM} + \mathbf{r}_{CM}\left(\sum_{j=1}^{3} m_j \bar{\mathbf{r}}_j \right)$$

Each sum $\Sigma \, m_j \bar{\mathbf{r}}_j$ of mass moments relative to the CM point is zero.

$$(\ddot{\mathbf{I}} \text{ relative to } \mathbf{r}) = M\left[(\mathbf{r}_{CM} \bullet \mathbf{r}_{CM})\mathbf{1} - \mathbf{r}_{CM}\mathbf{r}_{CM} \right] + \sum_{j=1}^{3} m_j \left[(\bar{\mathbf{r}}_j \bullet \bar{\mathbf{r}}_j)\mathbf{1} - \bar{\mathbf{r}}_j\bar{\mathbf{r}}_j \right] \tag{6.5.15}$$

$$= (\ddot{\mathbf{I}} \text{ for M concetrated at } \mathbf{r}_{CM}) + (\ddot{\mathbf{I}} \text{ relative to } \mathbf{r}_{CM})$$

This is the *parallel axis theorem*. The inertia of a body rotating around an arbitrary point is equal to that of a point mass *M* at the CM point $\mathbf{r}_{CM}$ plus the inertia of the body around its own CM.

Chapter 6.6. 3D Euler transformations and rotating vector frames

Many labs need to orient crystals or lasers using a *goniometer* like one shown undergoing an Euler rotational sequence in Fig. 6.6.1. Sketches and photographs in Fig. 6.6.1 thru Fig. 6.6.5 show a goniometric *rotation-analog-computer* that we will use to describe rotation mechanics. This device helps visualize both *R(3)* (real 3D vector rotations) and *U(2)* (complex 2D unitary transformations) labeled either by Euler angles *(αβγ)* or by Darboux ω-whirl-vector angles [φϑΘ].
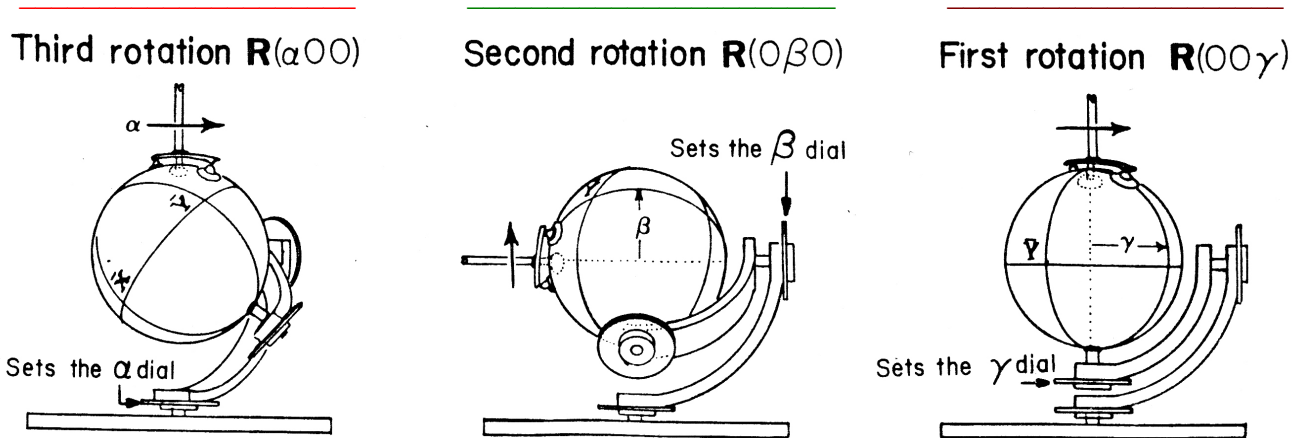
Fig. 6.6.1 Euler sequence R(αβγ) of z-rotation by α after y-rotation by β after z-rotation by γ.

a. Euler angle goniometer and vector 3D rotations

The 3-by-3 rotation matrix *R(αβγ)* describing an Euler rotation of real 3-vectors is a bit larger than the complex 2-by-2 spinor matrix (4.4.20). *R(αβγ)* is a real 3-by-3 matrix made using the same triple product rotation sequence **R**(αβγ) in (4.4.20) or Fig. 4.4.3 of Unit 4 or Fig. 6.6.1 above.

$$\langle R(\alpha\beta\gamma)\rangle = \langle R(\alpha 0 0)\rangle \qquad \langle R(0\beta 0)\rangle \qquad \langle R(00\gamma)\rangle$$

$$= \begin{pmatrix} \cos\alpha & -\sin\alpha & 0 \\ \sin\alpha & \cos\alpha & 0 \\ 0 & 0 & 1 \end{pmatrix} \begin{pmatrix} \cos\beta & 0 & \sin\beta \\ 0 & 1 & 0 \\ -\sin\beta & 0 & \cos\beta \end{pmatrix} \begin{pmatrix} \cos\gamma & -\sin\gamma & 0 \\ \sin\gamma & \cos\gamma & 0 \\ 0 & 0 & 1 \end{pmatrix} \qquad (6.6.1a)$$

Rotation matrix $\langle \mathbf{e}_A | \mathbf{e}_{\bar{B}}\rangle = \langle \mathbf{e}_A | R | \mathbf{e}_B\rangle$ below has row-*A* or column-*B* labeled by bra-$\langle \mathbf{e}_A |$ or ket-$|\mathbf{e}_{\bar{B}}\rangle$.

$$|\mathbf{e}_{\bar{X}}\rangle = R(\alpha\beta\gamma)|\mathbf{e}_X\rangle \qquad |\mathbf{e}_{\bar{Y}}\rangle = R(\alpha\beta\gamma)|\mathbf{e}_Y\rangle \qquad |\mathbf{e}_{\bar{Z}}\rangle = R(\alpha\beta\gamma)|\mathbf{e}_Z\rangle$$

$$(\langle \mathbf{e}_A | R(\alpha\beta\gamma)|\mathbf{e}_B\rangle) = \begin{array}{c} \langle \mathbf{e}_X| \\ \langle \mathbf{e}_Y| \\ \langle \mathbf{e}_Z| \end{array} \begin{pmatrix} \cos\alpha\cos\beta\cos\gamma - \sin\alpha\sin\gamma & -\cos\alpha\cos\beta\sin\gamma - \sin\alpha\cos\gamma & \cos\alpha\sin\beta \\ \sin\alpha\cos\beta\cos\gamma + \cos\alpha\sin\gamma & -\sin\alpha\cos\beta\sin\gamma + \cos\alpha\cos\gamma & \sin\alpha\sin\beta \\ -\cos\gamma\sin\beta & \sin\gamma\sin\beta & \cos\beta \end{pmatrix} \qquad (6.6.1b)$$

The third column contains the Cartesian components of the *R(αβγ)*-rotated Z-axis that is labeled by

$$\mathbf{e}_{\bar{Z}} = |\mathbf{e}_{\bar{Z}}\rangle = (\cos\alpha\,\sin\beta,\ \sin\alpha\,\sin\beta,\ \cos\beta), \qquad \text{or} \qquad \mathbf{e}_{\bar{Z}} = \mathbf{e}_X \cos\alpha\sin\beta + \mathbf{e}_Y\sin\alpha\sin\beta + \mathbf{e}_Z\cos\beta$$

It has the same *polar coordinate components (cosα sinβ, sinα sinβ, cosβ)* seen in Fig. 4.4.3 or (4.4.21). *R* is a matrix of nine *direction cosines* $...\mathbf{e}_X \bullet \mathbf{e}_{\bar{Y}} = \langle X|\bar{Y}\rangle = \cos\angle_X^{\bar{Y}}, \cdots etc.$ transforming vectors passively or actively. (Recall 2D case (4.B.2) used for passive (4.B.1) or active (4.B.5) transformation.)
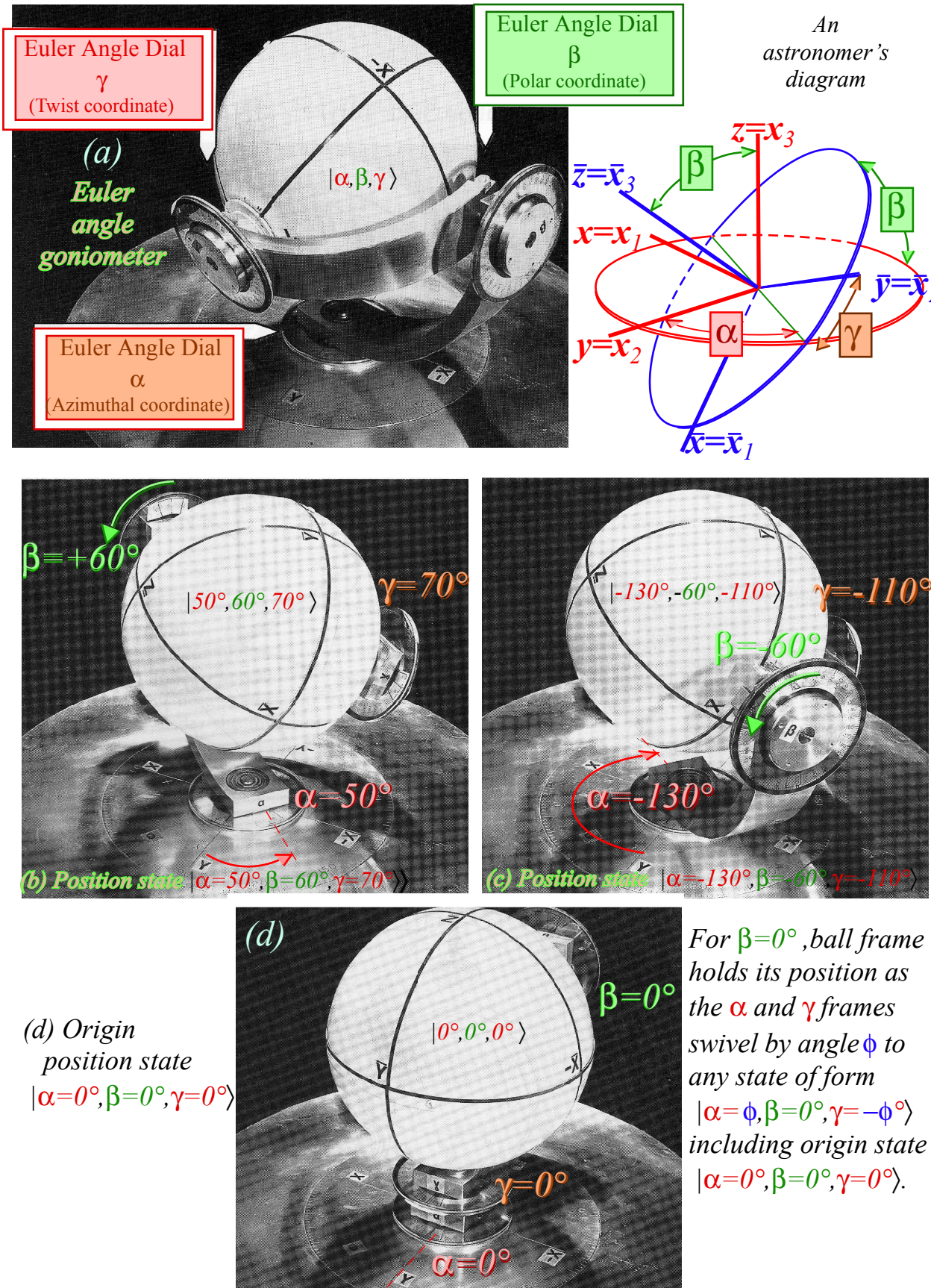
Fig. 6.6.2 (a-d) Euler angle position states and goniometer.

Fig. 6.6.2 Euler angle device relates body frame to lab frame through a sucession of frames and dials.

Metal frames labeled x′ and x″ in Fig. 6.6.3 connect the laboratory or LAB frame $\{X,Y,Z\}$ to the body or BOD frame $\{\bar{X},\bar{Y},\bar{Z}\}$. A series of three bearings and dials define the Euler angles *(αβγ)* of the relative LAB-to-BOD orientation. The device in Fig. 6.6.1-4 shows several key concepts.

First, it shows clearly that Euler angles are good *position coordinates*. While rotation *operations* are done in a definite $R_Z(\alpha) \leftarrow R_Y(\beta) \leftarrow R_Z(\gamma)$ order, the dials shown in Fig. 6.6.3 are path independent. Setting *(αβγ)* in any order gives a position state obtained by operations $R_Z(\alpha)R_Y(\beta)R_Z(\gamma)$ in Fig. 4.4.3 or Fig. 6.6.1. We say *(αβγ)* are *holonomic* (path-independent) coordinates.

Second, it shows how Euler angles are natural choices for lab or theory involving 3D rotation. Indeed, *(αβγ)* are the same as *yaw(α), pitch(β), and roll(γ)* used by an airplane pilot to track the bow or $\bar{Z}$ -axis of the craft body relative to Earth or stars.

Third, the convention used in Fig. 6.6.1-2 makes the first two Euler angles (α and β) into *azimuth* and *polar angle* of the *body zenith* $\bar{Z}$. This is the appropriate for atomic and molecular physics where the body zenith $\bar{Z}$ is a symmetry axis, radius vector, or other significant body point.

Fourth, Fig. 6.6.3 shows the <u>latter</u> two Euler angles (β and γ), more correctly, their negatives (-β and -γ) are also azimuth and polar angles, but for the LAB *zenith Z* relative to the *body frame*. Note that the last row of matrix (6.6.1b) has exactly the polar coordinate form using -β and -γ as azimuth and polar angle, respectively, as sketched in the upper right of Fig. 6.6.3.

Different conventions exist for Euler angles. The first were based on astronomical orientation of planetary orbits and celestial stellar tracks not unlike the arcs in the astronomer's diagram in Fig. 6.6.2(a). The zenith of an orbit plane does not appear in the sky so its azimuth and polar angle is useless. Instead astronomers record the azimuth of the points where the body rises or sets, the so-called *ascending or descending nodes*. These are located *±90°*, respectively, from the azimuth of the orbital zenith so older Euler definitions measure azimuth α from the *±Y*-axis instead of the *X*-axis. Astronomers may also use the *orbital elevation-υ* or the polar angle complement υ=π/2−β.

Euler angles and any 3D angular coordinates, are fundamentally *double valued*. Two settings, *(α=50°,β=60°,γ=70°)* in Fig. 6.6.2b of positive β and *(α-π=-130°,−β=-60°, γ-π=-110°)*, in Fig. 6.6.2c of negative β, both leave a body in the same lab-relative position. Calculus texts restrict polar angle θ=β to positive to avoid this! Recall in Fig. 4.4.4 thru Fig. 4.4.7 that 3D spin vectors rotate twice or by *4π (spin-up, spin-dn, spin-up, spin dn)* for each spinor rotation $(|x\rangle = |\uparrow\rangle, |y\rangle = |\downarrow\rangle, -|x\rangle = -|\uparrow\rangle, -|y\rangle = -|\downarrow\rangle)$. A mechanical demonstration of a full 4π rotation is shown in Fig. 6.6.4.

The case of β=0 (Fig. 6.6.2d) is quite singular since then α and γ coordinates are *infinite-valued* and the state $(\alpha, 0, \gamma)$ is the same position as *(α−ϕ,0,γ+ϕ)* for all ϕ. The singularity occurs at origin *(α=0,β=0,γ=0)* of *R(3)* and *U(2)* group parameter space or, more precisely, *(α=ϕ,β=0,γ=−ϕ)*, and another such singularity is at β=π. Singular ϕ−floppiness is a killer, literally, and corresponds to gyroscopic *gimbal-lock* dreaded by pilots who fly acrobatic maneuvers depending on mechanical gyroscopic instruments that have a linkage quite like the ones shown here. The Euler device in Fig. 6.6.2 provides an excellent demonstration of a gyro compass.
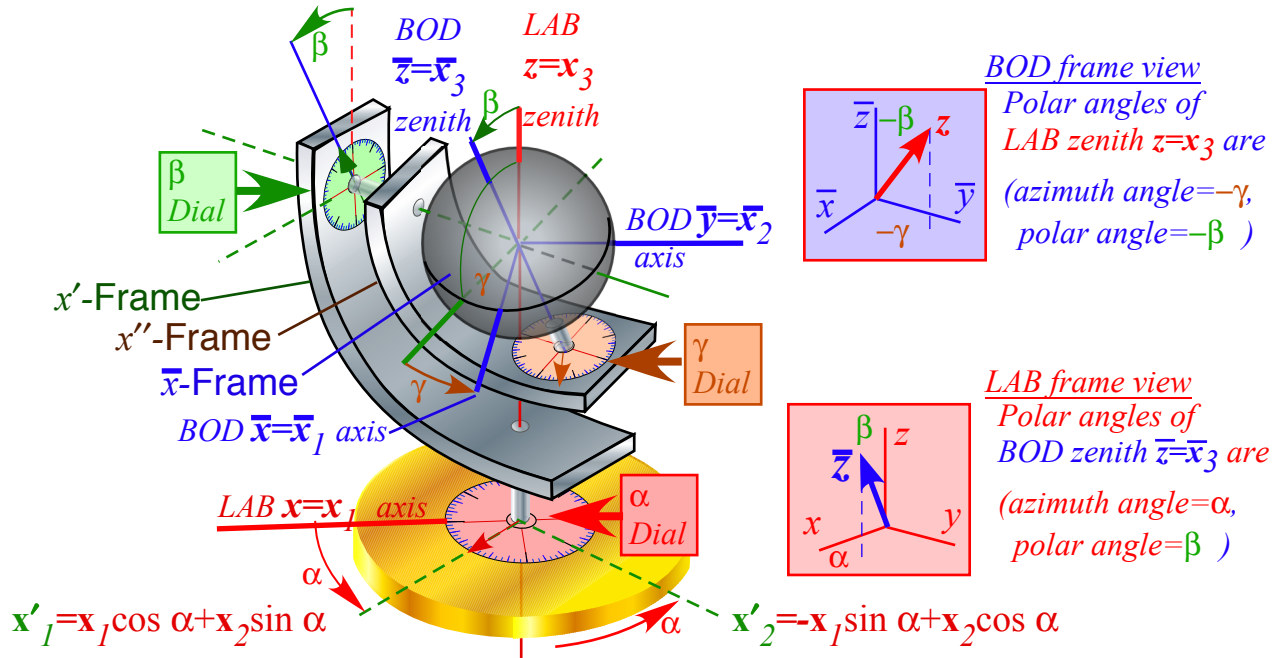
Fig. 6.6.3 Relating body frame to lab frame through a sucession of frames and dials.

b. Darboux rotations, whirl vector $\Theta=\Omega\tau$, and axis angles [φ,ϑ,Θ]

A multi-valued rotational origin is necessary to allow a Darboux crank axis-angle rotation $\mathbf{R}[\varphi,\vartheta,\Theta]$ of Fig. 6.6.4 to produce Euler position states (6.6.1) from an origin or original state $|000\rangle$.

$$\mathbf{R}(\alpha\beta\gamma)\,|000\rangle = |\alpha\beta\gamma\rangle = \mathbf{R}[\varphi,\vartheta,\Theta]\,|000\rangle = \mathbf{R}[\varphi,\vartheta,\Theta]\,|\varphi-\pi/2, 0, \pi/2-\varphi\rangle \qquad (6.6.2)$$

A device that demonstrates this is shown attached to the Euler angle goniometer in Fig. 6.6.4. However, gimbal-lock prevents motion from original position $|000\rangle$ until the goniometer x'-x''-frame pair is tucked under the axis-angle crank support at azimuth φ, that is, until the origin is reset from ($\alpha=0, \beta=0, \gamma=0$) to ($\varphi-\pi/2, 0, \pi/2-\varphi$). Note azimuth α points the x'-frame with its β-axis to an azimuth α-*90°*. Then, the continuous rotation by axis angle $\Theta=\omega t$ may begin in Fig. 6.6.4. *Euler angles* ($\alpha\beta\gamma$) in parentheses or *axis-angles* [$\varphi,\vartheta,\Omega t=\Theta$] in braces[] relate $\mathbf{R}$($\alpha\beta\gamma$)=$\mathbf{R}[\varphi,\vartheta,\Theta]$ by equating the four Θ-components{$\Theta_X, \Theta_Y, \Theta_Z, \Theta_0$} of crank (4.4.10) (or (4.4.30)) with oscillator variables {x_1, p_1, x_2, p_2} of state (4.4.20).

$$\mathbf{R}(\alpha\beta\gamma) = \begin{pmatrix} e^{-i\frac{\alpha+\gamma}{2}}\cos\frac{\beta}{2} & -e^{i\frac{\gamma-\alpha}{2}}\sin\frac{\beta}{2} \\ e^{i\frac{\alpha-\gamma}{2}}\sin\frac{\beta}{2} & e^{i\frac{\alpha+\gamma}{2}}\cos\frac{\beta}{2} \end{pmatrix} = \cos\frac{\alpha+\gamma}{2}\cos\frac{\beta}{2}\begin{pmatrix} 1 & 0 \\ 0 & 1 \end{pmatrix}$$

$$-i\begin{pmatrix} 0 & 1 \\ 1 & 0 \end{pmatrix}\sin\frac{\gamma-\alpha}{2}\sin\frac{\beta}{2} - i\begin{pmatrix} 0 & -i \\ i & 0 \end{pmatrix}\cos\frac{\gamma-\alpha}{2}\sin\frac{\beta}{2} - i\begin{pmatrix} 1 & 0 \\ 0 & -1 \end{pmatrix}\sin\frac{\alpha+\gamma}{2}\cos\frac{\beta}{2} \qquad (6.6.3)$$

$$\mathbf{R}[\Theta] = \begin{pmatrix} \cos\frac{\Theta}{2}-i\hat{\Theta}_Z\sin\frac{\Theta}{2} & -i\sin\frac{\Theta}{2}\left(\hat{\Theta}_X-i\hat{\Theta}_Y\right) \\ -i\sin\frac{\Theta}{2}\left(\hat{\Theta}_X+i\hat{\Theta}_Y\right) & \cos\frac{\Theta}{2}+i\hat{\Theta}_Z\sin\frac{\Theta}{2} \end{pmatrix} = \cos\frac{\Theta}{2}\begin{pmatrix} 1 & 0 \\ 0 & 1 \end{pmatrix}$$

$$-i\begin{pmatrix} 0 & 1 \\ 1 & 0 \end{pmatrix}\hat{\Theta}_X\sin\frac{\Theta}{2} \qquad -i\begin{pmatrix} 0 & -i \\ i & 0 \end{pmatrix}\hat{\Theta}_Y\sin\frac{\Theta}{2} \qquad -i\begin{pmatrix} 1 & 0 \\ 0 & -1 \end{pmatrix}\hat{\Theta}_Z\sin\frac{\Theta}{2} \qquad (6.6.4)$$

Shared 4D phasor coordinates (x_j=$Re\Psi_j$, p_j=$Im\Psi_j$) in (4.4.1c) relate Euler-*to*-Axis angles.

$$x_1 = \quad \cos[(\gamma+\alpha)/2]\cos\beta/2 \quad = \qquad\qquad\qquad\qquad\qquad \cos\Theta/2$$
$$-p_2 = \quad \sin[(\gamma-\alpha)/2]\sin\beta/2 \quad = \hat\Theta_X\sin\Theta/2 = \cos\varphi\ \sin\vartheta\sin\Theta/2$$
$$x_2 = \quad \cos[(\gamma-\alpha)/2]\sin\beta/2 \quad = \hat\Theta_Y\sin\Theta/2 = \sin\varphi\ \sin\vartheta\ \sin\Theta/2 \qquad\qquad (6.6.5a)$$
$$-p_1 = \quad \sin[(\gamma+\alpha)/2]\cos\beta/2 \quad = \hat\Theta_Z\sin\Theta/2 = \cos\vartheta \qquad \sin\Theta/2$$

Solving these relations yields the following Euler angles in terms of axis angles φ, ϑ, and Θ=Ωt.

$$\alpha=\varphi-\pi/2+T, \qquad\qquad \beta = 2\sin^{-1}(\sin\Theta/2\ \sin\vartheta), \qquad\qquad \gamma=\pi/2-\varphi+T \qquad (6.6.5b)$$

Here T= $\tan^{-1}(\tan(\Omega/2)\cos\vartheta)$. Inverting this gives axis-angles in terms of Euler angles.

$$\varphi=(\alpha-\gamma+\pi)/2, \qquad \vartheta=\tan^{-1}[\tan\beta/2/\sin(\alpha+\gamma)/2], \qquad \Theta=2\cos^{-1}[\cos\beta/2\cos(\alpha+\gamma)/2]. \quad (6.6.5c)$$

It is important to recall the practical difference between Euler angles ($\alpha\beta\gamma$) and axis angles $[\varphi,\vartheta,\Theta]$. Euler angles ($\alpha\beta\gamma$) are coordinates of rotated <u>states</u> of *position* while axis-angles $[\varphi,\vartheta,\Theta]$ are parameters of rotation <u>operators</u> or angular *velocity*. Euler angles ($\alpha\beta\gamma$) serve as convenient polar coordinates of spin vectors **S** (Recall Fig. 4.4.5) and for orbiting or spinning bodies as shown below. Axis angles $[\varphi,\vartheta,\Theta]$ are the polar coordinates and rotation angle of a crank-axis Ω for an operation. Euler angels ($\alpha\beta\gamma$) tell where **S** *is* while axis angles $[\varphi,\vartheta,\Omega]$ tells whence it came and where it's *going*.

A note of caution is in order with respect to exponential operator notation. Axis angle operations were given in (4.4.15) using a single exponential-of-a-sum expression.

$$\mathbf{R[\blacklozenge]} = e^{-i\blacklozenge\bullet\mathbf{S}} = e^{-i(\Theta_X\mathbf{S}_X+\Theta_Y\mathbf{S}_Y+\Theta_Z\mathbf{S}_Z)} = e^{-i\Theta(\hat\Theta_X\mathbf{S}_X+\hat\Theta_Y\mathbf{S}_Y+\hat\Theta_Z\mathbf{S}_Z)} \qquad\qquad (6.6.5d)$$

Euler angle operation (6.6.1) is a <u>product</u> of three <u>separate</u> single exponentials.

$$\mathbf{R}(\alpha\beta\gamma) = e^{-i\alpha\mathbf{S}_Z}e^{-i\beta\mathbf{S}_Y}e^{-i\gamma\mathbf{S}_Z} \qquad\qquad (6.6.5e)$$

Unless operators **A** and **B** commute, $e^{i\mathbf{A}}e^{i\mathbf{B}}$ is not $e^{i(\mathbf{A}+\mathbf{B})}$. In rare cases (such as here!) where two operators commute with their commutator you can write

$$e^{\mathbf{A}}e^{\mathbf{B}}e^{-[\mathbf{A},\mathbf{B}]} = e^{(\mathbf{A}+\mathbf{B})} = e^{\mathbf{B}}e^{\mathbf{A}}e^{[\mathbf{A},\mathbf{B}]} \ \text{ if: } [\mathbf{A},[\mathbf{A},\mathbf{B}]]=0=[\mathbf{A},[\mathbf{A},\mathbf{B}]]$$

This is the first part of what is known as the *Baker-Campbell-Hausdorf theorem*.

1. Double valued axis angle rotation

Fig. 6.6.5 follows an entire *720°* or 4π rotation that connects the two positions shown in Fig. 6.6.2. First relations (6.6.5a) find the axis angles $[\varphi$=*80°*, ϑ=*34°*, Θ=*129°*] for the initial Euler position state (α=*50°*, β=*60°*, γ=*70°*) in Fig. 6.6.2(b) and Fig. 6.6.3.

$$\mathbf{R}(\alpha=50°,\beta=60°,\gamma=70°)\ |000\rangle = \mathbf{R}[\varphi=80°,\vartheta=34°,\Theta=129°]\ |000\rangle \qquad\qquad (6.6.6a)$$

It starts from a "1st" origin state in Fig. 6.6.5(a). (Note figure notation: ϕ=φ, θ=ϑ, ω=Θ)

$$|000\rangle = |\varphi-\pi/2, 0, \pi/2-\varphi\rangle = |\alpha=-10°,\beta=0°,\gamma=10°\rangle = \mathbf{R}[\varphi,\vartheta,\Theta=0°]\ |000\rangle \qquad (6.6.6b)$$

A 2π rotation (a-g) by Θ=ω = *360°* gives the "2nd" origin state in Fig. 6.6.5(g).

$$\mathbf{R}[\varphi=80°,\vartheta=34°,\Theta=360°]\ |000\rangle = |\alpha=170°,\beta=0°,\gamma=190°\rangle \qquad\qquad (6.6.6c)$$
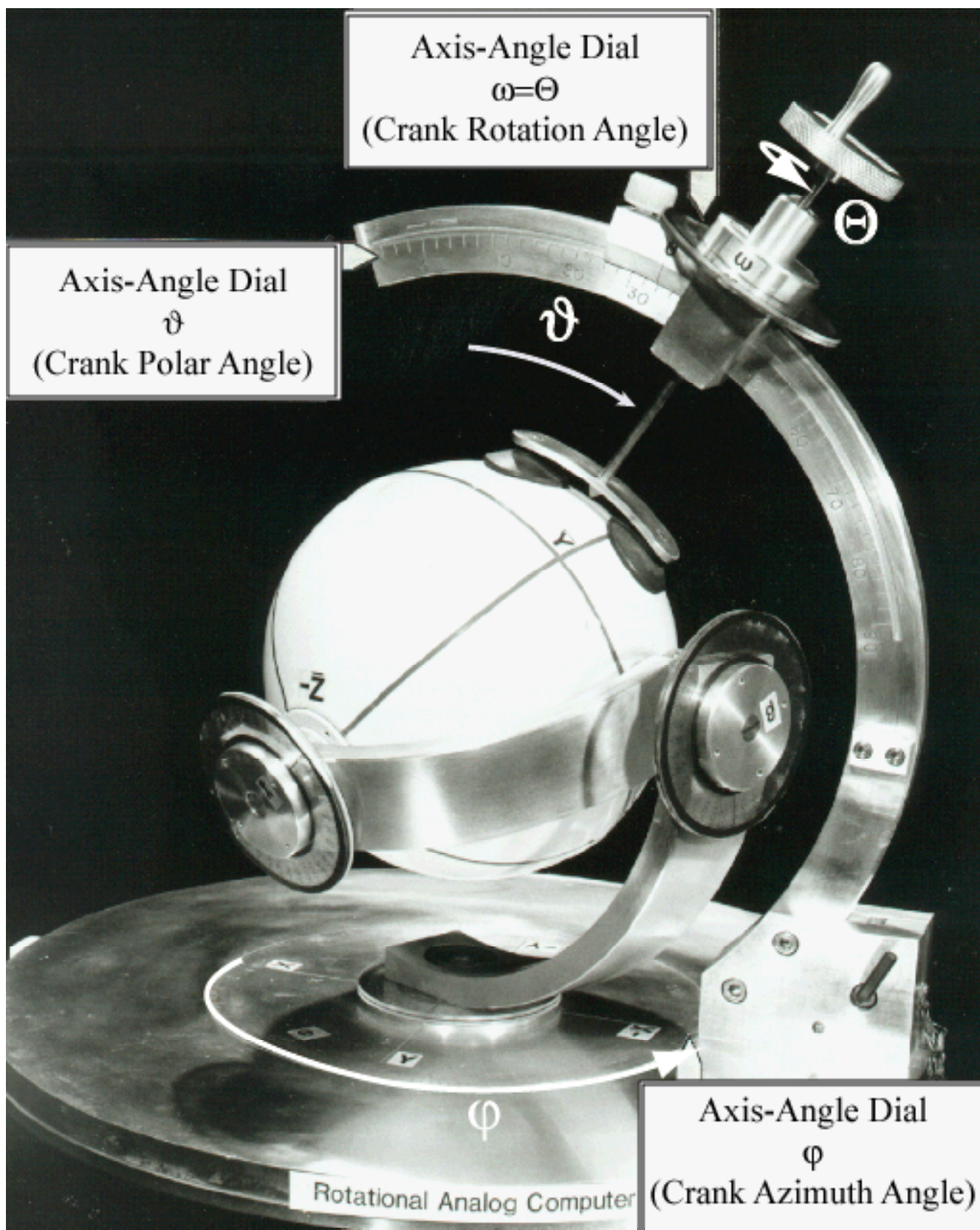
Fig. 6.6.4 Mechanical crank axis angles [φ,ϑ,Θ] operating on sphere having Euler angles (α,β,γ)

Fig. 6.6.5 Rotational 4π sequence 1st Row: (a) First origin state ω=Θ=0, (b-f) First position states.
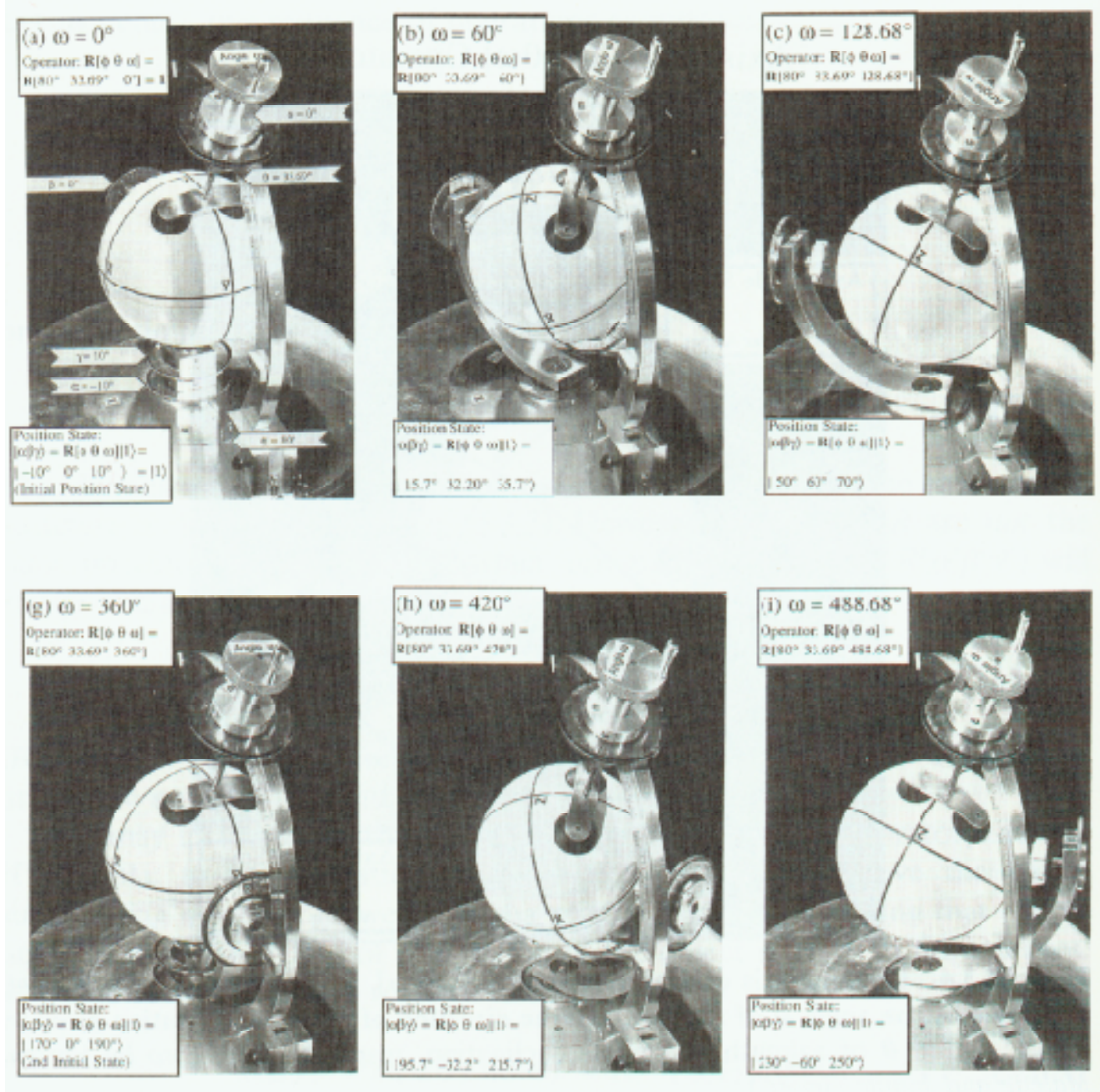
Fig. 6.6.5 Rotation 2nd Row: (g) 2nd origin state ω=Θ=2π, (h-l) 2nd position states (negative-β).

The ball "looks" the same in the 2nd initial state of Fig. 6.6.5(i) or Fig. 6.6.2(b) as in the 1st.

$$\mathbf{R}[\varphi=80°, \vartheta=34°, \Theta=489°]\,|000\rangle = |\alpha=230°, \beta=-60°, \gamma=250°\rangle \qquad (6.6.6d)$$

However, "looks" by classical eyes are deceiving. In fact, the αγ-Euler angles and the goniometer x′-frame for each "2nd" position in figures 6.6.5(g-l) are π-flipped from those above them in figures 6.6.5(a-f). Also, β is negative. Another "full" 2π rotation (either way) is needed to finish a full-U(2) rotation of *0-modulo-4π* and return the apparatus to its first initial position in Fig. 6.6.5(c).

First position states have positive-β >0.
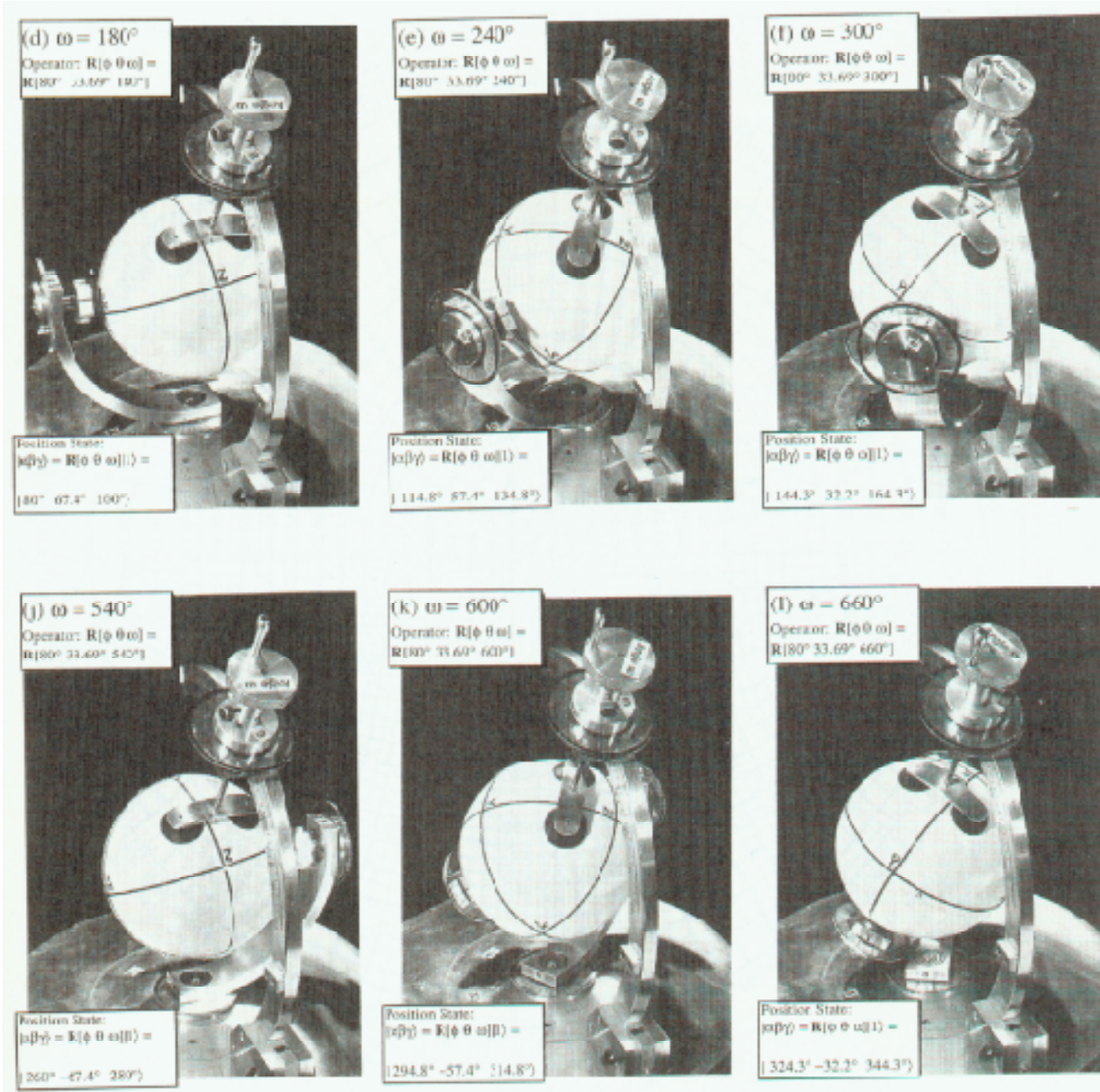
2nd position states have negative-β <0.

There is a double-valued nature of the 3D-space we occupy. It has been noted repeatedly in Unit 4 comparisons of the real 3-D *R(3)* spin-*vector* world *versus* the complex 2-D *U(2) spinor* world in Fig. 4.4.5. Photon polarization spin-vector **S** goes twice (4π) around *R(3)* space while polarization **E**-vector or Ψ-spinor goes just once around *U(2)* space in Fig. 4.4.6. Also, spinor reflections only need half the angle of the rotations they accomplish. They also provide a more elegant formula and graphical "slide-rule" for rotation group products. As we show now, it's all "done with mirrors!"

2. Mirror reflections and Hamilton's turns

In Section 4.4 we noted that *mirror reflection* operations are more fundamental than rotations and are done by real Pauli matrices such as σ_X and σ_Z or their combination σ_ϕ below.

$$\sigma_X = \begin{pmatrix} 0 & 1 \\ 1 & 0 \end{pmatrix} \;,\; \sigma_Z = \begin{pmatrix} 1 & 0 \\ 0 & -1 \end{pmatrix} \;,\; \sigma_\phi = \begin{pmatrix} \cos\phi & \sin\phi \\ \sin\phi & -\cos\phi \end{pmatrix} = \sigma_X \cos\phi + \sigma_Z \sin\phi \;,$$

Action of σ_ϕ displayed in Fig. 6.6.6 reflects through a plane tilted at half-angle $\phi/2$ to the *x*-axis. The product $\sigma_\phi\sigma_X$ is a rotation $\mathbf{R}[\phi]$ by angle ϕ, while $\sigma_X\sigma_\phi$ is the opposite rotation $\mathbf{R}[-\phi]$ by $(-\phi)$.

$$\sigma_\phi\sigma_X = \begin{pmatrix} \cos\phi & \sin\phi \\ \sin\phi & -\cos\phi \end{pmatrix}\begin{pmatrix} 1 & 0 \\ 0 & -1 \end{pmatrix}, \qquad \sigma_X\sigma_\phi = \begin{pmatrix} 1 & 0 \\ 0 & -1 \end{pmatrix}\begin{pmatrix} \cos\phi & \sin\phi \\ \sin\phi & -\cos\phi \end{pmatrix}$$

$$= \begin{pmatrix} \cos\phi & -\sin\phi \\ \sin\phi & \cos\phi \end{pmatrix} = R[\phi] \;, \qquad = \begin{pmatrix} \cos\phi & \sin\phi \\ -\sin\phi & \cos\phi \end{pmatrix} = R[-\phi]$$

(6.6.7)
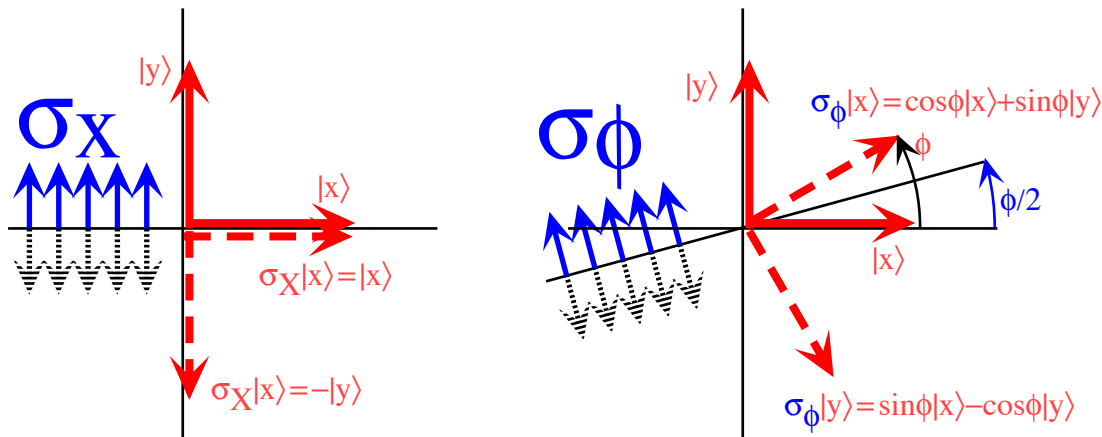
Fig. 6.6.6 Mirror reflections σ_X through xz-plane and σ_ϕ through rotated plane.

Hamilton saw this as a neat way to visualize three-dimensional rotations. Simply install two mirrors so they intersect on a Θ crank vector with half-angle $\Theta/2$ between the first and the second as shown in Fig. 6.6.7. It is like a clothing store mirror which lets you rotate an image of yourself by Θ as you adjust the angle $\Theta/2$ between mirrors. A unit normal vector $\mathbf{N_1}$ and $\mathbf{N_2}$ is constructed from each mirror plane and a $\Theta/2$ arc-vector drawn between the first and second plane normals. This arc is called *Hamilton's turn* vector $(\mathbf{N_1}{\rightarrow}\mathbf{N_2})$. It is these Hamilton turns that can be "added" like vectors to give *U(2)* group products!

Notice that only the <u>relative</u> angle $\Theta/2$ or $\pi-\Theta/2$ between mirrors is important in defining rotation $\mathbf{R}[\Theta]$; their absolute position is irrelevant. You can swivel the two mirrors anywhere around the Θ-axis. The trick to making products is to swivel the Hamilton turn arc $\mathbf{N_1}{\rightarrow}\mathbf{N_2}$ for the first rotation $\mathbf{R}[\Theta]$ around so it meets head-to-tail with the Hamilton turn arc $\mathbf{N'_1}{\rightarrow}\mathbf{N'_2}$ of the second rotation as $\mathbf{R}[\Theta']$ as shown in Fig. 6.6.8. Then the two mirrors associated with $\mathbf{N_2}$ and $\mathbf{N'_1}$ lie on top of each other and cancel since two reflections by the same mirror is *no reflection*. That leaves only the first mirror $(\mathbf{N_1})$ and the last $(\mathbf{N'_2})$, and the resultant Hamilton-turn arc $\mathbf{N_1}{\rightarrow}\mathbf{N'_2}$ is the arc of the desired product $\mathbf{R}[\Theta'']=\mathbf{R}[\Theta']\mathbf{R}[\Theta]$.
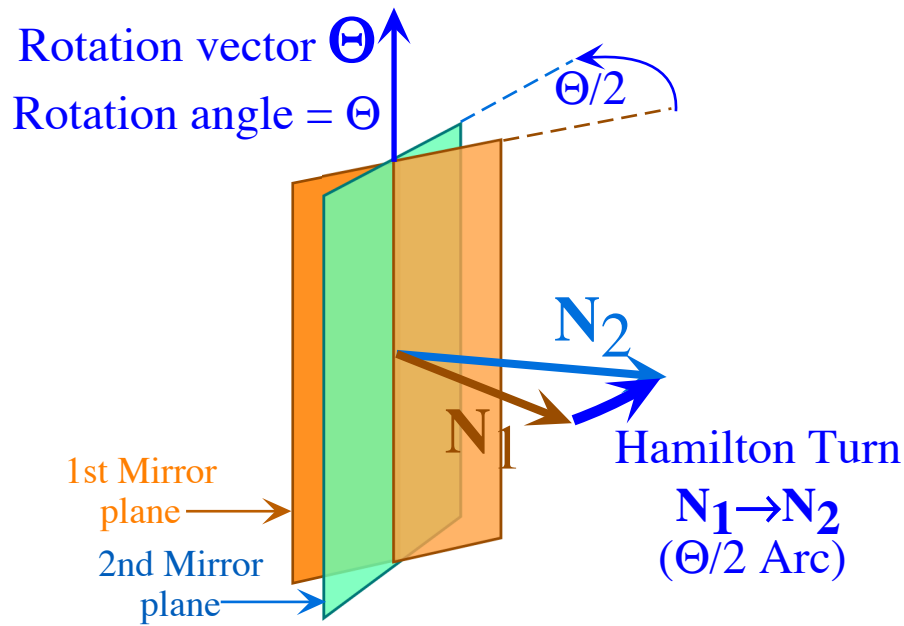
Fig. 6.6.7 Mirror reflection planes, normals, and Hamilton-turn arc vector.
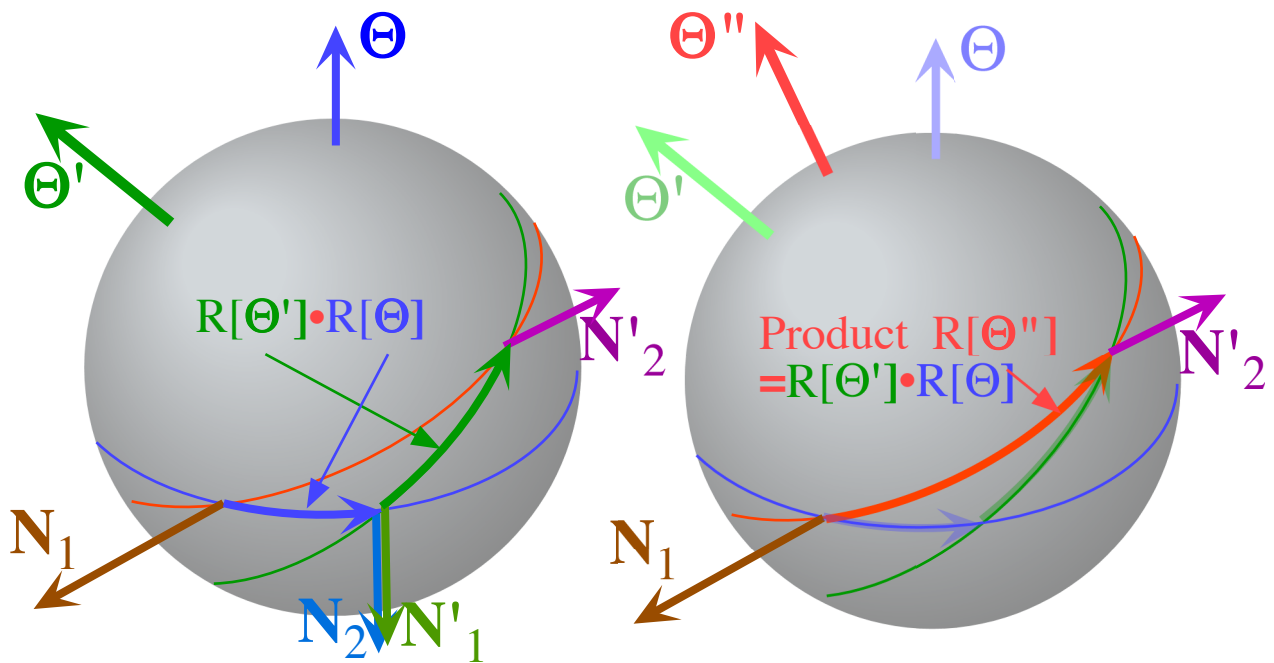
Fig. 6.6.8 Adding Hamilton-turn arcs to compute a U(2) product $\mathbf{R}[\Theta''] = \mathbf{R}[\Theta']\mathbf{R}[\Theta]$.

It is important to note that all Hamilton-turn arcs lie on *great* or *equatorial* circles and slide along the equatorial circles of the rotation axis vector Θ of the rotation $\mathbf{R}[\Theta]$.

   Also, note that each Hamilton arc $\Theta/2$, $\Theta'/2$, or $\Theta''/2$ is half of the actual angle Θ, Θ', or Θ'' of rotation $\mathbf{R}[\Theta]$, $\mathbf{R}[\Theta']$, or $\mathbf{R}[\Theta'']$, respectively. That means that an arc $\Theta/2$ between $\mathbf{N_1}$ and $\mathbf{N_2}$ and its supplement angles ($\Theta \pm 2\pi)/2 = \Theta/2 \pm \pi$ between $\mathbf{N_1}$ and $-\mathbf{N_2}$ represent the same classical rotation by Θ. For classical objects, a rotation by $\Theta \pm 2\pi$ is the same as one by Θ. However, for a quantum spin-1/2 object, the arc pointing from $\mathbf{N_1}$ to the antipodal

normal -N_2 represents a Θ-rotation with an extra π-phase factor $e^{\pm i\pi} = -1$, that is, -$R[\Theta]$. Recall rotation by 2π of the *U(2)* polarization state in Fig. 4.4.6 always comes up the same state, but it's π-out of phase. Hamilton's turns account for this.

3. Similarity transformation and Hamilton's turns

Finally, the Hamilton-turn "vector addition" on a sphere gives different results if the vectors are added in the reverse order to give $R[\Theta''']=R[\Theta]R[\Theta']$ instead of $R[\Theta'']=R[\Theta']R[\Theta]$. The arc-diagram for this forms a spherical parallelogram as shown in Fig. 6.6.9. It also shows the effect of a similarity transformation of rotation R [Θ''] by rotation $R[\Theta]$ to give rotation $R[\Theta''']$.

$$R[\Theta]\ R[\Theta'']\ R[-\Theta] = R[\Theta''']\quad (6.6.8a)\qquad\qquad R[-\Theta]\ R[\Theta''']\ R[\Theta] = R[\Theta'']\quad (6.6.8b)$$

As in (6.6.4), a rotation $R[\Theta]$ of a rotation $R[\Theta'']$ is just that; everything associated with the rotation $R[\Theta'']$ gets rotated by the full angle Θ around axis Θ. This includes its crank vector Θ'' and now its Hamilton-turn arc that in Fig. 6.6.9 gets moved by exactly two $R[\Theta]$ Hamilton-turn arcs into path of the $R[\Theta''']$ turn arc below it, that is, two $R[\Theta]$ Hamilton-turn $\Theta/2$ arcs amount to one whole angle Θ. Fig. 6.6.9 shows similarity transformation of rotation $R[\Theta''']$ by rotation $R[\Theta']$ to gives $R[\Theta'']$.

$$R[\Theta']\ R[\Theta''']\ R[-\Theta'] = R[\Theta'']\qquad\qquad\qquad\qquad (6.6.8c)$$

An infinite number of rotations transform $R[\Theta'']$ into $R[\Theta''']$ but just one crank direction has a smallest and largest angles Θ and $2\pi-\Theta$. You should locate this crank and Hamilton-turn on Fig. 6.6.9. (The four crank vectors Θ, Θ', Θ'', and Θ''' also define a spherical parallelogram below.)
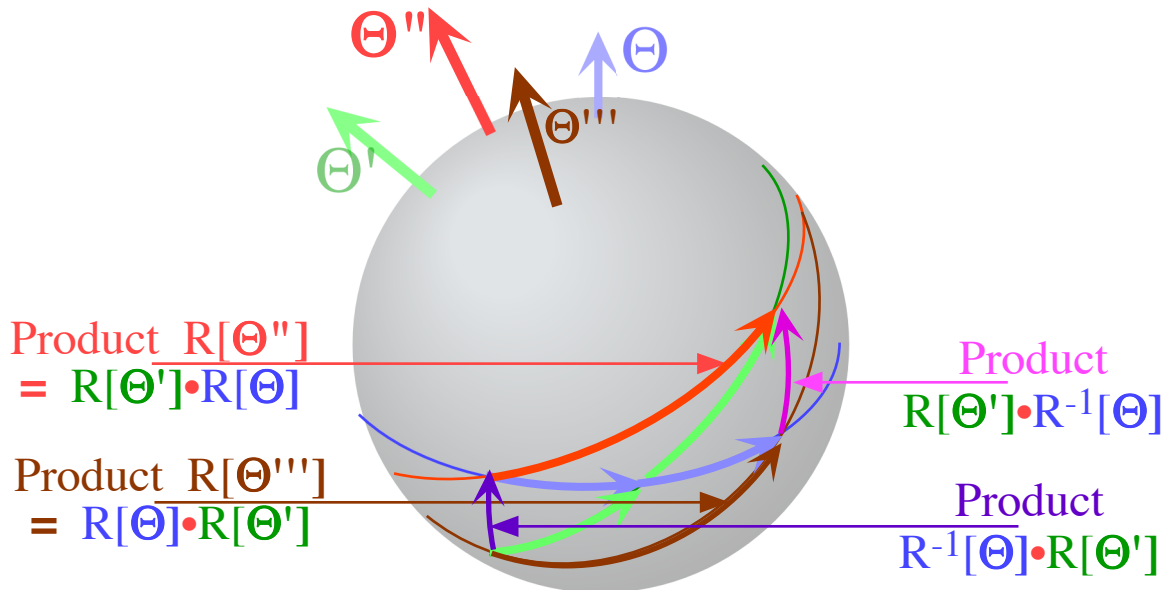
Fig. 6.6.9 Hamilton-turn arc parallelogram with $R[\Theta'']=R[\Theta']R[\Theta]$ and $R[\Theta''']=R[\Theta]R[\Theta']$

The geometry of minimal or *geodesic* transformations is important for classical and quantum dynamics as will be shown in Unit 7.

4. Combining rotations: U(2) group products

The product of $\mathbf{R}[\Theta']\,\mathbf{R}[\Theta]$ of any two rotations is another rotation operator $\mathbf{R}[\Theta'']$ which can be computed using Hamilton's axis-angle expansion (4.4.15) as follows.

$$\mathbf{R}[\Theta']\mathbf{R}[\Theta] = \left(\cos\frac{\Theta'}{2}\,\mathbf{1} - i\sin\frac{\Theta'}{2}\,\hat{\Theta}'\bullet\boldsymbol{\sigma}\right)\left(\cos\frac{\Theta}{2}\,\mathbf{1} - i\sin\frac{\Theta}{2}\,\hat{\Theta}\bullet\boldsymbol{\sigma}\right)$$

$$= \cos\frac{\Theta'}{2}\cos\frac{\Theta}{2}\,\mathbf{1} - i\left[\cos\frac{\Theta'}{2}\sin\frac{\Theta}{2}\,\hat{\Theta} + \cos\frac{\Theta}{2}\sin\frac{\Theta'}{2}\,\hat{\Theta}'\right]\bullet\boldsymbol{\sigma} - \sin\frac{\Theta'}{2}\sin\frac{\Theta}{2}\left(\hat{\Theta}'\bullet\boldsymbol{\sigma}\right)\left(\hat{\Theta}\bullet\boldsymbol{\sigma}\right) \qquad (6.6.9)$$

The Hamilton-Jordan-Pauli identity (4.4.12) is used to reduce $(\Theta'\bullet\sigma)(\Theta\bullet\sigma)$.

$$\mathbf{R}[\Theta']\mathbf{R}[\Theta] = \left(\cos\frac{\Theta''}{2}\right)\mathbf{1} - i\left[\sin\frac{\Theta''}{2}\,\hat{\Theta}''\right]\bullet\boldsymbol{\sigma} = \mathbf{R}[\Theta'']$$

$$= \left(\cos\frac{\Theta'}{2}\cos\frac{\Theta}{2}\right)\mathbf{1} - i\left[\cos\frac{\Theta'}{2}\sin\frac{\Theta}{2}\,\hat{\Theta} + \cos\frac{\Theta}{2}\sin\frac{\Theta'}{2}\,\hat{\Theta}' + \sin\frac{\Theta'}{2}\sin\frac{\Theta}{2}\,\hat{\Theta}'\times\hat{\Theta}\right]\bullet\boldsymbol{\sigma} \qquad (6.6.10\ a)$$

It is straightforward to solve for the new product angle Θ'' and axis Θ'' .

$$\left(\cos\frac{\Theta''}{2}\right) = \left(\cos\frac{\Theta'}{2}\cos\frac{\Theta}{2}\right)$$

$$\left[\sin\frac{\Theta''}{2}\,\hat{\Theta}''\right] = \left[\cos\frac{\Theta'}{2}\sin\frac{\Theta}{2}\,\hat{\Theta} + \cos\frac{\Theta}{2}\sin\frac{\Theta'}{2}\,\hat{\Theta}' + \sin\frac{\Theta'}{2}\sin\frac{\Theta}{2}\,\hat{\Theta}'\times\hat{\Theta}\right] \qquad (6.6.10\ b)$$

This is the *U(2) group product* formula that in Fig. 6.6.7 is done with mirrors!.

5. Similarity transformation of rotation axes

Euler's factoring (6.6.1) of axis-angle expression (4.4.15) is not unique. Rotation $\mathbf{R}[\varphi,\vartheta,\Theta]$ by Θ about axis Θ of polar angle (φ,ϑ) is a similarity transformation $\mathbf{T}$ of Z-axis-twist rotation $e^{-i\Theta S_Z}$.

$$\mathbf{R}[\varphi,\vartheta,\Theta] = \mathbf{T}\,e^{-i\Theta S_Z}\,\mathbf{T}^\dagger \qquad (6.6.11a)$$

The desired transformation $\mathbf{T}$ is just the Euler operation $\mathbf{R}(\varphi\vartheta 0)$ such as was diagrammed in Fig. 6.6.1, only one omits the twist γ since it just cancels out. Effectively, we take the Θ-axis from polar-angle $[\varphi,\vartheta]$ to the Z-axis with an inverse Euler-op $\mathbf{T}^\dagger = \mathbf{R}^\dagger(\varphi\vartheta 0)$, then do the Z-twist $e^{-i\Theta S_Z}$, and finally, return the axis to its original (φ,ϑ)-position with the Euler rotation (*sans* twist) $\mathbf{T}=\mathbf{R}(\varphi\vartheta 0)$.

$$\mathbf{R}[\varphi,\vartheta,\Theta] = \mathbf{R}(\varphi\vartheta 0)\,e^{-i\Theta S_Z}\,\mathbf{R}^\dagger(\varphi\vartheta 0) = \mathbf{R}(\varphi\vartheta 0)\,\mathbf{R}(00\Theta)\,\mathbf{R}^\dagger(\varphi\vartheta 0) \qquad (6.6.11b)$$

Euler rotations are given by (6.6.1). (Note: $\mathbf{R}^\dagger(0\vartheta 0) = \mathbf{R}(0-\vartheta 0)$ and $\mathbf{R}^\dagger S^\dagger = (S R)^\dagger$)

$$\mathbf{R}[\varphi,\vartheta,\Theta] = \mathbf{R}(\varphi 00)\,\mathbf{R}(0\vartheta 0)\,\mathbf{R}(00\Theta)\,\mathbf{R}(0-\vartheta 0)\,\mathbf{R}(-\varphi 00) \qquad (6.6.11c)$$

$$\mathbf{R}[\varphi,\vartheta,\Theta] = e^{-i\varphi S_Z}\ e^{-i\vartheta S_Y}\,e^{-i\Theta S_Z}\ e^{+i\vartheta S_Y}\ e^{+i\varphi S_Z} \qquad (6.6.11d)$$

So axis-defined $\mathbf{R}[\varphi,\vartheta,\Theta]$ factors into <u>five</u> monomial exponentials instead of three factors found in the much simpler Euler rotation $\mathbf{R}(\alpha\beta\gamma)$ of (6.6.1). (Check that this gives the same 2-by-2 matrix in (4.4.15a).) Doing rotations with just Y and Z axes keeps complex matrix arithmetic to a minimum since often Z-axis rotations are diagonal and Y-rotations, if not diagonal, are generally real.

Now the application of σ-rules to the derivation of the expression for a general rotation $\mathbf{R}[\Theta]$ of an arbitrary unit 3-vector $\mathbf{e}_L$ or unit spinor σ_L is tricky. But, it's something that a physicist should do at least once! Therefore we leave the following results as exercises.

$$\mathbf{R}[\Theta] \cdot \boldsymbol{\sigma}_L \cdot \mathbf{R}[\Theta]^n = \left(\cos\frac{\Theta}{2}\, \mathbf{1} - i\sin\frac{\Theta}{2}\, \hat{\Theta}_K \boldsymbol{\sigma}_K \right) \cdot \boldsymbol{\sigma}_L \cdot \left(\cos\frac{\Theta}{2}\, \mathbf{1} + i\sin\frac{\Theta}{2}\, \hat{\Theta}_N \boldsymbol{\sigma}_N \right)$$

$$= \boldsymbol{\sigma}_L' = \boldsymbol{\sigma}_L \cos\Theta - \varepsilon_{LKM} \hat{\Theta}_K \boldsymbol{\sigma}_M \sin\Theta + \left(1 - \cos\Theta\right) \hat{\Theta}_L \left(\hat{\Theta}_N \boldsymbol{\sigma}_N \right)$$

$$(6.6.12)$$

You should also demonstrate that this is equivalent to the following 3-vector expression.

$$\overline{\mathbf{e}}_L = R \cdot \mathbf{e}_L = \mathbf{e}_L \cos\Theta - \varepsilon_{LKM} \hat{\Theta}_K \mathbf{e}_M \sin\Theta + \left(1 - \cos\Theta\right) \hat{\Theta}_L \left(\hat{\Theta}_N \mathbf{e}_N \right)$$

$$= \mathbf{e}_L \cos\Theta + \hat{\boldsymbol{\Theta}} \times \mathbf{e}_L \sin\Theta + \left(1 - \cos\Theta\right) \hat{\boldsymbol{\Theta}} \left(\hat{\boldsymbol{\Theta}} \bullet \mathbf{e}_L \right)$$

$$(6.6.13)$$

The 3-vector transformations are more complicated than the 2-spinor ones but are functions of whole angles Θ of rotation unlike *2*-space spinor operations that have half-angles $\Theta/2$ or square-root cosines $\cos\frac{\Theta}{2} = \sqrt{\frac{1+\cos\Theta}{2}}$. (Recall (4.4.14).) Direction-cosine rotation components $\mathbf{e}_M \bullet \overline{\mathbf{e}}_L$ are as follows.

$$\left\langle \mathbf{e}_M \middle| R \middle| \mathbf{e}_L \right\rangle = R_{ML} = \mathbf{e}_M \bullet \overline{\mathbf{e}}_L = \delta_{ML} \cos\Theta - \varepsilon_{LKM} \hat{\Theta}_K \sin\Theta + \left(1 - \cos\Theta\right) \hat{\Theta}_M \hat{\Theta}_L \quad (6.6.14)$$

Nine R_{LM} give a 3D Darboux rotation matrix $R[\Theta]=R[\varphi\vartheta\Theta]$ with axis angle parameters of *whirl angle* $\Theta=\omega t$ and the *unit whirl axis*: $(\hat{\Theta}_X, \hat{\Theta}_Y, \hat{\Theta}_Z) = (\cos\varphi\sin\vartheta, \sin\varphi\sin\vartheta, \cos\vartheta)$ in Fig. 6.6.10.

$$\begin{pmatrix} R_{XX} & R_{XY} & R_{XZ} \\ R_{YX} & R_{YY} & R_{YZ} \\ R_{ZX} & R_{ZY} & R_{ZZ} \end{pmatrix} = \begin{pmatrix} \mathbf{e}_X \bullet \overline{\mathbf{e}}_X & \mathbf{e}_X \bullet \overline{\mathbf{e}}_Y & \mathbf{e}_X \bullet \overline{\mathbf{e}}_Z \\ \mathbf{e}_Y \bullet \overline{\mathbf{e}}_X & \mathbf{e}_Y \bullet \overline{\mathbf{e}}_Y & \mathbf{e}_Y \bullet \overline{\mathbf{e}}_Z \\ \mathbf{e}_Z \bullet \overline{\mathbf{e}}_X & \mathbf{e}_Z \bullet \overline{\mathbf{e}}_Y & \mathbf{e}_Z \bullet \overline{\mathbf{e}}_Z \end{pmatrix} = \qquad (6.6.15)$$

$$\begin{pmatrix} \cos\Theta + \left(1-\cos\Theta\right)\hat{\Theta}_X^2 & \left(1-\cos\Theta\right)\hat{\Theta}_X\hat{\Theta}_Y - \hat{\Theta}_Z\sin\Theta & \left(1-\cos\Theta\right)\hat{\Theta}_X\hat{\Theta}_Z + \hat{\Theta}_Y\sin\Theta \\ \left(1-\cos\Theta\right)\hat{\Theta}_X\hat{\Theta}_Y + \hat{\Theta}_Z\sin\Theta & \cos\Theta + \left(1-\cos\Theta\right)\hat{\Theta}_Y^2 & \left(1-\cos\Theta\right)\hat{\Theta}_Y\hat{\Theta}_Z - \hat{\Theta}_X\sin\Theta \\ \left(1-\cos\Theta\right)\hat{\Theta}_X\hat{\Theta}_Z - \hat{\Theta}_Y\sin\Theta & \left(1-\cos\Theta\right)\hat{\Theta}_Y\hat{\Theta}_Z + \hat{\Theta}_X\sin\Theta & \cos\Theta + \left(1-\cos\Theta\right)\hat{\Theta}_Z^2 \end{pmatrix}$$

This should equal Euler's $R(\alpha\beta\gamma)$ in (6.6.1) or 3D rotation $\mathbf{R}[\varphi,\vartheta,\Theta]$ in (6.6.11) after Euler-to-axis angle conversions (6.6.5) relating 2D spinor rotation $\mathbf{R}[\varphi,\vartheta,\Theta]$ in (6.6.4) to $\mathbf{R}(\alpha\beta\gamma)$ in (6.6.3).

6. Geometry of spin precession

   Fig. 6.6.10 shows 3-views of a spin $\mathbf{S}_{\alpha\beta}$ vector (rotating) around a cone centered on a unit whirl axis $\hat{\boldsymbol{\Omega}} = \hat{\boldsymbol{\Theta}} = [\hat{\Omega}_A, \hat{\Omega}_B, \hat{\Omega}_C] = [\hat{\Omega}_Z, \hat{\Omega}_X, \hat{\Omega}_Y] = [\cos\vartheta,\ \cos\varphi\sin\vartheta,\ \sin\varphi\sin\vartheta]$. It is like Fig. 4.4.2 but Ω has zero azimuth $\varphi=0$ so $\hat{\Omega}$ lies in the *AB* -plane $\hat{\boldsymbol{\Omega}} = [\hat{\Omega}_A, \hat{\Omega}_B, 0] = [\cos\vartheta, \sin\vartheta, 0]$. The initial spin state $\left| \uparrow_A \right\rangle = \binom{1}{0}$ *(up-A)* has spin vector $[S_A, S_B, S_C] = S[1,0,0]$ pointing up-*A*-axis at $(\alpha=0, \beta=0)$. Then $\mathbf{S}_{00}$ rotates around $\hat{\boldsymbol{\Omega}}$ by angle $\Theta = \Omega \cdot t$ at angular rate Ω to become $\mathbf{S}_{\alpha\beta} = [S_A, S_B, S_C] = S[\cos\beta, \cos\alpha\sin\beta, \sin\alpha\sin\beta]$. Here we use the $\{A,B,C\}$ polarization symmetry labels *Asymmetry, Balance, Circulation* to denote, respectively, Cartesian $\{Z,X,Y\}$ components of spin state as defined by (4.4.16) and operator $\mathsf{R}=e^{-\mathsf{i}\mathsf{H}t}$ as defined by (4.4.18) in Sec. 4.4.

   Note that the crank $\boldsymbol{\Omega}$ swings spin $\mathbf{S}$ to a maximum polar angle $\beta = 2\vartheta$ that is twice the polar angle ϑ of crank $\boldsymbol{\Omega}$ as measured from *A*-axis where the spin was initially. Rotation angle $\Theta=\Omega\cdot t$ is π as it passes through the

AB –plane that it also contains $\hat{\Omega}$ and the spin vector $\mathbf{S}_{00}$ at *t=0*. Then spin $\mathbf{S}_{\alpha\beta(t=\pi/\Omega)}$ is at its lowest and most distant position relative to the *A*-axis.

Let us compare the $[S_A, S_B, S_C] = [S_Z, S_X, S_Y]$ component geometry of vector $\mathbf{S}_{\alpha\beta}$ in Fig. 6.6.10 with the *Z*-column vector of matrix (6.6.15) for a crank with $\varphi=0$ or $[\hat{\Theta}_Z, \hat{\Theta}_X, \hat{\Theta}_Y] = [\cos\vartheta, \sin\vartheta, 0] = [\hat{\Theta}_A, \hat{\Theta}_B, \hat{\Theta}_C]$.

The *A*-altitude of the spin vector is given by trigonometry of Fig. 6.6.10 views (a), (b) or (c).

$$S_A = S_Z = S\cos\beta = S\frac{1+\cos\Theta}{2} + S\frac{1-\cos\Theta}{2}\cos 2\vartheta = S(\cos^2\vartheta + \sin^2\vartheta\cos\Theta) = S(\cos\Theta + (1-\cos\Theta)\cos^2\vartheta)$$

$$= S(1 - 2\sin^2\vartheta\sin^2\frac{\Omega\cdot t}{2}) \quad where: \quad \Theta = \Omega\cdot t \tag{6.6.16a}$$

Its minimum value is $S\cos 2\vartheta$ as we should expect from the doubling of the cone half-angle. The range of motion of expectation value S_A is the altitude $2S\sin^2\vartheta$ of a right triangle shown by (c) view (top left).

As the *A*-component of spin oscillates so does the *B*-component and the *C*-component, each with different time dependence. Looking straight down the Ω -crank axis shows uniform circular motion in the upper left hand part (d) of Fig. 6.6.10. With *C*-axis normal to Ω ($\varphi=0$), the *C*-component oscillation is along cone base radius $S\sin\vartheta$ projected onto the *C*-axis times $-\sin\Omega\cdot t$ as shown by view (a) or (b).

$$S_C = S_Y = S\sin\alpha\sin\beta = -S\sin\vartheta\sin\Omega\cdot t \tag{6.6.16c}$$

The minus sign is due to the counter-clockwise rotation that first goes toward the negative *C*-axis.

The *B*-component oscillates along a $\cos\vartheta$ projection of the cone base diameter $S\sin\vartheta$.

$$S_B = S_X = S\cos\alpha\sin\beta = S\sin\vartheta\cos\vartheta(1-\cos\Theta) = S\sin 2\vartheta\sin^2\frac{\Omega\cdot t}{2} \tag{6.6.16b}$$

The range of expectation value S_B is the base $S\sin 2\vartheta = 2S\sin\vartheta\cos\vartheta$ of the right triangle in the (c) view.

Each of these values is consistent with the *Z*-column of (6.6.15). For these, the crank azimuth φ is not zero as it is in Fig. 6.6.10. To rectify this situation, it is only necessary to rotate the *B*-component and *C*-component by that azimuth angle φ using a matrix for φ -rotation around the *A*-axis.

$$\begin{pmatrix} S_B \\ S_C \end{pmatrix} = \begin{pmatrix} S_X \\ S_Y \end{pmatrix} = S\begin{pmatrix} \sin\beta\cos\alpha \\ \sin\beta\sin\alpha \end{pmatrix} = S\sin\vartheta\begin{bmatrix} \cos\varphi & -\sin\varphi \\ \sin\varphi & \cos\varphi \end{bmatrix}\begin{pmatrix} \cos\vartheta(1-\cos\Theta) \\ \sin\Omega\cdot t \end{pmatrix} = S\begin{bmatrix} \cos\varphi & -\sin\varphi \\ \sin\varphi & \cos\varphi \end{bmatrix}\begin{pmatrix} \sin 2\vartheta\sin^2\frac{\Omega\cdot t}{2} \\ -\sin\vartheta\sin\Omega\cdot t \end{pmatrix}$$

The *A*-altitude S_A is independent of the azimuth angle φ. Of the three expectation values, only S_A is guaranteed to be *100% certain* value +S *("up")* and then only at *certain times* $t = 0, 2\pi/\Omega, 4\pi/\Omega, ...$. Other values are *averages* of quantum *up*-and-*down* values $+S=+\frac{\hbar}{2}$ or $-S=-\frac{\hbar}{2}$ allowed inside any *B* or *C* analyzer. The values (6.6.16) vary with time unless $\vec{s}$ and $\hat{\Omega}$ coincide. ($\vartheta = 0$ here.)

If we increase crank polar angle to a "magic angle" $\vartheta_{magic} = \cos^{-1} 3^{-1/2} \cong 54.7°$ and azimuth to $\varphi=\pi/4$ as in Fig. 4.4.2, then each analyzer *A*, *B*, and *C* will experience, in turn, a *moment of certainty* when they are *sure* to find the spin "up" in their direction. (Verify this.)
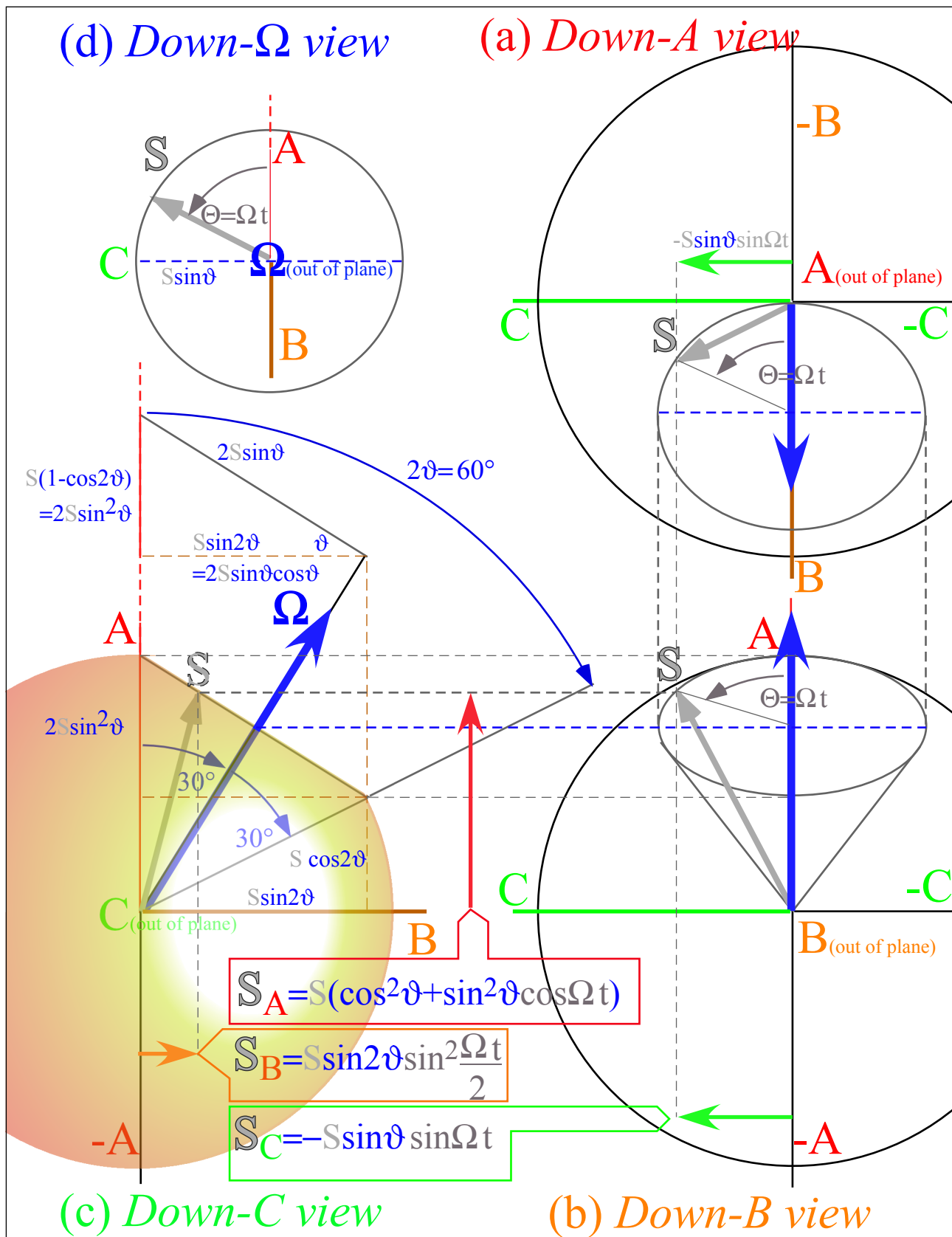
Fig. 6.6.10 Geometry of 3D rotation R[φ=0,ϑ,Θ]by Θ=Ωt of S vector initially on Z=A axis

Chapter 6.7. Euler rotational kinematics and dynamics

The relations between the Darboux whirl-vector ω or Ω of angular velocity, the various LAB and BOD components $\{L_x, L_y, L_z\}_{(LAB)}$ and $\{L_{\bar{x}}, L_{\bar{y}}, L_{\bar{z}}\}_{(BOD)}$ of angular momentum, and the individual Euler angular velocities $\{\dot{\alpha}, \dot{\beta}, \dot{\gamma}\}$ are developed here using the Euler-Axis relations of Sec. 6.6.

a. Euler angular velocity relations

The Euler device in Fig. 6.6.3 can be viewed as four connected Merry-Go-Rounds consisting of the LAB-*x*-frame $\{x = x_1, y = x_2, z = x_3\}$ (presumably inertial, but not necessarily so) connected by bearing and dial α to the x′-frame $\{x' = x_1', y' = x_2', z' = x_3'\}$ connected by bearing and dial β to the x″-frame $\{x'' = x_1'', y'' = x_2'', z'' = x_3''\}$ holding bearing and dial γ for BOD $\bar{x}_3$ -frame $\{\bar{x} = \bar{x}_1, \bar{y} = \bar{x}_2, \bar{z} = \bar{x}_3\}$.

　　　Velocity as seen by each intermediate frame is added to its rotational velocity $\omega \times \mathbf{r}$ relative to a frame whose rotation axis ω supports it, so velocity $\dot{\mathbf{r}}'$ seen in x′-frame added to $\omega_\alpha \times \mathbf{r}$ is LAB$\dot{\mathbf{r}}^{LAB}$.

$$\dot{\mathbf{r}}^{LAB} = \dot{\mathbf{r}}' + \omega_\alpha \times \mathbf{r} \quad \text{where:} \qquad \omega_\alpha = \dot{\alpha}\mathbf{x}_3 = \dot{\alpha}(-\sin\beta\cos\gamma\,\bar{\mathbf{x}}_1 + \sin\beta\sin\gamma\,\bar{\mathbf{x}}_2 + \cos\beta\,\bar{\mathbf{x}}_3) \quad (6.7.1)$$

Rotation ω_α is about LAB z=x_3-axis whose BOD coordinates $\mathbf{x}_3\cdot\bar{\mathbf{x}}_k$ are the 3rd row of matrix (6.6.1b).

Then x′-frame dial β supports the x″-frame. Coordinates of ω_β appear in Fig. 6.6.3.

$$\dot{\mathbf{r}}' = \dot{\mathbf{r}}'' + \omega_\beta \times \mathbf{r} \qquad \text{where:} \qquad \omega_\beta = \dot{\beta}(-\sin\alpha\,\mathbf{x}_1 + \cos\alpha\,\mathbf{x}_2) = \dot{\beta}(\sin\gamma\,\bar{\mathbf{x}}_1 + \cos\gamma\,\bar{\mathbf{x}}_2) \qquad (6.7.2)$$

Then x″-frame dial γ has the $\bar{\mathbf{x}}_3$ -axis whose LAB coordinates $\bar{\mathbf{x}}_3\cdot\mathbf{x}_k$ are the 3rd column of (6.6.1b).

$$\dot{\mathbf{r}}'' = \dot{\bar{\mathbf{r}}}^{BOD} + \omega_\gamma \times \mathbf{r} \;\; \text{where:} \qquad \omega_\gamma = \dot{\gamma}(\sin\beta\cos\alpha\,\mathbf{x}_1 + \sin\beta\sin\alpha\,\mathbf{x}_2 + \cos\beta\,\mathbf{x}_3) = \dot{\gamma}\bar{\mathbf{x}}_3 \qquad (6.7.3)$$

The relations collapse into a single LAB-BOD relation by eliminating the "middle-men"$\dot{\mathbf{r}}'$ and $\dot{\mathbf{r}}''$.

$$\dot{\mathbf{r}}^{LAB} = \dot{\mathbf{r}}' + \omega_\alpha \times \mathbf{r} = \dot{\mathbf{r}}'' + \omega_\beta \times \mathbf{r} + \omega_\alpha \times \mathbf{r} = \dot{\bar{\mathbf{r}}}^{BOD} + \omega_\gamma \times \mathbf{r} + \omega_\beta \times \mathbf{r} + \omega_\alpha \times \mathbf{r} \qquad (6.7.4)$$

This repeats a Galilean-sum-rule of rotational relativity derived in (3.7.14) of Unit 3.

$$\dot{\mathbf{r}}^{LAB} = \dot{\bar{\mathbf{r}}}^{BOD} + (\omega_\gamma + \omega_\beta + \omega_\alpha) \times \mathbf{r} = \dot{\bar{\mathbf{r}}}^{BOD} + \omega \times \mathbf{r} \qquad (6.7.5a)$$

Angular velocity ω has LAB $\{\mathbf{x}_1, \mathbf{x}_2, \mathbf{x}_3\}$ or BOD $\{\bar{\mathbf{x}}_{\bar{1}}, \bar{\mathbf{x}}_{\bar{2}}, \bar{\mathbf{x}}_{\bar{3}}\}$ frame components ω_j or$\omega_{\bar{j}}$.

$$\omega = \omega_\gamma + \omega_\beta + \omega_\alpha = \omega_1\mathbf{x}_1 + \omega_2\mathbf{x}_2 + \omega_3\mathbf{x}_3 = \omega_{\bar{1}}\bar{\mathbf{x}}_{\bar{1}} + \omega_{\bar{2}}\bar{\mathbf{x}}_{\bar{2}} + \omega_{\bar{3}}\bar{\mathbf{x}}_{\bar{3}}$$

$$\omega = (-\dot{\beta}\sin\alpha + \dot{\gamma}\sin\beta\cos\alpha)\mathbf{x}_1 + (\dot{\beta}\cos\alpha + \dot{\gamma}\sin\beta\sin\alpha)\mathbf{x}_2 + (\dot{\alpha} + \dot{\gamma}\cos\beta)\mathbf{x}_3 \qquad (6.7.5b)$$

$$\omega = (+\dot{\beta}\sin\gamma - \dot{\alpha}\sin\beta\cos\gamma)\bar{\mathbf{x}}_1 + (\dot{\beta}\cos\gamma + \dot{\alpha}\sin\beta\sin\gamma)\bar{\mathbf{x}}_2 + (\dot{\gamma} + \dot{\alpha}\cos\beta)\bar{\mathbf{x}}_3$$

A LAB-BOD symmetry *(α to $-\gamma$, β to $-\beta$, γ to $-\alpha$)* is evident in these LAB and BOD Jacobian relations.

$$\begin{pmatrix} \omega_1 \\ \omega_2 \\ \omega_3 \end{pmatrix} = \begin{pmatrix} 0 & -\sin\alpha & \cos\alpha\sin\beta \\ 0 & \cos\alpha & \sin\alpha\sin\beta \\ 1 & 0 & \cos\beta \end{pmatrix} \begin{pmatrix} \dot{\alpha} \\ \dot{\beta} \\ \dot{\gamma} \end{pmatrix} (6.7.5c) \qquad \begin{pmatrix} \omega_{\bar{1}} \\ \omega_{\bar{2}} \\ \omega_{\bar{3}} \end{pmatrix} = \begin{pmatrix} -\sin\beta\cos\gamma & \sin\gamma & 0 \\ \sin\beta\sin\gamma & \cos\gamma & 0 \\ \cos\beta & 0 & 1 \end{pmatrix} \begin{pmatrix} \dot{\alpha} \\ \dot{\beta} \\ \dot{\gamma} \end{pmatrix} (6.7.5d)$$

Their inverses are LAB and BOD "Kajobians" below. Together they define rotational mechanics.

$$\begin{pmatrix} \dot{\alpha} \\ \dot{\beta} \\ \dot{\gamma} \end{pmatrix} = \begin{pmatrix} -\cos\alpha\cot\beta & -\sin\alpha\cot\beta & 1 \\ -\sin\alpha & \cos\alpha & 0 \\ \cos\alpha\csc\beta & \sin\alpha\csc\beta & 0 \end{pmatrix} \begin{pmatrix} \omega_1 \\ \omega_2 \\ \omega_3 \end{pmatrix} \quad (6.7.5e) \qquad \begin{pmatrix} \dot{\alpha} \\ \dot{\beta} \\ \dot{\gamma} \end{pmatrix} = \begin{pmatrix} -\cos\gamma\csc\beta & \sin\gamma\csc\beta & 0 \\ \sin\gamma & \cos\gamma & 0 \\ \cot\beta\cos\gamma & -\cot\beta\sin\gamma & 1 \end{pmatrix} \begin{pmatrix} \omega_{\bar{1}} \\ \omega_{\bar{2}} \\ \omega_{\bar{3}} \end{pmatrix} \quad (6.7.5f)$$

b. Euler angular momentum relations

The Euler velocity relations yield angular momentum in terms of a Lagrangian $L(\dot{\alpha},\dot{\beta},\dot{\gamma};\alpha,\beta,\gamma)$.

$$J_\alpha = \frac{\partial L}{\partial\dot{\alpha}} \ , \qquad J_\beta = \frac{\partial L}{\partial\dot{\beta}} \ , \qquad J_\gamma = \frac{\partial L}{\partial\dot{\gamma}} \ . \qquad (6.7.6)$$

This is consistent with fundamental definitions (1.12.10) in Unit 1, (2.4.1) in Unit 2, and (3.6.4) in Unit 3. J_μ are Euler's version of GCC momentum p_μ and $(\alpha\beta\gamma)$ are the angular GCC (q^1, q^2, q^3).

The Cartesian momentum components J_m or $J_{\bar{m}}$ go with angular velocity components $\omega_k = \dot{\Theta}_k$ or $\omega_{\bar{k}} = \dot{\Theta}_{\bar{k}}$ in (6.7.5) that refer to Cartesian frames LAB or BOD, respectively.

LAB: $\left(J_1 = \dfrac{\partial L}{\partial\omega_1}, \ J_2 = \dfrac{\partial L}{\partial\omega_2}, \ J_3 = \dfrac{\partial L}{\partial\omega_3} \right)$ (6.7.7a) $\qquad$ BOD: $\left(J_{\bar{1}} = \dfrac{\partial L}{\partial\omega_{\bar{1}}}, \ J_{\bar{2}} = \dfrac{\partial L}{\partial\omega_{\bar{2}}}, \ J_{\bar{3}} = \dfrac{\partial L}{\partial\omega_{\bar{3}}} \right)$ (6.7.7b)

Strangely, there are no *well-defined* Cartesian-coordinate LAB angles $(\Theta_1, \Theta_2, \Theta_3)$ or BOD angles $(\Theta_{\bar{1}}, \Theta_{\bar{2}}, \Theta_{\bar{3}})$ to go with angular velocities ω_k or $\omega_{\bar{k}}$. Only their derivatives are definable.

$$(\dot{\Theta}_1, \dot{\Theta}_2, \dot{\Theta}_3) = (\omega_1, \omega_2, \omega_3). \qquad (6.7.8a) \qquad\qquad (\dot{\Theta}_{\bar{1}}, \dot{\Theta}_{\bar{2}}, \dot{\Theta}_{\bar{3}}) = (\omega_{\bar{1}}, \omega_{\bar{2}}, \omega_{\bar{3}}). \qquad (6.7.8b)$$

The Θ_k-angles are *non-holonomic* or *non-integrable* coordinates as noted in regard to derivative constraints (3.9.25) in Unit 3. Differential $d\Theta_k = \omega_k dt$ or derivative $\dot{\Theta}_k$ is locally defined but integrals $\int d\Theta_k = \int \omega_k\, dt$ are path-dependent. Cartesian Θ_k angles cannot define global orientation as Euler $(\alpha\beta\gamma)$ do in Fig. 6.6.2.

Cartesian momentum J_m or $J_{\bar{m}}$ in (6.7.7) relate to Euler angles by Jacobian derivative chain-sums over Euler velocity $(\dot{\alpha},\dot{\beta},\dot{\gamma})$ but not angles (α,β,γ) since coordinates cannot be explicit functions of velocity ω_k or $\omega_{\bar{k}}$. So J_m or $J_{\bar{m}}$ in (6.7.9) use transposed and inverted velocity matrices (6.7.5) to give (6.7.10).

$$J_m = \frac{\partial L}{\partial\omega_m} = \frac{\partial L}{\partial\omega_m} = \frac{\partial L}{\partial\dot{\alpha}}\frac{\partial\dot{\alpha}}{\partial\omega_m} + \frac{\partial L}{\partial\dot{\beta}}\frac{\partial\dot{\beta}}{\partial\omega_m} + \frac{\partial L}{\partial\dot{\gamma}}\frac{\partial\dot{\gamma}}{\partial\omega_m} = J_\alpha\frac{\partial\dot{\alpha}}{\partial\omega_m} + J_\beta\frac{\partial\dot{\beta}}{\partial\omega_m} + J_\gamma\frac{\partial\dot{\gamma}}{\partial\omega_m} \quad (6.7.9a)$$

$$J_{\bar{k}} = \frac{\partial L}{\partial\omega_{\bar{k}}} = \frac{\partial L}{\partial\omega_{\bar{k}}} = \frac{\partial L}{\partial\dot{\alpha}}\frac{\partial\dot{\alpha}}{\partial\omega_{\bar{k}}} + \frac{\partial L}{\partial\dot{\beta}}\frac{\partial\dot{\beta}}{\partial\omega_{\bar{k}}} + \frac{\partial L}{\partial\dot{\gamma}}\frac{\partial\dot{\gamma}}{\partial\omega_{\bar{k}}} = J_\alpha\frac{\partial\dot{\alpha}}{\partial\omega_{\bar{k}}} + J_\beta\frac{\partial\dot{\beta}}{\partial\omega_{\bar{k}}} + J_\gamma\frac{\partial\dot{\gamma}}{\partial\omega_{\bar{k}}} \quad (6.7.9b)$$

Euler $\{J_\alpha, J_\beta, J_\gamma\}$-to-$\{J_m, J_{\bar{m}}\}$ matrices are transposed cartesian $\{\omega_m, \omega_{\bar{m}}\}$-to-$\{\dot{\alpha},\dot{\beta},\dot{\gamma}\}$ matrices (6.7.5e-f).

$$\begin{pmatrix} J_1 \\ J_2 \\ J_3 \end{pmatrix} = \begin{pmatrix} -\cos\alpha\cot\beta & -\sin\alpha & \cos\alpha\csc\beta \\ -\sin\alpha\cot\beta & \cos\alpha & \sin\alpha\csc\beta \\ 1 & 0 & 0 \end{pmatrix} \begin{pmatrix} J_\alpha \\ J_\beta \\ J_\gamma \end{pmatrix} \quad (6.7.10a) \qquad \begin{pmatrix} J_{\bar{1}} \\ J_{\bar{2}} \\ J_{\bar{3}} \end{pmatrix} = \begin{pmatrix} -\cos\gamma\csc\beta & \sin\gamma & \cot\beta\cos\gamma \\ \sin\gamma\csc\beta & \cos\gamma & -\cot\beta\sin\gamma \\ 0 & 0 & 1 \end{pmatrix} \begin{pmatrix} J_\alpha \\ J_\beta \\ J_\gamma \end{pmatrix} \quad (6.7.10b)$$

Momentum $\{J_m, J_{\bar{m}}\}$-to-$\{J_\alpha, J_\beta, J_\gamma\}$ matrices are transposed velocity $\{\dot{\alpha},\dot{\beta},\dot{\gamma}\}$-to-$\{\omega_m, \omega_{\bar{m}}\}$ matrices (6.7.5c-d).

$$\begin{pmatrix} J_\alpha \\ J_\beta \\ J_\gamma \end{pmatrix} = \begin{pmatrix} 0 & 0 & 1 \\ -\sin\alpha & \cos\alpha & 0 \\ \cos\alpha\sin\beta & \sin\alpha\sin\beta & \cos\beta \end{pmatrix} \begin{pmatrix} J_1 \\ J_2 \\ J_3 \end{pmatrix} \quad (6.7.10c) \qquad \begin{pmatrix} J_\alpha \\ J_\beta \\ J_\gamma \end{pmatrix} = \begin{pmatrix} -\sin\beta\cos\gamma & \sin\beta\sin\gamma & \cos\beta \\ \sin\gamma & \cos\gamma & 0 \\ 0 & 0 & 1 \end{pmatrix} \begin{pmatrix} J_{\bar{1}} \\ J_{\bar{2}} \\ J_{\bar{3}} \end{pmatrix} \quad (6.7.10d)$$

Since coordinates have *zero* velocity dependence, coordinate and velocity Jacobians are *identical*.

$$\text{\textit{Lemma 1}: } (\tfrac{\partial x^a}{\partial \dot{q}^m} \equiv 0 \equiv \tfrac{\partial q^n}{\partial \dot{x}^b}) \text{ \textit{implies}: } \tfrac{\partial \dot{x}^a}{\partial \dot{q}^m} \equiv \tfrac{\partial x^a}{\partial q^m} \text{ \textit{and}: } \tfrac{\partial \dot{q}^n}{\partial \dot{x}^b} \equiv \tfrac{\partial q^n}{\partial x^b} \qquad (3.5.4)_{repeated}$$

But, velocity *is* coordinate dependent for curved coordinates, that is, for analytic non-constant **J**.

$$\text{\textit{Lemma 2}: } (\tfrac{\partial^2 x^a}{\partial q^m \partial q^n} \equiv \tfrac{\partial^2 x^a}{\partial q^n \partial q^m}) \text{ \textit{implies}: } \tfrac{d}{dt}\tfrac{\partial x^a}{\partial q^m} \equiv \tfrac{\partial \dot{x}^a}{\partial q^m} \text{ \textit{and}: } \tfrac{d}{dt}\tfrac{\partial q^n}{\partial x^b} \equiv \tfrac{\partial \dot{q}^n}{\partial x^b} \qquad (3.5.6)_{repeated}$$

All this assumes a coordinate differential $dx^a = \dot{x}^a dt$ is velocity $\dot{x}^a$ times a time differential dt.

$$dx^a = \tfrac{\partial x^a}{\partial q^\mu} dq^\mu \text{ implies: } \tfrac{dx^a}{dt} \equiv \dot{x}^a = \tfrac{\partial x^a}{\partial q^\mu}\dot{q}^\mu \equiv \tfrac{dq^\mu}{dt}$$

c. Euler-Lagrange equations of motion

Lagrange definition of momentum p or J_m by *velocity* partial derivative $\tfrac{\partial L}{\partial \dot{q}^\mu} = p_\mu$ or $\tfrac{\partial L}{\partial \dot{\Theta}_m} = J_m$ and Lagrange

equation of force $F = \dot{p}$ or torque $\dot{J}_m$ by *coordinate* partial derivative $\tfrac{\partial L}{\partial q^\mu} = \dot{p}_\mu$ or $\tfrac{\partial L}{\partial \Theta_m} = \dot{J}_m$ are the same form in any

coordinate system or frame due to symmetry of Jacobian matrices $\mathbf{J}_m^{\bar{m}} = \tfrac{\partial x^{\bar{m}}}{\partial q^m}$.

LAB- momenta J_m transform to Euler $J_b = \{J_\alpha, J_\beta, J_\gamma\}$ in (6.7.10c) by Jacobian $\mathbf{J}_m^b = \tfrac{\partial \Theta_m}{\partial \beta_b}$ as in (6.7.11a).

Torques $\dot{J}_m$ and $\dot{J}_b = \{\dot{J}_\alpha, \dot{J}_\beta, \dot{J}_\gamma\}$ involve Jacobian time derivatives as in (6.7.12) below.

$$J_b = \frac{\partial L}{\partial \dot{\beta}_b} = \frac{\partial \Theta_m}{\partial \beta_b} J_m \quad (6.7.11a) \qquad\qquad \dot{J}_b = \frac{\partial L}{\partial \beta_b} \qquad (6.7.11b)$$

Inverse $\mathbf{K}_b^m = \tfrac{\partial \beta_b}{\partial \Theta_m}$ transforms Euler $J_b = \{J_\alpha, J_\beta, J_\gamma\}$ to LAB J_m in (6.7.10a) and (6.7.11c).

$$J_m = \frac{\partial L}{\partial \dot{\Theta}_m} = J_b \frac{\partial \beta_b}{\partial \Theta_m} \quad (6.7.11c) \qquad\qquad \dot{J}_m = \frac{\partial L}{\partial \Theta_m} \qquad (6.7.11d)$$

Cartesian BOD-momenta transform by Jacobian $\mathbf{J}_{\bar{m}}^b = \tfrac{\partial \Theta_{\bar{m}}}{\partial \beta_b}$ in (6.7.10d) or by $\mathbf{K}_b^{\bar{m}} = \tfrac{\partial \beta_b}{\partial \Theta_{\bar{m}}}$ in (6.7.10b).

$$J_{\bar{m}} = \frac{\partial L}{\partial \dot{\Theta}_{\bar{m}}} = J_b \frac{\partial \beta_b}{\partial \Theta_{\bar{m}}} \quad (6.7.11e) \qquad\qquad \dot{J}_{\bar{m}} = \frac{\partial L}{\partial \Theta_{\bar{m}}} \qquad (6.7.11f)$$

Terms in $\dot{J}_1 = \tfrac{\partial L}{\partial \Theta_1}$ of (6.7.9) and (6.7.11d) relate to (6.7.11) thru six chain-sum terms of $\tfrac{\partial L}{\partial \Theta_1}$.

$$\dot{J}_1 = \tfrac{d}{dt}[\tfrac{\partial L}{\partial \dot{\alpha}}\tfrac{\partial \dot{\alpha}}{\partial \dot{\Theta}_1} + \tfrac{\partial L}{\partial \dot{\beta}}\tfrac{\partial \dot{\beta}}{\partial \dot{\Theta}_1} + \tfrac{\partial L}{\partial \dot{\gamma}}\tfrac{\partial \dot{\gamma}}{\partial \dot{\Theta}_1}] = \tfrac{\partial L}{\partial \Theta_1} = \tfrac{\partial L}{\partial \alpha}\tfrac{\partial \alpha}{\partial \Theta_1} + \tfrac{\partial L}{\partial \beta}\tfrac{\partial \beta}{\partial \Theta_1} + \tfrac{\partial L}{\partial \gamma}\tfrac{\partial \gamma}{\partial \Theta_1} + \tfrac{\partial L}{\partial \dot{\alpha}}\tfrac{\partial \dot{\alpha}}{\partial \Theta_1} + \tfrac{\partial L}{\partial \dot{\beta}}\tfrac{\partial \dot{\beta}}{\partial \Theta_1} + \tfrac{\partial L}{\partial \dot{\gamma}}\tfrac{\partial \dot{\gamma}}{\partial \Theta_1} \qquad (6.7.12)$$

Lemma 1 applies on the left and *Lemma 2* on the right. Euler equations (6.7.11) result term-by-term.

$$\dot{J}_1 = \tfrac{d}{dt}[\tfrac{\partial L}{\partial \dot{\alpha}}\tfrac{\partial \alpha}{\partial \Theta_1} + \tfrac{\partial L}{\partial \dot{\beta}}\tfrac{\partial \beta}{\partial \Theta_1} + \tfrac{\partial L}{\partial \dot{\gamma}}\tfrac{\partial \gamma}{\partial \Theta_1}] = \tfrac{\partial L}{\partial \alpha}\tfrac{\partial \alpha}{\partial \Theta_1} + \tfrac{\partial L}{\partial \beta}\tfrac{\partial \beta}{\partial \Theta_1} + \tfrac{\partial L}{\partial \gamma}\tfrac{\partial \gamma}{\partial \Theta_1} + \tfrac{\partial L}{\partial \dot{\alpha}}\tfrac{d}{dt}\tfrac{\partial \alpha}{\partial \Theta_1} + \tfrac{\partial L}{\partial \dot{\beta}}\tfrac{d}{dt}\tfrac{\partial \beta}{\partial \Theta_1} + \tfrac{\partial L}{\partial \dot{\gamma}}\tfrac{d}{dt}\tfrac{\partial \gamma}{\partial \Theta_1} \qquad (6.7.13a)$$

$$\dot{J}_1 = \frac{d}{dt}[J_\alpha \frac{\partial \alpha}{\partial \Theta_1} + J_\beta \frac{\partial \beta}{\partial \Theta_1} + J_\gamma \frac{\partial \gamma}{\partial \Theta_1}] = \dot{J}_\alpha \frac{\partial \alpha}{\partial \Theta_1} + \dot{J}_\beta \frac{\partial \beta}{\partial \Theta_1} + \dot{J}_\gamma \frac{\partial \gamma}{\partial \Theta_1} + J_\alpha \frac{d}{dt}\frac{\partial \alpha}{\partial \Theta_1} + J_\beta \frac{d}{dt}\frac{\partial \beta}{\partial \Theta_1} + J_\gamma \frac{d}{dt}\frac{\partial \gamma}{\partial \Theta_1} \qquad (6.7.13b)$$

LAB-Euler velocity transformation matrices (6.7.5) are repeated below in Jacobian notation.

$$\begin{pmatrix} \frac{\partial \omega_1}{\partial \dot\alpha} & \frac{\partial \omega_1}{\partial \dot\beta} & \frac{\partial \omega_1}{\partial \dot\gamma} \\ \frac{\partial \omega_2}{\partial \dot\alpha} & \frac{\partial \omega_2}{\partial \dot\beta} & \frac{\partial \omega_2}{\partial \dot\gamma} \\ \frac{\partial \omega_3}{\partial \dot\alpha} & \frac{\partial \omega_3}{\partial \dot\beta} & \frac{\partial \omega_3}{\partial \dot\gamma} \end{pmatrix} = \begin{pmatrix} \frac{\partial \Theta_1}{\partial \alpha} & \frac{\partial \Theta_1}{\partial \beta} & \frac{\partial \Theta_1}{\partial \gamma} \\ \frac{\partial \Theta_2}{\partial \alpha} & \frac{\partial \Theta_2}{\partial \beta} & \frac{\partial \Theta_2}{\partial \gamma} \\ \frac{\partial \Theta_3}{\partial \alpha} & \frac{\partial \Theta_3}{\partial \beta} & \frac{\partial \Theta_3}{\partial \gamma} \end{pmatrix} \qquad (6.7.14a)$$

$$\begin{pmatrix} \frac{\partial \dot\alpha}{\partial \omega_1} & \frac{\partial \dot\alpha}{\partial \omega_2} & \frac{\partial \dot\alpha}{\partial \omega_3} \\ \frac{\partial \dot\beta}{\partial \omega_1} & \frac{\partial \dot\beta}{\partial \omega_2} & \frac{\partial \dot\beta}{\partial \omega_3} \\ \frac{\partial \dot\gamma}{\partial \omega_1} & \frac{\partial \dot\gamma}{\partial \omega_2} & \frac{\partial \dot\gamma}{\partial \omega_3} \end{pmatrix} = \begin{pmatrix} \frac{\partial \alpha}{\partial \Theta_1} & \frac{\partial \alpha}{\partial \Theta_2} & \frac{\partial \alpha}{\partial \Theta_3} \\ \frac{\partial \beta}{\partial \Theta_1} & \frac{\partial \beta}{\partial \Theta_2} & \frac{\partial \beta}{\partial \Theta_3} \\ \frac{\partial \gamma}{\partial \Theta_1} & \frac{\partial \gamma}{\partial \Theta_2} & \frac{\partial \gamma}{\partial \Theta_3} \end{pmatrix} = \qquad (6.7.14b)$$

$$= \begin{pmatrix} 0 & -\sin\alpha & \cos\alpha\sin\beta \\ 0 & \cos\alpha & \sin\alpha\sin\beta \\ 1 & 0 & \cos\beta \end{pmatrix} \begin{matrix} \text{Euler}(\dot\alpha\dot\beta\dot\gamma) \\ \text{veloc. to} \\ \text{LAB}[\dot\Theta_\mathbf{a}] \end{matrix}$$

$$\begin{pmatrix} -\cos\alpha\cot\beta & -\sin\alpha\cot\beta & 1 \\ -\sin\alpha & \cos\alpha & 0 \\ \cos\alpha\csc\beta & \sin\alpha\csc\beta & 0 \end{pmatrix} \begin{matrix} \text{LAB}[\dot\Theta_\mathbf{a}] \\ \text{veloc. to} \\ \text{Euler}(\dot\alpha\dot\beta\dot\gamma) \end{matrix}$$

Momentum transformation is matrix transpose going opposite way as in (6.7.10a) and (6.7.10c).

$$\begin{pmatrix} 0 & 0 & 1 \\ -\sin\alpha & \cos\alpha & 0 \\ \cos\alpha\sin\beta & \sin\alpha\sin\beta & \cos\beta \end{pmatrix} \begin{matrix} \text{LAB}[J_\mathbf{a}] \\ \text{mom. to} \\ \text{Euler}(J_\phi) \end{matrix}$$

$$\begin{pmatrix} -\cos\alpha\cot\beta & -\sin\alpha & \cos\alpha\csc\beta \\ -\sin\alpha\cot\beta & \cos\alpha & \sin\alpha\csc\beta \\ 1 & 0 & 0 \end{pmatrix} \begin{matrix} \text{Euler}(J_\phi) \\ \text{mom. to} \\ \text{LAB}[J_\mathbf{a}] \end{matrix}$$

Similar transformations (6.7.5d) or (6.7.5f) connect Euler-angular and BOD-Cartesian quantities.

$$\begin{pmatrix} \frac{\partial \omega_{\bar1}}{\partial \dot\alpha} & \frac{\partial \omega_{\bar1}}{\partial \dot\beta} & \frac{\partial \omega_{\bar1}}{\partial \dot\gamma} \\ \frac{\partial \omega_{\bar2}}{\partial \dot\alpha} & \frac{\partial \omega_{\bar2}}{\partial \dot\beta} & \frac{\partial \omega_{\bar2}}{\partial \dot\gamma} \\ \frac{\partial \omega_{\bar3}}{\partial \dot\alpha} & \frac{\partial \omega_{\bar3}}{\partial \dot\beta} & \frac{\partial \omega_{\bar3}}{\partial \dot\gamma} \end{pmatrix} = \begin{pmatrix} \frac{\partial \Theta_{\bar1}}{\partial \alpha} & \frac{\partial \Theta_{\bar1}}{\partial \beta} & \frac{\partial \Theta_{\bar1}}{\partial \gamma} \\ \frac{\partial \Theta_{\bar2}}{\partial \alpha} & \frac{\partial \Theta_{\bar2}}{\partial \beta} & \frac{\partial \Theta_{\bar2}}{\partial \gamma} \\ \frac{\partial \Theta_{\bar3}}{\partial \alpha} & \frac{\partial \Theta_{\bar3}}{\partial \beta} & \frac{\partial \Theta_{\bar3}}{\partial \gamma} \end{pmatrix} \quad (6.7.14c)$$

$$\begin{pmatrix} \frac{\partial \dot\alpha}{\partial \omega_{\bar1}} & \frac{\partial \dot\alpha}{\partial \omega_{\bar2}} & \frac{\partial \dot\alpha}{\partial \omega_{\bar3}} \\ \frac{\partial \dot\beta}{\partial \omega_{\bar1}} & \frac{\partial \dot\beta}{\partial \omega_{\bar2}} & \frac{\partial \dot\beta}{\partial \omega_{\bar3}} \\ \frac{\partial \dot\gamma}{\partial \omega_{\bar1}} & \frac{\partial \dot\gamma}{\partial \omega_{\bar2}} & \frac{\partial \dot\gamma}{\partial \omega_{\bar3}} \end{pmatrix} = \begin{pmatrix} \frac{\partial \alpha}{\partial \Theta_{\bar1}} & \frac{\partial \alpha}{\partial \Theta_{\bar2}} & \frac{\partial \alpha}{\partial \Theta_{\bar3}} \\ \frac{\partial \beta}{\partial \Theta_{\bar1}} & \frac{\partial \beta}{\partial \Theta_{\bar2}} & \frac{\partial \beta}{\partial \Theta_{\bar3}} \\ \frac{\partial \gamma}{\partial \Theta_{\bar1}} & \frac{\partial \gamma}{\partial \Theta_{\bar2}} & \frac{\partial \gamma}{\partial \Theta_{\bar3}} \end{pmatrix} = \quad (6.7.14d)$$

$$= \begin{pmatrix} -\sin\beta\cos\gamma & \sin\gamma & 0 \\ \sin\beta\sin\gamma & \cos\gamma & 0 \\ \cos\beta & 0 & 1 \end{pmatrix} \begin{matrix} \text{Euler}(\alpha\beta\gamma) \\ \text{coord. to} \\ \text{BOD}[\Theta_\mathbf{a}] \end{matrix}$$

$$\begin{pmatrix} -\cos\gamma\csc\beta & \sin\gamma\csc\beta & 0 \\ \sin\gamma & \cos\gamma & 0 \\ \cot\beta\cos\gamma & -\cot\beta\sin\gamma & 1 \end{pmatrix} \begin{matrix} \text{BOD}[\Theta_{\bar{\mathbf{a}}}] \\ \text{coord. to} \\ \text{Euler}(\alpha\beta\gamma) \end{matrix}$$

Again, transposed matrices do momentum transforms oppositely as in (6.7.10b) and (6.7.10d).

$$\begin{pmatrix} -\sin\beta\cos\gamma & \sin\beta\sin\gamma & \cos\beta \\ \sin\gamma & \cos\gamma & 0 \\ 0 & 0 & 1 \end{pmatrix} \begin{matrix} \text{BOD}[J_{\bar{\mathbf{a}}}] \\ \text{mom. to} \\ \text{Euler}(J_\phi) \end{matrix}$$

$$\begin{pmatrix} -\cos\gamma\csc\beta & \sin\gamma & \cot\beta\cos\gamma \\ \sin\gamma\csc\beta & \cos\gamma & -\cot\beta\sin\gamma \\ 0 & 0 & 1 \end{pmatrix} \begin{matrix} \text{Euler}(J_\phi) \\ \text{mom. to} \\ \text{BOD}[J_{\bar{\mathbf{a}}}] \end{matrix}$$

A product of (6.7.14a) and (6.7.14d) gives the original rotation $R(\alpha\beta\gamma)$ in (6.6.1) from LAB-to-BOD.

$$\begin{pmatrix} \frac{\partial \Theta_1}{\partial \alpha} & \frac{\partial \Theta_1}{\partial \beta} & \frac{\partial \Theta_1}{\partial \gamma} \\ \frac{\partial \Theta_2}{\partial \alpha} & \frac{\partial \Theta_2}{\partial \beta} & \frac{\partial \Theta_2}{\partial \gamma} \\ \frac{\partial \Theta_3}{\partial \alpha} & \frac{\partial \Theta_3}{\partial \beta} & \frac{\partial \Theta_3}{\partial \gamma} \end{pmatrix} \cdot \begin{pmatrix} \frac{\partial \alpha}{\partial \Theta_{\bar1}} & \frac{\partial \alpha}{\partial \Theta_{\bar2}} & \frac{\partial \alpha}{\partial \Theta_{\bar3}} \\ \frac{\partial \beta}{\partial \Theta_{\bar1}} & \frac{\partial \beta}{\partial \Theta_{\bar2}} & \frac{\partial \beta}{\partial \Theta_{\bar3}} \\ \frac{\partial \gamma}{\partial \Theta_{\bar1}} & \frac{\partial \gamma}{\partial \Theta_{\bar2}} & \frac{\partial \gamma}{\partial \Theta_{\bar3}} \end{pmatrix} = \begin{pmatrix} 0 & -\sin\alpha & \cos\alpha\sin\beta \\ 0 & \cos\alpha & \sin\alpha\sin\beta \\ 1 & 0 & \cos\beta \end{pmatrix} \cdot \begin{pmatrix} -\cos\gamma\csc\beta & \sin\gamma\csc\beta & 0 \\ \sin\gamma & \cos\gamma & 0 \\ \cot\beta\cos\gamma & -\cot\beta\sin\gamma & 1 \end{pmatrix} \quad (6.6.15a)$$

$$
= \begin{vmatrix} \dfrac{\partial \Theta_1}{\partial \Theta_{\bar{1}}} & \dfrac{\partial \Theta_1}{\partial \Theta_{\bar{2}}} & \dfrac{\partial \Theta_1}{\partial \Theta_{\bar{3}}} \\[1ex] \dfrac{\partial \Theta_2}{\partial \Theta_{\bar{1}}} & \dfrac{\partial \Theta_2}{\partial \Theta_{\bar{2}}} & \dfrac{\partial \Theta_2}{\partial \Theta_{\bar{3}}} \\[1ex] \dfrac{\partial \Theta_3}{\partial \Theta_{\bar{1}}} & \dfrac{\partial \Theta_3}{\partial \Theta_{\bar{2}}} & \dfrac{\partial \Theta_3}{\partial \Theta_{\bar{3}}} \end{vmatrix} = R(\alpha\beta\gamma) = \begin{pmatrix} \cos\alpha\cos\beta\cos\gamma - \sin\alpha\sin\gamma & -\cos\alpha\cos\beta\sin\gamma - \sin\alpha\cos\gamma & \cos\alpha\sin\beta \\ \sin\alpha\cos\beta\cos\gamma + \cos\alpha\sin\gamma & -\sin\alpha\cos\beta\sin\gamma + \cos\alpha\cos\gamma & \sin\alpha\sin\beta \\ -\cos\gamma\sin\beta & \sin\gamma\sin\beta & \cos\beta \end{pmatrix}
$$

Inverse rotation $R(-\gamma-\beta-\alpha)=R^{-1}(\alpha\beta\gamma)$ going from BOD-to-LAB is a transpose $R^T(\alpha\beta\gamma)$ of (6.6.1) since R is an orthogonal matrix ($R^{-1}=R^T$ or $R=(R^T)^{-1}$), and that gives a related factorization of $R(\alpha\beta\gamma)$.

$$
R(\alpha\beta\gamma) = \left(R^T(\alpha\beta\gamma)\right)^{-1} = \begin{pmatrix} -\cos\alpha\cot\beta & -\sin\alpha & \cos\alpha\csc\beta \\ -\sin\alpha\cot\beta & \cos\alpha & \sin\alpha\csc\beta \\ 1 & 0 & 0 \end{pmatrix} \begin{pmatrix} -\sin\beta\cos\gamma & \sin\beta\sin\gamma & \cos\beta \\ \sin\gamma & \cos\gamma & 0 \\ 0 & 0 & 1 \end{pmatrix} \quad \text{(6.7.15b)}
$$

Poincare invariant energy and Hamilton equations

Angular velocity ω and momentum **J** transform by inverse Jacobians. So $\vec{\omega}\cdot\vec{J}$ is another example of a Poincare invariant (2.6.9) or (3.8.5c). Also, $\tfrac{1}{2}\vec{\omega}\cdot\vec{J}$ is invariant kinetic energy $T = \tfrac{1}{2}(H+L) = \tfrac{1}{2}p_\mu \dot{q}^\mu$.

$$
T = \tfrac{1}{2}(H+L) = \tfrac{1}{2}(J_\alpha\dot{\alpha} + J_\beta\dot{\beta} + J_\gamma\dot{\gamma}) = \tfrac{1}{2}(J_1\omega_1 + J_2\omega_2 + J_3\omega_3) = \tfrac{1}{2}(J_{\bar{1}}\omega_{\bar{1}} + J_{\bar{2}}\omega_{\bar{2}} + J_{\bar{3}}\omega_{\bar{3}}) = \tfrac{1}{2}\vec{\omega}\cdot\vec{J} \quad \text{(6.7.16)}
$$

Scalar product $\vec{\omega}\cdot\vec{J}$ of angular momentum and velocity is frame-invariant. Without external torque or potential, $\vec{J}$ is constant in LAB-frame and ω moves on tangent plane $\vec{\omega}\cdot\vec{J} = 2T$ normal to LAB-fixed $\vec{J}$ in Fig. 6.5.3. The $\omega\cdot\textbf{I}\cdot\omega$-ellipse and its BOD frame roll without slipping on the tangent plane. The ω-ellipse contacts the plane at ω, precisely where a BOD point is instantaneously stationary in the LAB-frame.

Kinetic energy is $T(\dot{\alpha},\dot{\beta},\dot{\gamma};\alpha,\beta,\gamma) = \tfrac{1}{2}\vec{\omega}\cdot\vec{J}$ in *any* frame or potential $V(\alpha\beta\gamma)$. Hamiltonian $H = T+V$ is constant if $L=T-V$ is time-independent. Kinetic energy T is constant if V is negligible. Then energy is simply: $H=T=L=E$, as it is for free or for constrained rotors discussed below. Hamilton's equations for Hamiltonian H $(J_\alpha, J_\beta, J_\gamma; \alpha, \beta, \gamma)$ have a LAB form, a BOD form, and an Euler form as shown below.

$$
\dot{J}_m = -\frac{\partial H}{\partial \Theta_m} \quad \text{(6.7.17a)} \qquad\qquad \dot{J}_{\bar{m}} = -\frac{\partial H}{\partial \Theta_{\bar{m}}} \quad \text{(6.7.17b)} \qquad\qquad (\dot{J}_\alpha, \dot{J}_\beta, \dot{J}_\gamma) = -\left(\frac{\partial H}{\partial \alpha}, \frac{\partial H}{\partial \beta}, \frac{\partial H}{\partial \gamma}\right)
$$

$$
\dot{\Theta}_m = \frac{\partial H}{\partial J_m} \qquad\qquad\qquad\qquad \dot{\Theta}_{\bar{m}} = \frac{\partial H}{\partial J_{\bar{m}}} \qquad\qquad\qquad\qquad (\dot{\alpha}, \dot{\beta}, \dot{\gamma}) \;=\; \left(\frac{\partial H}{\partial \dot{\alpha}}, \frac{\partial H}{\partial \dot{\beta}}, \frac{\partial H}{\partial \dot{\gamma}}\right) \quad \text{(6.7.17c)}
$$

d. Constrained *vs.* Free rigid rotors

Rigid-rotor Lagrangian or Hamiltonian has a LAB-defined kinetic energy from (6.5.5) or (6.7.16).

$$
L = \tfrac{1}{2}\vec{\omega}\cdot\vec{J} = \tfrac{1}{2}\omega\cdot\textbf{I}\cdot\omega = \tfrac{1}{2}\omega_m I_{mn}\omega_n = KE \quad \text{(6.7.18a)} \qquad\qquad H = \tfrac{1}{2}\textbf{J}\cdot\textbf{I}^{-1}\cdot\textbf{J} = \tfrac{1}{2}J_m I_{mn}^{-1} J_n = KE \quad \text{(6.7.18b)}
$$

Potential V is assumed constant or zero for a free-rotor (meaning potential-free) but also for a rotor constrained by frictionless bearings with *infinite* bearing raceway potential V that guides the rotor but takes *zero* work to or from the *KE* of H or of L. Let us compare constrained-*versus*-free rotor kinetics.

1. Constant-ω constrained rotor (LAB frame view)

Fig. 6.7.1a shows a linear rotor with its angular rotation axis ω fixed by a bearing along the LAB $z=x_3$ axis. Body axis $\overline{z} = x_{\overline{3}}$ is welded to the *z*-axle at a constant polar angle β. LAB-defined inertia I_{mn} for mass *m* on body radius $\mathbf{r} = r\mathbf{x}_{\overline{3}}$ vary with angle α and β by (6.5.1), but only $α=Θ_3 = \dot{α}·t$ varies in time.

$$\mathbf{I} = m(r^2 - \mathbf{rr}) \quad \text{where:} \quad \mathbf{r} = r\mathbf{x}_{\overline{3}} = r(\cos α \sin β, \sin α \sin β, \cos β)$$

$$\begin{pmatrix} I_{11} & I_{12} & I_{13} \\ I_{21} & I_{22} & I_{23} \\ I_{31} & I_{32} & I_{33} \end{pmatrix} = mr^2 \begin{pmatrix} 1-\cos^2 α \sin^2 β & -\sin α \cos α \sin^2 β & -\cos α \sin β \cos β \\ I_{21} = I_{12} & 1-\sin^2 α \sin^2 β & -\sin α \sin β \cos β \\ I_{31} = I_{13} & I_{32} = I_{23} & \sin^2 β \end{pmatrix} \qquad (6.7.19a)$$

Angular velocity vector ω constrained to one LAB-*z*-component.

$$\mathbf{ω} = (ω_1, ω_2, ω_3) = (0,0,\dot{α}) \qquad (6.7.19b)$$

This yields a time-varying 3-component angular momentum vector **J** given by tensor relation **J=I•ω** of (6.5.5). The **J**-vector is sketched in relation to radius vector **r** and angular velocity ω in Fig. 6.7.1b.

$$\begin{pmatrix} J_1 \\ J_2 \\ J_3 \end{pmatrix} = \begin{pmatrix} I_{11} & I_{12} & I_{13} \\ I_{21} & I_{22} & I_{23} \\ I_{31} & I_{32} & I_{33} \end{pmatrix} \begin{pmatrix} ω_1 \\ ω_2 \\ ω_3 \end{pmatrix} = \begin{pmatrix} I_{11} & I_{12} & I_{13} \\ I_{21} & I_{22} & I_{23} \\ I_{31} & I_{32} & I_{33} \end{pmatrix} \begin{pmatrix} 0 \\ 0 \\ \dot{α} \end{pmatrix} = mr^2 \begin{pmatrix} -\cos α \sin β \cos β \\ -\sin α \sin β \cos β \\ \sin^2 β \end{pmatrix} \dot{α} \quad (6.7.20a)$$

The J-vector traces a cone of polar angle π/2–β=*const.* in the lab as it rotates by $α=Θ_3$ at rate $\dot{α} = ω_3$.

$$\begin{pmatrix} J_1 \\ J_2 \\ J_3 \end{pmatrix} = \begin{pmatrix} \cos α & -\sin α & 0 \\ \sin α & \cos α & 0 \\ 0 & 0 & 1 \end{pmatrix} \begin{pmatrix} -\cos β \\ 0 \\ \sin β \end{pmatrix} j = \begin{pmatrix} \cos α & -\sin α & 0 \\ \sin α & \cos α & 0 \\ 0 & 0 & 1 \end{pmatrix} \begin{pmatrix} \sin β & 0 & -\cos β \\ 0 & 1 & 0 \\ -\cos β & 0 & \sin β \end{pmatrix} \begin{pmatrix} 0 \\ 0 \\ j \end{pmatrix} \quad \begin{array}{l} \textit{where :} \\ j=mr^2\dot{α}\sin β \\ (6.7.20b) \end{array}$$

Energy (6.7.16) depends on azimuthal angular velocity ($ω_3 = \dot{α}$) but not on angle $α=Θ_3$ itself, so $\dot{J}_α = 0$.

$$L = T = \tfrac{1}{2}\vec{\mathbf{ω}}•\mathbf{J} = \tfrac{1}{2}\vec{\mathbf{ω}}•\vec{\mathbf{I}}•\vec{\mathbf{ω}} = \tfrac{1}{2}mr^2\dot{α}^2 \sin^2 β = \tfrac{1}{2}mr^2ω_3^2 \sin^2 β \qquad (6.7.21)$$

So energy *L=T=KE* is constant if both $ω_3 = \dot{α}$ and β are constant. If β is fixed then so is $\dot{α}$.

LAB-frame Lagrange equations (6.7.11) or (6.7.13) and (6.7.20) should be consistent with velocity constraints $(ω_1,ω_2,ω_3) = (0,0,\dot{α})$ that fix Euler angles β, γ, and leave only the 3rd $ω_a$ and angle α free.

$$J_1 = \frac{\partial L}{\partial ω_1} = I_{13}ω_3 \qquad J_2 = \frac{\partial L}{\partial ω_2} = I_{23}ω_3 \qquad J_3 = \frac{\partial L}{\partial ω_3} = I_{33}ω_3 \qquad (6.7.22a)$$

$$= -(mr^2 \cos α \sin β \cos β)ω_3 \qquad = -(mr^2 \sin α \sin β \cos β)ω_3 \qquad = (mr^2 \sin^2 β)ω_3$$

Evaluating $\frac{\partial L}{\partial ω_m}$ using Jacobian components (6.7.14b) gives consistent results for LAB **J**.

$$J_1 = \frac{\partial L}{\partial ω_1} = \frac{\partial L}{\partial \dot{α}}\frac{\partial \dot{α}}{\partial ω_1} \qquad J_2 = \frac{\partial L}{\partial ω_2} = \frac{\partial L}{\partial \dot{α}}\frac{\partial \dot{α}}{\partial ω_2} \qquad J_3 = \frac{\partial L}{\partial ω_3} = \frac{\partial L}{\partial \dot{α}}\frac{\partial \dot{α}}{\partial ω_3} \qquad (6.7.22b)$$

$$= -\dot{α}mr^2 \sin^2 β \cos α \cot β \qquad = -\dot{α}mr^2 \sin^2 β \sin α \cot β \qquad = \dot{α}mr^2 \sin^2 β$$

But, **J**-motion equations for torques $\dot{J}_\beta$ are upset by constraints. Lagrangian (6.7.21) is a function of β so its usual equation $\dot{J}_\beta = \frac{\partial L}{\partial \beta}$ is nonzero. Constraint equation $c=\beta$ adds a Lagrange-multiplier torque $\lambda \frac{\partial c}{\partial \beta} = \lambda$ to constrain **J**-motion to $\dot{J}_\beta = 0$ for constant β. (J_β is really *undefined* due to *infinite* β-bearing potentials!)

$$\dot{J}_\beta = \frac{\partial L}{\partial \beta} + \lambda \frac{\partial c}{\partial \beta}(= 0 \text{ if: } \lambda = -mr^2\dot{\alpha}^2 \sin\beta\cos\beta) \tag{6.7.23}$$

This λ is a centripetal (center-pulling) torque holding β constant and is maximum at β=π/4. If J_β, J_γ and $\dot{J}_\alpha$ are zero, so are all $\dot{J}_m$ terms in (6.7.13b) except $J_\alpha \frac{d}{dt}\frac{\partial\alpha}{\partial\Theta_m}$ for *m=1,2*. Jacobian $\frac{\partial\alpha}{\partial\Theta_m}$ in (6.7.14b) give $\dot{J}_m$ that are consistent with simple time derivatives of (6.7.20a) or (6.7.22a).

$$\begin{aligned}
\dot{J}_1 &= \frac{\partial L}{\partial\Theta_1} = \frac{\partial L}{\partial\dot{\alpha}}\frac{d}{dt}\frac{\partial\alpha}{\partial\Theta_1} & \dot{J}_2 &= \frac{\partial L}{\partial\Theta_2} = \frac{\partial L}{\partial\dot{\alpha}}\frac{d}{dt}\frac{\partial\alpha}{\partial\Theta_2} & \dot{J}_3 &= \frac{\partial L}{\partial\Theta_3} = \frac{\partial L}{\partial\dot{\alpha}}\frac{d}{dt}\frac{\partial\alpha}{\partial\Theta_3} \\
&= mr^2\dot{\alpha}\sin^2\beta(\dot{\alpha}\sin\alpha\cot\beta) & &= -mr^2\dot{\alpha}\sin^2\beta(\dot{\alpha}\cos\alpha\cot\beta) & &= mr^2\dot{\alpha}\sin^2\beta \cdot (0) \\
&= mr^2\dot{\alpha}^2\sin\alpha\sin\beta\cos\beta & &= -mr^2\dot{\alpha}^2\cos\alpha\sin\beta\cos\beta & &= 0
\end{aligned} \tag{6.7.24}$$

2. Constant-ω constrained rotor (BOD frame view)

Body axis $\pm\bar{\mathbf{z}}=\pm\mathbf{x}_{\bar{3}}$ is welded to LAB *z*-axle ($\mathbf{z}=\mathbf{x}_3$) at constant polar-angle β. Azimuth-angle $\alpha = \dot{\alpha}\cdot t$ moves in Fig. 6.7.1a. Any vector ($\mathbf{x}_1$, $\mathbf{x}_2$, $\mathbf{x}_3$) or tensor ($\mathbf{x}_1\mathbf{x}_1$, $\mathbf{x}_1\mathbf{x}_2$,… $\mathbf{x}_3\mathbf{x}_3$) rotates to BOD by $R(\alpha\beta0)$.

$$\mathbf{x}_{\bar{k}} = \mathbf{R}(\alpha\beta0)\cdot\mathbf{x}_k \tag{6.7.25a} \qquad\qquad \mathbf{x}_{\bar{j}}\mathbf{x}_{\bar{k}} = \mathbf{R}(\alpha\beta0)\cdot\mathbf{x}_j\mathbf{x}_k\cdot\mathbf{R}^{\mathbf{T}}(\alpha\beta0) \tag{6.7.25b}$$

The inverse matrix $R^{-1}(\alpha\beta\gamma)$ (or transpose $R^T(\alpha\beta\gamma)$) makes a LAB-to-BOD coordinate change-of-basis.

$$\begin{pmatrix} x_{\bar{1}} \\ x_{\bar{2}} \\ x_{\bar{3}} \end{pmatrix} = R^T(\alpha\beta0)\cdot\begin{pmatrix} x_1 \\ x_2 \\ x_3 \end{pmatrix} \tag{6.7.25c} \qquad \begin{pmatrix} I_{\bar{1}\bar{1}} & I_{\bar{1}\bar{2}} & I_{\bar{1}\bar{3}} \\ I_{\bar{2}\bar{1}} & I_{\bar{2}\bar{2}} & I_{\bar{2}\bar{3}} \\ I_{\bar{3}\bar{1}} & I_{\bar{3}2} & I_{\bar{3}\bar{3}} \end{pmatrix} = R^T(\alpha\beta0)\cdot\begin{pmatrix} I_{11} & I_{12} & I_{13} \\ I_{21} & I_{22} & I_{23} \\ I_{31} & I_{32} & I_{33} \end{pmatrix}\cdot R(\alpha\beta0) \tag{6.7.25d}$$

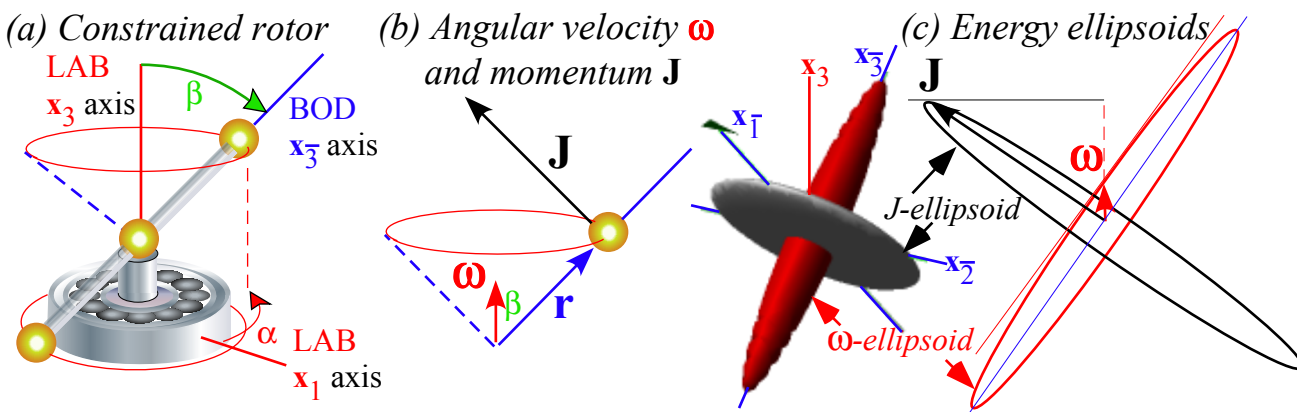*(a) Constrained rotor   (b) Angular velocity ω and momentum J   (c) Energy ellipsoids*

Fig. 6.7.1 Elementary ω-constrained rotor and angular velocity-momentum geometry.

Examples below use matrix representations based on matrix $R=R(\alpha\beta0)$ derived from (6.6.1) with γ=0.

$$\overline{\mathbf{z}} = \mathbf{x}_{\overline{3}} \qquad = \mathbf{R}(\alpha\beta 0)\cdot\mathbf{x}_3 \qquad\qquad \overline{\mathbf{z}\mathbf{z}} = \mathbf{x}_{\overline{3}}\mathbf{x}_{\overline{3}} \qquad\qquad = \mathbf{R}(\alpha\beta 0)\cdot \quad \mathbf{x}_3\mathbf{x}_3 \quad \cdot\mathbf{R}^{\mathbf{T}}(\alpha\beta 0)$$

$$\begin{pmatrix} \cos\alpha\sin\beta \\ \sin\alpha\sin\beta \\ \cos\beta \end{pmatrix} = R(\alpha\beta 0)\cdot \begin{pmatrix} 0 \\ 0 \\ 1 \end{pmatrix} \begin{pmatrix} \cos^2\alpha\sin^2\beta & \sin\alpha\cos\alpha\sin^2\beta & \cos\alpha\sin\beta\cos\beta \\ I_{21}=I_{12} & \sin^2\alpha\sin^2\beta & \sin\alpha\sin\beta\cos\beta \\ I_{31}=I_{13} & I_{32}=I_{23} & \cos^2\beta \end{pmatrix} \begin{aligned} &= R(\alpha\beta 0)\cdot \begin{pmatrix} 0 & 0 & 0 \\ 0 & 0 & 0 \\ 0 & 0 & 1 \end{pmatrix} \cdot R^T(\alpha\beta 0) \end{aligned}$$

For example, a LAB inertia matrix like (6.7.19) transforms by $R^{\mathrm{T}}(\alpha\beta 0)$ to a diagonal BOD-based matrix.

$$\begin{pmatrix} I_{\overline{1}} & 0 & 0 \\ 0 & I_{\overline{2}} & 0 \\ 0 & 0 & I_{\overline{3}} \end{pmatrix} = \begin{pmatrix} I & 0 & 0 \\ 0 & I & 0 \\ 0 & 0 & \iota \end{pmatrix} = R^T \begin{pmatrix} I+(\iota-I)\cos^2\alpha\sin^2\beta & (\iota-I)\sin\alpha\cos\alpha\sin^2\beta & (\iota-I)\cos\alpha\sin\beta\cos\beta \\ (\iota-I)\sin\alpha\cos\alpha\sin^2\beta & I+(\iota-I)\sin^2\alpha\sin^2\beta & (\iota-I)\sin\alpha\sin\beta\cos\beta \\ (\iota-I)\cos\alpha\sin\beta\cos\beta & (\iota-I)\sin\alpha\sin\beta\cos\beta & I\sin^2\beta+(\iota)\cos^2\beta \end{pmatrix} R \quad (6.7.26)$$

I-matrix (6.7.26) has an extra "*iota*" of longitudinal inertia in the 3rd eigenvalue ($I_{\overline{3}} = \iota = \varepsilon mr^2$) due to thickness of radius rod holding *m*-masses at body frame $\pm\overline{\mathbf{z}}=\pm\,\mathbf{x}_{\overline{3}}$. The previous example (6.7.19) had only transverse inertia ($I_{\overline{1}} = mr^2 = I_{\overline{2}} = I$). Adding ι lets us define an *inverse* inertia matrix I^{-1} that a valid Hamiltonian needs. BOD-frame Lagrangian contains *I*-matrix eigenvalues $\{I_{\overline{1}} = I, I_{\overline{2}} = I, I_{\overline{3}} = \iota\}$ in (6.7.13) while a Hamiltonian function of **J** contains inverse I^{-1}-matrix eigenvalues $\{I_{\overline{1}}^{-1} = \tfrac{1}{I}, I_{\overline{2}}^{-1} = \tfrac{1}{I}, I_{\overline{3}}^{-1} = \tfrac{1}{\iota}\}$ below.

$$H = \tfrac{1}{2}\mathbf{J}\bullet\mathbf{I}^{-1}\bullet\mathbf{J} = \tfrac{1}{2}J_m I_{mn}^{-1}J_n = \tfrac{1}{2}J_{\overline{m}}I_{\overline{mn}}^{-1}J_{\overline{n}} = \tfrac{1}{2}\left(\frac{J_{\overline{1}}^2}{I_{\overline{1}}}+\frac{J_{\overline{2}}^2}{I_{\overline{2}}}+\frac{J_{\overline{3}}^2}{I_{\overline{3}}}\right)_{principle-BOD-axes} \qquad (6.7.27a)$$

$$L = \tfrac{1}{2}\boldsymbol{\omega}\bullet\mathbf{I}\bullet\boldsymbol{\omega} = \tfrac{1}{2}\omega_m I_{mn}\omega_n = \tfrac{1}{2}\omega_{\overline{m}}I_{\overline{mn}}\omega_{\overline{n}} = \tfrac{1}{2}\left(I_{\overline{1}}\omega_{\overline{1}}^2+I_{\overline{2}}\omega_{\overline{2}}^2+I_{\overline{3}}\omega_{\overline{3}}^2\right) = E = \tfrac{1}{2}\mathbf{J}\bullet\boldsymbol{\omega}$$

BOD-frame inertia $I_{\overline{m},\overline{n}}$ and eigenvalues $I_{\overline{m}}$ are constant if a rigid-body is rigidly fixed to its BOD-frame of *I* and I^{-1} eigenvectors $\{\overline{\mathbf{x}}_{\overline{1}},\overline{\mathbf{x}}_{\overline{2}},\overline{\mathbf{x}}_{\overline{3}}\}$ that define axes of *J*-ellipsoid *(H=E)* or ω-ellipsoid *(L=E)* in (6.7.27a). *J*-ellipsoid radii $\{a,b,c\}$ in $\{J_{\overline{1}},J_{\overline{2}},J_{\overline{3}}\}$-space are proportional to square roots $\sqrt{I_{\overline{m}}}$ of eigen-inertia $I_{\overline{m}}$.

$$\frac{H}{E} = \frac{J_{\overline{1}}^2}{a^2}+\frac{J_{\overline{2}}^2}{b^2}+\frac{J_{\overline{3}}^2}{c^2} = 1 \quad \text{where:} \quad a = \frac{\sqrt{I_{\overline{1}}}}{\sqrt{2E}}, \quad b = \frac{\sqrt{I_{\overline{2}}}}{\sqrt{2E}}, \quad c = \frac{\sqrt{I_{\overline{3}}}}{\sqrt{2E}}. \qquad (6.7.27b)$$

In contrast, ω -ellipsoid radii $\{A,B,C\}$ in $\{\omega_{\overline{1}},\omega_{\overline{2}},\omega_{\overline{3}}\}$-space are *inversely* proportional to $\sqrt{I_{\overline{m}}}$.

$$\frac{L}{E} = \frac{\omega_{\overline{1}}^2}{A^2}+\frac{\omega_{\overline{2}}^2}{B^2}+\frac{\omega_{\overline{3}}^2}{C^2} = 1 \quad \text{where:} \quad A = \frac{1}{\sqrt{2EI_{\overline{1}}}}, \quad B = \frac{1}{\sqrt{2EI_{\overline{2}}}}, \quad C = \frac{1}{\sqrt{2EI_{\overline{3}}}}. \qquad (6.7.27c)$$

As a result, the ω-ellipsoid $L = \tfrac{1}{2}\boldsymbol{\omega}\bullet\mathbf{I}\bullet\boldsymbol{\omega}$ has a shape that matches the body it represents with its major (minor) axis along the longest (shortest) body dimension. For the *J*-ellipsoid $H = \tfrac{1}{2}\mathbf{J}\bullet\mathbf{I}\bullet\mathbf{J}$ it is *vice-versa*. An ω-ellipsoid of *I*-matrix (6.7.26) for a rod of low iota ($\iota \ll I$) is a cigar-like shaft shown in Fig. 6.7.1c. It inflates to an infinitely long ($C\to\infty$) cylinder if ι goes to zero as in *I*-matrix (6.7.19). The same limit ($\iota\to 0$) deflates the discus-like *J*-ellipsoid in Fig. 6.7.1c into a flat ($c\to 0$) disc of radius $a=b$.

BOD-frame H and L functions (6.7.27) have only momentum $J_{\bar{m}}$ or velocity $\omega_{\bar{m}}$ components and constants $I_{\bar{m}}$ and E. So, BOD-$J_{\bar{m}}$ and $\omega_{\bar{m}}$ are constant by equations (6.7.11) or (6.7.17) of (non)-motion.

$$\dot{J}_{\bar{m}} = \frac{\partial L}{\partial \Theta_{\bar{m}}} = 0 = -\frac{\partial H}{\partial \Theta_{\bar{m}}} \quad \Rightarrow \text{implies:} \Rightarrow \quad const. = J_{\bar{m}} = \frac{\partial L}{\partial \dot{\Theta}_{\bar{m}}} = \frac{\partial L}{\partial \omega_{\bar{m}}} = I_{\bar{m}\bar{n}}\omega_{\bar{n}} \qquad (6.7.28)$$

LAB-frame J_n or ω_n components are related by rotation $R(\alpha\beta0)$ in (6.7.25c) to BOD-frame $J_{\bar{m}}$ or $\omega_{\bar{m}}$.

$$J_{\bar{m}} = R^T_{\bar{m},n}(\alpha\beta0)J_n = J_n R_{n,\bar{m}}(\alpha\beta0) \quad (6.7.29a) \qquad \omega_{\bar{m}} = R^T_{\bar{m},n}(\alpha\beta0)\omega_n = \omega_n R_{n,\bar{m}}(\alpha\beta0) \quad (6.7.\,29b)$$

$$J_n = R_{n,\bar{m}}(\alpha\beta0)J_{\bar{m}} \qquad\qquad (6.7.\,29c) \qquad \omega_n = R_{n,\bar{m}}(\alpha\beta0)\omega_{\bar{m}} \qquad\qquad (6.7.\,29d)$$

Time derivative $\dot{\mathbf{R}} = \boldsymbol{\varepsilon}_\omega \cdot \mathbf{R}$ of rotation $\mathbf{R}[\boldsymbol{\omega}\cdot t] = e^{\boldsymbol{\varepsilon}\cdot\boldsymbol{\omega}\cdot t} = e^{\boldsymbol{\varepsilon}_\omega\cdot t}$ acting on vector $\mathbf{v}$ gives: $\dot{\mathbf{R}}\vec{\mathbf{v}} = \boldsymbol{\varepsilon}_\omega\cdot\mathbf{R}\vec{\mathbf{v}} = \boldsymbol{\omega}\times(\mathbf{R}\vec{\mathbf{v}})$.

$$\dot{J}_n = \dot{R}_{n,\bar{m}}(\alpha\beta0)J_{\bar{m}} + R_{n,\bar{m}}(\alpha\beta0)\dot{J}_{\bar{m}} \qquad\qquad \dot{\omega}_n = \dot{R}_{n,\bar{m}}(\alpha\beta0)\omega_{\bar{m}} + R_{n,\bar{m}}(\alpha\beta0)\dot{\omega}_{\bar{m}}$$

$$= (\boldsymbol{\omega}\times\mathbf{RR}^T\mathbf{J})_n + \quad 0 \qquad (6.7.30a) \qquad\qquad = (\boldsymbol{\omega}\times\mathbf{RR}^T\boldsymbol{\omega})_n + \quad 0 \qquad (6.7.30a)$$

$$= (\boldsymbol{\omega}\times\mathbf{J})_n \qquad\qquad\qquad\qquad = (\boldsymbol{\omega}\times\boldsymbol{\omega})_n = 0$$

So LAB torque $\dot{J}_n$ is nonzero and $\vec{\mathbf{J}}$ moves in the LAB unless it is aligned with ω, but ω is fixed in *both* frames by a constraint $\alpha = \omega_3 t = \dot{\alpha}t$ of (6.7.19b) as enforced by the frictionless bearing in Fig. 6.7.1a. Results (6.7.30) for $\vec{\mathbf{J}}$ and $\dot{\vec{\mathbf{J}}}$ agree with Jacobian results (6.7.22) and time derivatives (6.7.24).

$$\boldsymbol{\omega}\times\vec{\mathbf{J}} = \begin{vmatrix} \mathbf{x}_1 & \mathbf{x}_2 & \mathbf{x}_3 \\ 0 & 0 & \omega_3 \\ J_1 & J_2 & J_3 \end{vmatrix} = \begin{pmatrix} -\omega_3 J_2 \\ \omega_3 J_1 \\ 0 \end{pmatrix} = mr^2\dot{\alpha}^2\sin\beta\cos\beta\begin{pmatrix} \sin\alpha \\ -\cos\alpha \\ 0 \end{pmatrix}$$

$\vec{\mathbf{J}}$ is LAB-moving and $\vec{\boldsymbol{\omega}}$ is LAB-fixed while both $\vec{\boldsymbol{\omega}}$ and $\vec{\mathbf{J}}$ are BOD-fixed for the constrained rotor above.

In a *free* rotor discussed next, $\vec{\mathbf{J}}$ is LAB-fixed but BOD-moving while $\vec{\boldsymbol{\omega}}$ moves in both LAB and BOD frames. By definition, a Darboux whirl $\vec{\boldsymbol{\omega}}$-vector must be a line of *instantaneous* stationary points in *both* LAB and BOD frames, but like "eyes" of hurricanes, unconstrained $\vec{\boldsymbol{\omega}}$ vectors are generally moving in both the LAB frame (as in Fig. 6.7.2b) and in the BOD frame.

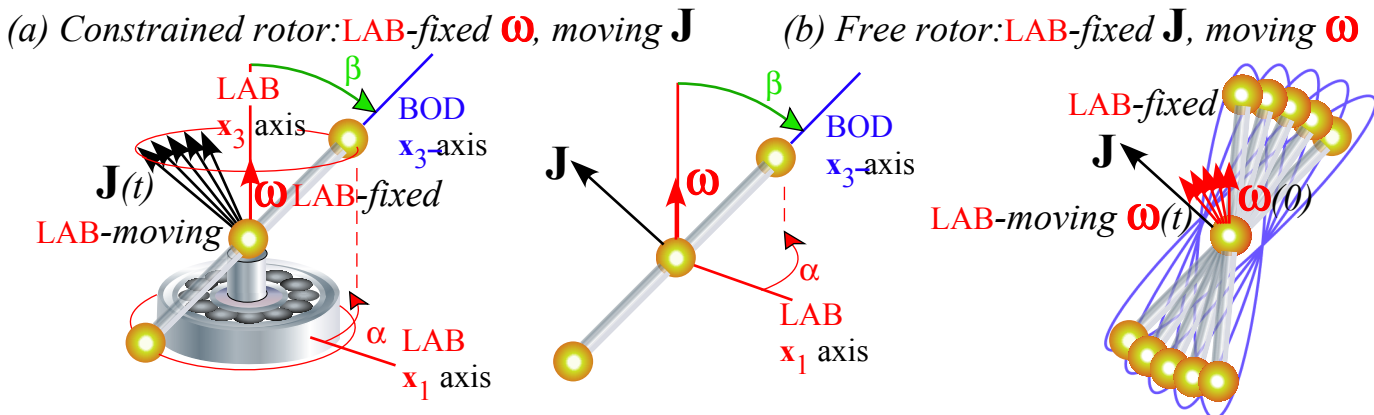*(a) Constrained rotor:*LAB-*fixed* $\boldsymbol{\omega}$*, moving* $\mathbf{J}$ *(b) Free rotor:*LAB-*fixed* $\mathbf{J}$*, moving* $\boldsymbol{\omega}$

Fig. 6.7.2 Free rotor cut loose from LAB-constraining ω-axis changes dynamics accordingly.

f. Free rigid symmetric rotor

Freeing the constrained rotor removes the constraint $c=\beta$ that made the polar angle β a constant parameter and recovers a variable β with well-defined velocity $\dot\beta$ and momentum $J_\beta = \frac{\partial L}{\partial \dot\beta}$. Breaking connection to the bearing in Fig. 6.7.2(a) lets the rotor tumble so $\dot J_\beta = \frac{\partial L}{\partial \beta}$ may vary as may azimuth angular velocity $\{\dot\alpha, \dot\gamma\}$ and momentum $\{J_\alpha = \frac{\partial L}{\partial \dot\alpha}, J_\gamma = \frac{\partial L}{\partial \dot\gamma} \dot\gamma\}$ in Euler-Hamilton-Lagrange equations (6.7.11) or (6.7.17).

Lagrangian(6.7.17) has BOD-based terms $\frac{1}{2} I_{\bar m} \omega_{\bar m}^2$ involving constants $I_{\bar m}$ and velocity $\omega_{\bar m}$. The latter relates to Euler angles (α,β,γ) and velocity $(\dot\alpha,\dot\beta,\dot\gamma)$ by Jacobian relations (6.7.5d) that are squared below.

$$\omega_{\bar 1}^2 = (-\dot\alpha \sin\beta \cos\gamma + \dot\beta \sin\gamma)^2 = \dot\alpha^2 \sin^2\beta \cos^2\gamma - 2\dot\alpha\dot\beta \sin\beta \sin\gamma \cos\gamma + \dot\beta^2 \sin^2\gamma$$
$$\omega_{\bar 2}^2 = (+\dot\alpha \sin\beta \sin\gamma + \dot\beta \cos\gamma)^2 = \dot\alpha^2 \sin^2\beta \sin^2\gamma + 2\dot\alpha\dot\beta \sin\beta \sin\gamma \cos\gamma + \dot\beta^2 \cos^2\gamma \qquad (6.7.31)$$
$$\omega_{\bar 3}^2 = (+\dot\alpha \cos\beta + \dot\gamma)^2 \qquad\quad = \dot\alpha^2 \cos^2\beta + 2\dot\alpha\dot\gamma \cos\beta + \dot\gamma^2$$

1. Free symmetric-top rotor (Euler angle view)

The rotor in Fig. 6.7.2 is called a *prolate symmetric-top rotor* since its cylindrical symmetry makes its first two inertial constants equal ($I_{\bar 1} = I_{\bar 2} = I_{II} > I_{\bar 3} = \iota$) and larger than the third ($I_{\bar 3} = \iota$). The opposite case, an *oblate* symmetric-top, is a ring or discus shaped object with ($I_{II} < I_{\bar 3}$). (Discs and rings have ($I_{II} = \frac{1}{2} I_{\bar 3}$).)
The symmetric-top Lagrangian reduces to a simpler form by cancellation in (6.7.31).

$$L_{sym-top} = \frac{1}{2} I_{II}(\omega_{\bar 1}^2 + \omega_{\bar 2}^2) + \frac{1}{2} I_{\bar 3}\omega_{\bar 3}^2 = \frac{1}{2} I_{II}(\dot\alpha^2 \sin^2\beta + \dot\beta^2) + \frac{1}{2} I_{\bar 3}(\dot\alpha \cos\beta + \dot\gamma)^2 \qquad (6.7.32a)$$

The rigid *spherical-top* Lagrangian with three equal inertia ($I_{\bar 1} = I_{\bar 2} = I_{\bar 3} = I_{III}$) further simplifies.

$$L_{sph-top} = \frac{1}{2} I_{III}(\omega_{\bar 1}^2 + \omega_{\bar 2}^2 + \omega_{\bar 3}^2) = \frac{1}{2} I_{III}(\dot\alpha^2 + \dot\beta^2 + 2\dot\alpha\dot\gamma \cos\beta + \dot\gamma^2) \qquad (6.7.32b)$$

Metric $g_{\mu\nu}$ forms (3.3.13) or (3.5.10) for $L_{sym-top}$ lead to Lagrange-Euler equations and momentum.

$$L_{sym-top} = \frac{1}{2} g_{\mu\nu}\dot\mu\dot\nu =$$

$$\frac{1}{2}\begin{pmatrix} \dot\alpha & \dot\beta & \dot\gamma \end{pmatrix}\begin{pmatrix} g_{\alpha\alpha} & g_{\alpha\beta} & g_{\alpha\gamma} \\ g_{\beta\alpha} & g_{\beta\beta} & g_{\beta\gamma} \\ g_{\gamma\alpha} & g_{\gamma\beta} & g_{\gamma\gamma} \end{pmatrix}\begin{pmatrix} \dot\alpha \\ \dot\beta \\ \dot\gamma \end{pmatrix} = \frac{1}{2}\begin{pmatrix} \dot\alpha & \dot\beta & \dot\gamma \end{pmatrix}\begin{pmatrix} I_{II}\sin^2\beta + I_{\bar 3}\cos^2\beta & 0 & I_{\bar 3}\cos\beta \\ 0 & I_{II} & 0 \\ I_{\bar 3}\cos\beta & 0 & I_{\bar 3} \end{pmatrix}\begin{pmatrix} \dot\alpha \\ \dot\beta \\ \dot\gamma \end{pmatrix} \qquad (6.7.33)$$

Covariant momentum p_μ is a Lagrangian $\frac{\partial L}{\partial \dot q^\mu}$ derivative and a linear combination $g_{\mu\nu}\dot q^\nu$ of velocity. Metric coefficients $g_{\alpha\beta}, g_{\beta\alpha}, g_{\beta\gamma}$, and $g_{\gamma\beta}$ are zero since the β axis is normal to that of α and γ. (Recall Fig. 6.6.3.)

$$J_\mu = g_{\mu\nu}\dot\nu = \frac{\partial L_{sym-top}}{\partial \dot\mu} = \begin{pmatrix} J_\alpha \\ J_\beta \\ J_\gamma \end{pmatrix} = \begin{pmatrix} g_{\alpha\alpha} & g_{\alpha\beta} & g_{\alpha\gamma} \\ g_{\beta\alpha} & g_{\beta\beta} & g_{\beta\gamma} \\ g_{\gamma\alpha} & g_{\gamma\beta} & g_{\gamma\gamma} \end{pmatrix}\begin{pmatrix} \dot\alpha \\ \dot\beta \\ \dot\gamma \end{pmatrix} = \begin{pmatrix} I_{II}\sin^2\beta + I_{\bar 3}\cos^2\beta & 0 & I_{\bar 3}\cos\beta \\ 0 & I_{II} & 0 \\ I_{\bar 3}\cos\beta & 0 & I_{\bar 3} \end{pmatrix}\begin{pmatrix} \dot\alpha \\ \dot\beta \\ \dot\gamma \end{pmatrix} \qquad (6.7.34)$$

Inverse metric relation $g^{\upsilon\mu}p_\mu$ gives velocity $\dot{q}^\upsilon$ as momentum derivative $\frac{\partial H}{\partial p_\upsilon}$ of Euler-Hamiltonian $H_{sym\text{-}top}$.

$$\dot{\upsilon}=g^{\upsilon\mu}J_\mu=\frac{\partial H_{sym\text{-}top}}{\partial J_\upsilon}=\begin{pmatrix}\dot\alpha\\\dot\beta\\\dot\gamma\end{pmatrix}=\begin{pmatrix}g^{\alpha\alpha}&g^{\alpha\beta}&g^{\alpha\gamma}\\g^{\beta\alpha}&g^{\beta\beta}&g^{\beta\gamma}\\g^{\gamma\alpha}&g^{\gamma\beta}&g^{\gamma\gamma}\end{pmatrix}\begin{pmatrix}J_\alpha\\J_\beta\\J_\gamma\end{pmatrix}=\begin{pmatrix}\dfrac{1}{I_{II}\sin^2\beta}&0&\dfrac{-\cos\beta}{I_{II}\sin^2\beta}\\[2ex]0&\dfrac{1}{I_{II}}&0\\[2ex]\dfrac{-\cos\beta}{I_{II}\sin^2\beta}&0&\dfrac{1}{I_{\bar3}}+\dfrac{\cos^2\beta}{I_{II}\sin^2\beta}\end{pmatrix}\begin{pmatrix}J_\alpha\\J_\beta\\J_\gamma\end{pmatrix}\quad(6.7.35a)$$

$$H_{sym\text{-}top}=\tfrac12 g^{\mu\upsilon}J_\mu J_\upsilon=\frac{(J_\alpha-J_\gamma\cos\beta)^2}{2I_{II}\sin^2\beta}+\frac{J_\beta^2}{2I_{II}}+\frac{J_\gamma^2}{2I_{\bar3}}\qquad(6.7.35b)$$

Momentum time derivative $\dot{p}_\mu$ or torque $\dot{J}_\upsilon$ is either coordinate derivative $\frac{\partial L}{\partial q^\mu}$ of $L_{sym\text{-}top}$ or $-\frac{\partial H}{\partial q^\mu}$ of $H_{sym\text{-}top}$.

$$\begin{pmatrix}\dot{J}_\alpha\\\dot{J}_\beta\\\dot{J}_\gamma\end{pmatrix}=\begin{pmatrix}\frac{\partial L}{\partial\alpha}\\\frac{\partial L}{\partial\beta}\\\frac{\partial L}{\partial\gamma}\end{pmatrix}=\begin{pmatrix}0\\(I_{II}-I_{\bar3})\dot\alpha^2\sin\beta\cos\beta-I_{\bar3}\dot\alpha\dot\gamma\sin\beta\\0\end{pmatrix}=\begin{pmatrix}-\frac{\partial H}{\partial\alpha}\\-\frac{\partial H}{\partial\beta}\\-\frac{\partial H}{\partial\gamma}\end{pmatrix}=\begin{pmatrix}0\\\dfrac{(J_\alpha-J_\gamma\cos\beta)(J_\alpha\cos\beta-J_\gamma)}{I_{II}\sin^3\beta}\\0\end{pmatrix}\quad(6.7.36)$$

LAB-symmetry (isotropy) makes $J_\alpha=k_\alpha$ constant, and cylindrical BOD symmetry ($I_{\bar1}=I_{\bar2}=I_{II}$) gives constant $J_\gamma=k_\gamma$. Torque $\dot{J}_\alpha$ (or $\dot{J}_\gamma$) is zero if and only if $L_{sym\text{-}top}$ or $H_{sym\text{-}top}$ are independent of α (or γ).

The factors that give torque $\dot{J}_\beta$ in (6.7.36) convert by (6.7.34) to $\dot\alpha$ and $\dot\gamma$ velocity terms below.

$$J_\alpha-J_\gamma\cos\beta=I_{II}\dot\alpha\sin^2\beta\quad(6.7.37a)\qquad\qquad J_\alpha\cos\beta-J_\gamma=(I_{II}-I_{\bar3})\dot\alpha\sin^2\beta\cos\beta-I_{\bar3}\dot\gamma\sin^2\beta\quad(6.7.37b)$$

If β or $J_\beta=I_{II}\dot\beta$ is constant then $\dot{J}_\beta$ is zero and so is one or both of (6.7.37). If LAB momentum is J on **z**-axis $(J_1,J_2,J_3)=(0,0,J)$ then (6.7.10c) gives Euler $(J_\alpha,J_\beta,J_\gamma)=(J,0,J\cos\beta)$. Then J_β and $\dot\beta=\frac{J_\beta}{I_{II}}$ are *zero*.

$$\begin{pmatrix}J_\alpha\\J_\beta\\J_\gamma\end{pmatrix}=\begin{pmatrix}0&0&1\\-\sin\alpha&\cos\alpha&0\\\cos\alpha\sin\beta&\sin\alpha\sin\beta&\cos\beta\end{pmatrix}\begin{pmatrix}0\\0\\J\end{pmatrix}=\begin{pmatrix}J\\0\\J\cos\beta\end{pmatrix}\;implies:\begin{cases}J_\alpha-J_\gamma\cos\beta=J\sin^2\beta\\J_\alpha\cos\beta-J_\gamma=0\end{cases}\quad(6.7.38)$$

(6.7.37b) is zero but (6.7.37a) is a constant $J\sin^2\beta=I_{II}\dot\alpha\sin^2\beta$ like J_3 for β-constrained rotor in (6.7.22a). Constant BOD-twist rate $\dot\gamma$ from (6.7.35a) lets a free rotor turn like a constrained rotor at LAB-rate $\dot\alpha=\frac{J}{I_{II}}$.

$$\dot\gamma=\frac{-J_\alpha\cos\beta}{I_{II}\sin^2\beta}+\frac{J_\gamma}{I_{\bar3}}+\frac{J_\gamma\cos^2\beta}{I_{II}\sin^2\beta}=\left(\frac{1}{I_{\bar3}}-\frac{1}{I_{II}}\right)J\cos\beta=\frac{I_{II}-I_{\bar3}}{I_{\bar3}}\dot\alpha\cos\beta=\frac{I_{II}-I_{\bar3}}{I_{II}I_{\bar3}}J_{\bar3}=\frac{I_{II}-I_{\bar3}}{I_{II}}\omega_{\bar3}\quad(6.7.39)$$

With constant $\dot\gamma$ and β in (6.7.10b), BOD-frame sees LAB **z**-axis or $\mathbf{J}=(J_1,J_2,J_3)=(0,0,J)$ trace a β-cone by $\bar{\mathbf{J}}=(J_{\bar1},J_{\bar2},J_{\bar3})$ given below, while the LAB-frame sees BOD $\bar{\mathbf{z}}$-axis trace its β-cone going the other way.

$$\begin{pmatrix} J_{\bar{1}} \\ J_{\bar{2}} \\ J_{\bar{3}} \end{pmatrix} = \begin{pmatrix} -\cos\gamma\csc\beta & \sin\gamma & \cot\beta\cos\gamma \\ \sin\gamma\csc\beta & \cos\gamma & -\cot\beta\sin\gamma \\ 0 & 0 & 1 \end{pmatrix} \begin{pmatrix} J \\ 0 \\ J\cos\beta \end{pmatrix} = \begin{pmatrix} -J\sin\beta\cos\gamma \\ J\sin\beta\sin\gamma \\ J\cos\beta \end{pmatrix} \qquad (6.7.40)$$

The BOD $\bar{\mathbf{J}} = J(-\sin\beta\cos\gamma, \sin\beta\sin\gamma, \cos\beta) = J\mathbf{z}$ vector matches the $\langle\mathbf{z}|$-row of $R(\alpha\beta\gamma)$-matrix (6.6.1b).

Constant $\dot\alpha$, $\dot\gamma$ and β in (6.7.5c-d) give angular velocity $\boldsymbol{\omega}$ seen in LAB and $\bar{\boldsymbol{\omega}}$ seen in BOD-frame.

$$\begin{pmatrix} \omega_1 \\ \omega_2 \\ \omega_3 \end{pmatrix} = \begin{pmatrix} 0 & -\sin\alpha & \cos\alpha\sin\beta \\ 0 & \cos\alpha & \sin\alpha\sin\beta \\ 1 & 0 & \cos\beta \end{pmatrix} \begin{pmatrix} \dot\alpha \\ 0 \\ \dot\gamma \end{pmatrix} \qquad\qquad \begin{pmatrix} \omega_{\bar{1}} \\ \omega_{\bar{2}} \\ \omega_{\bar{3}} \end{pmatrix} = \begin{pmatrix} -\sin\beta\cos\gamma & \sin\gamma & 0 \\ \sin\beta\sin\gamma & \cos\gamma & 0 \\ \cos\beta & 0 & 1 \end{pmatrix} \begin{pmatrix} \dot\alpha \\ 0 \\ \dot\gamma \end{pmatrix}$$

$$= \dot\alpha\begin{pmatrix} 0 \\ 0 \\ 1 \end{pmatrix} + \dot\gamma\begin{pmatrix} \cos\alpha\sin\beta \\ \sin\alpha\sin\beta \\ \cos\beta \end{pmatrix} = \dot\alpha\mathbf{z} + \dot\gamma\bar{\mathbf{z}} \quad (6.7.41a) \qquad = \dot\alpha\begin{pmatrix} -\sin\beta\cos\gamma \\ \sin\beta\sin\gamma \\ \cos\beta \end{pmatrix} + \dot\gamma\begin{pmatrix} 0 \\ 0 \\ 1 \end{pmatrix} = \dot\alpha\mathbf{z} + \dot\gamma\bar{\mathbf{z}} \quad (6.7.41b)$$

The $\boldsymbol{\omega}$ vector traces a *LAB-cone* as α varies in (6.7.41a), and the $\bar{\boldsymbol{\omega}}$ vector traces a *BOD-cone* as γ varies in (6.7.41b). Both cones are shown for prolate tops in Fig. 6.7.3(a-c) where the BOD-cone rolls outside the LAB-cone. For a spherical top in Fig. 6.7.3(d) the LAB-cone collapses onto the LAB-axis. For oblate tops the BOD-cone can "hula" with the LAB-cone *inside* it as in Fig. 6.7.3(e). (It shows the most-oblate case.)
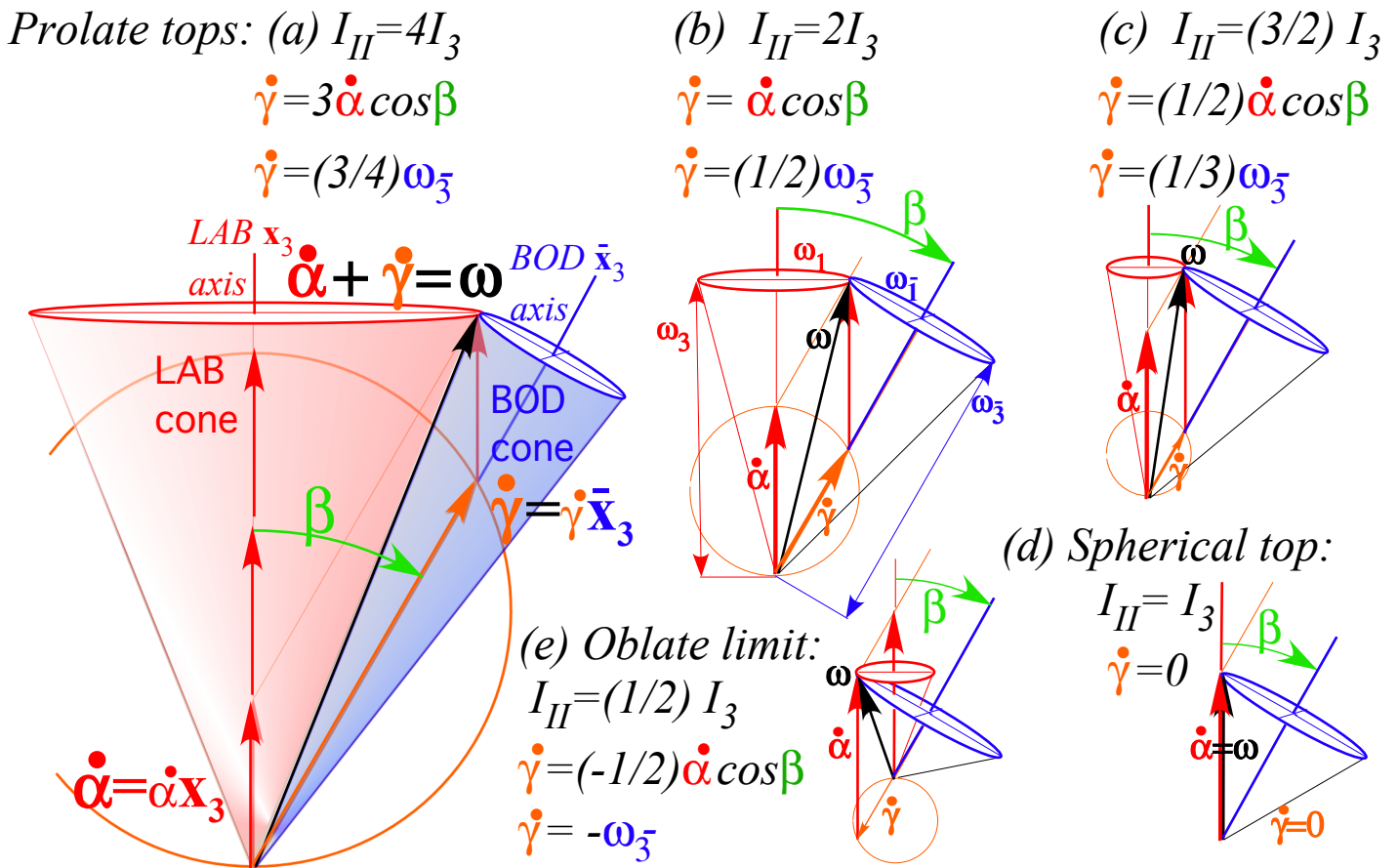

Fig. 6.7.3 Symmetric top ω-cones for β=30° and inertial ratios: (a) $\frac{I_{II}-I_3}{I_3}$ =3, (b) 1, (c) $\frac{1}{2}$, (d) 0, (e) -$\frac{1}{2}$.

2. Symmetric-top kinetic geometry

Detailed geometry of angular velocity vectors reveals the kinetic relations between LAB and BOD views. Fig. 6.7.4(a) expands on prolate case (c) of Fig. 6.7.3. Fig. 6.7.4(b) details the most-oblate case (e). The most-oblate case ($I_{\bar{3}} = 2I_{\bar{1}} = 2I_{\bar{2}}$) applies to flat symmetric *n*-sided polygonal-ring molecules for *n>2*. The most-prolate limit ($I_{\bar{3}} = \iota < I_{\bar{1}} = I_{\bar{2}}$) is a diatomic (*n=2*) molecule like Fig. 6.7.1. Each inertia eigenvalue $I_{\bar{a}}$ for a classical body is less than the sum $I_{\bar{b}} + I_{\bar{c}}$ of its other two. Each $I_{\bar{a}}$ may approach but not equal zero.

Fig. 6.7.4 is based on geometric relations (6.7.41) between Cartesian and Euler angular velocity and angular momentum relations (6.7.37) thru (6.7.40) that assumes LAB $(J_1, J_2, J_3) = (0,0,J)$ is on $\mathbf{z}=\mathbf{x}_3$-axis.

$$\omega_1 = \dot{\gamma}\sin\beta \qquad\qquad\qquad\qquad \omega_{\bar{1}} = -\dot{\alpha}\sin\beta$$
$$\omega_2 = 0 \qquad\qquad (6.7.42a) \qquad\qquad \omega_{\bar{2}} = 0 \qquad\qquad (6.7.42b)$$
$$\omega_3 = \dot{\alpha} + \dot{\gamma}\cos\beta \qquad\qquad\qquad\qquad \omega_{\bar{3}} = \dot{\alpha}\cos\beta + \dot{\gamma}$$

It is a zero-azimuth ($\alpha = 0 = \gamma$) projection of Fig. 6.7.3 onto the (ω_1, ω_3)-plane or ($\omega_{\bar{1}}, \omega_{\bar{3}}$)-plane. LAB fixed Euler α-dial and BOD fixed γ-dial compete to spin BOD points relative to LAB points.

Between $\mathbf{x}_3$ and $\bar{\mathbf{x}}_3$ is a line ω along which BOD and LAB points have for an instant zero speed relative to each other. For points on that "hurricane-eye-line" vector ω, the rotation in the LAB-frame around its $\mathbf{x}_3$-axis at rate $\dot{\alpha}$ exactly cancels the BOD-frame rotation at rate $\dot{\gamma}$ around its $\bar{\mathbf{x}}_3$ -axis.

LAB cone base radius $\omega_1 = \dot{\gamma}\sin\beta$ (Fig. 6.7.4(a) top) spins at $\dot{\alpha}$ to produce a linear "velocity" $\omega_1\dot{\alpha} = \dot{\alpha}\dot{\gamma}\sin\beta$ that exactly cancels a "velocity" $\omega_{\bar{1}}\dot{\gamma} = -\dot{\alpha}\dot{\gamma}\sin\beta$ produced by the rate $\dot{\gamma}$ of BOD base cone radius $\omega_{\bar{1}} = -\dot{\gamma}\sin\beta$ at the tip of the ω vector joining the two radii. Meanwhile, vector ω rotates at rate $\dot{\alpha}$ in concert with BOD $\bar{\mathbf{x}}_3$ axis around LAB axis $\mathbf{x}_3$ and, *vice-versa*, ω and $\mathbf{x}_3$ rotate at rate $\dot{\gamma}$ around $\bar{\mathbf{x}}_3$.

The ellipsoid $\frac{1}{2}\boldsymbol{\omega}\cdot\mathbf{I}\cdot\boldsymbol{\omega}=E$ and BOD ω-cone is fixed to its $\bar{\mathbf{x}}_3$ frame. The BOD ω-cone rolls on the LAB ω-cone like one conical gear on another. Fig. 6.7.4 shows ω-ellipsoid (6.7.27c) tangent to the LAB cone base plane that is normal to the $\mathbf{z}=\mathbf{x}_3$-axis and to angular momentum **J**. Not shown is the *J*-ellipsoid $\frac{1}{2}\mathbf{J}\cdot\mathbf{I}^{-1}\cdot\mathbf{J}=E$ (6.7.27b). The *J*-ellipsoid has a tangent plane at **J** that is always normal to ω.

BOD-frame angular momentum *J* relates to BOD-velocity ω by inertial eigen-relations $J_{\bar{a}} = I_{\bar{a}}\omega_{\bar{a}}$. LAB-frame $\mathbf{z}=\mathbf{x}_3$-axis has its direction defined here by $(J_1, J_2, J_3) = (0,0,J)$ and (6.7.39).

$$J = J_3 = I_{II}\dot{\alpha} = I_{\bar{1}}\dot{\alpha} = I_{\bar{2}}\dot{\alpha} \qquad\qquad\qquad (6.7.43a)$$

Note that LAB wobble frequency $\dot{\alpha}$ is related to *J* by $I_{II} = I_{\bar{1}} = I_{\bar{2}}$ and not by $I_{\bar{3}}$. BOD velocity and momentum involve $I_{\bar{1}} = I_{\bar{2}}$ and $I_{\bar{3}}$ as do BOD wobble frequencies $\dot{\gamma}$ and $\omega_{\bar{3}}$ in (6.7.42b).

$$J_{\bar{3}} = J\cos\beta = J_3\cos\beta = I_{\bar{1}}\dot{\alpha}\cos\beta = I_{\bar{3}}\omega_{\bar{3}} \qquad where: \omega_{\bar{3}} = \dot{\alpha}\cos\beta + \dot{\gamma} \qquad (6.7.43b)$$

$$\omega_{\bar{3}} = \frac{I_{\bar{1}}}{I_{\bar{3}}}\dot{\alpha}\cos\beta = \frac{J}{I_{\bar{3}}}\cos\beta \quad (6.7.43c) \qquad\qquad \dot{\gamma} = \frac{I_{\bar{1}} - I_{\bar{3}}}{I_{\bar{3}}}\dot{\alpha}\cos\beta = \frac{I_{\bar{1}} - I_{\bar{3}}}{I_{\bar{1}}}\omega_{\bar{3}} \qquad (6.7.43d)$$

As $I_{\bar{3}}$ approaches zero, the BOD ω-cone angle shrinks and BOD frequencies $\dot{\gamma}$ and $\omega_{\bar{3}}$ grow ever larger and more nearly equal for a given fixed momentum *J*, polar inclination angle β , and LAB frequency $\dot{\alpha}$.

(a) Prolate geometry

$I_{II}=I_1=I_2=(3/2)\,I_3$

LAB $axis$ $\mathbf{x}_3$

$\omega_1=\dot\gamma\sin\beta$

BOD $\mathbf{x}_{\bar3}$ $axis$

$\omega_{\bar1}=-\dot\alpha\sin\beta$

$\dot\alpha+\dot\gamma\cos\beta=\omega_3$

$\dot\alpha+\dot\gamma=\omega$

$\dot\alpha=J_3/I_1=J/I_1$

$\dot\alpha\cos\beta=J_{\bar3}/I_1$

$\qquad=\omega_{\bar3}I_3/I_1$

ω•I•ω=*2E*
prolate
ellipsoid

$\omega_{\bar3}=\dot\alpha\cos\beta+\dot\gamma$

$\qquad=\dot\alpha(I_1/I_3)\cos\beta$

$BOD-\bar{\mathbf{x}}_1$ $axis$

$\dot\alpha$

β

β

$\dot\gamma$

$LAB-\mathbf{x}_1$ $axis$

$\dot\gamma=\omega_{\bar3}-\dot\alpha\cos\beta$

$\quad=(\dot\alpha\cos\beta)(I_1-I_3)/I_3$

$\quad=\ \ \omega_{\bar3}\ (I_1-I_3)/I_1$

(b) Oblate geometry

$I_{II}=I_1=I_2=(1/2)\,I_3$

$\dot\alpha$

$\dot\alpha+\dot\gamma=\omega$

$\mathbf{x}_{\bar3}$

β

β

ω•I•ω=*2E*
oblate
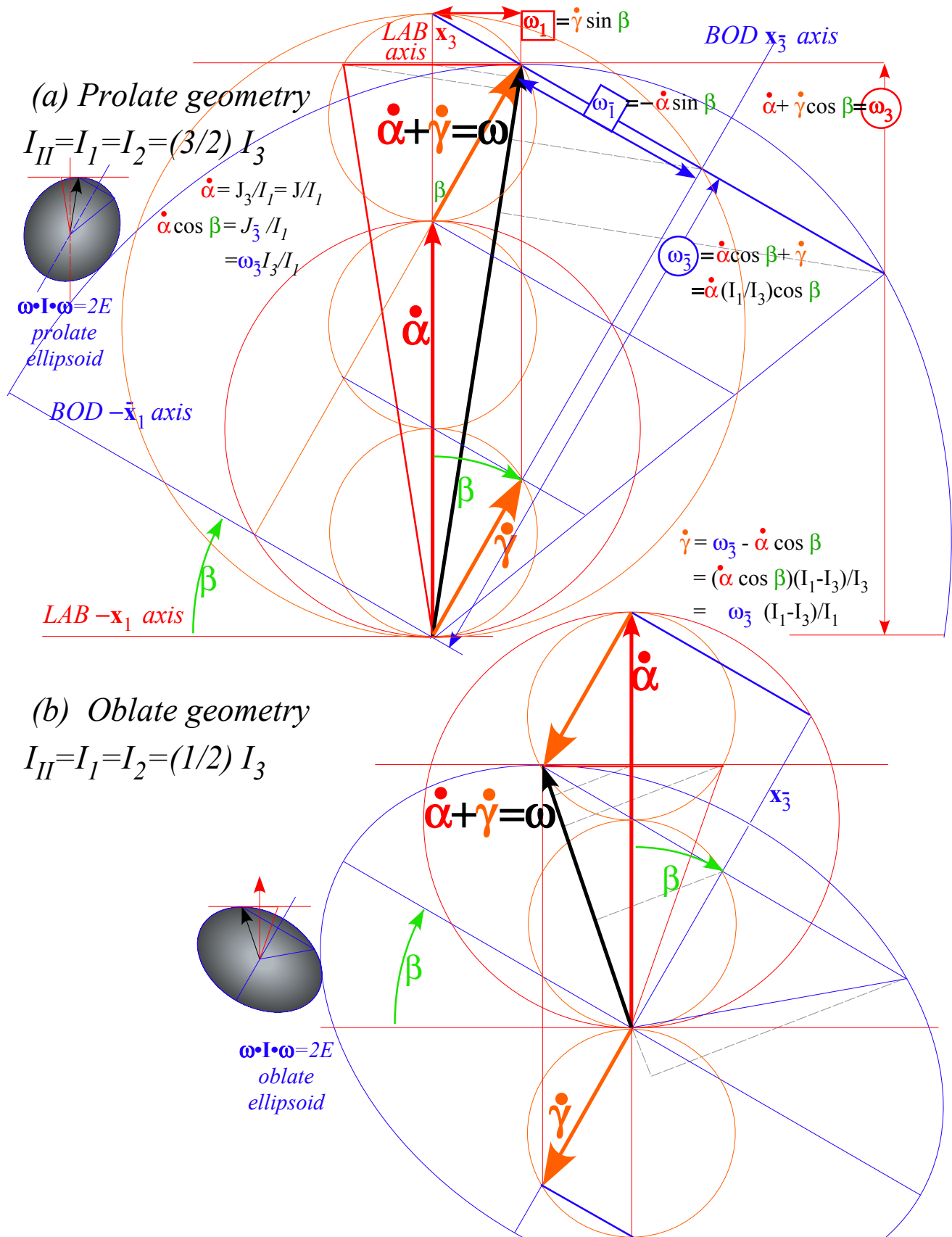*ellipsoid*

$\dot\gamma$

Fig. 6.7.4 Detailed geometry of symmetric top kinetics. (a) Prolate case. (b) Most-oblate case

3. Free rotor equations (Cartesian BOD and LAB views)

Determining conservation of a canonical momentum p_υ in Lagrangian and Hamiltonian mechanics is often just a matter of noting that its conjugate coordinate q^υ does not appear in L or H so that a momentum time derivative $\dot{p}_\upsilon = \frac{\partial L}{\partial q^\upsilon} = -\frac{\partial H}{\partial q^\upsilon}$ goes to zero with a coordinate partial derivative of either function.

    However, no simple inspection of Cartesian rotor L or H functions (6.7.27) for dependence on Cartesian-coordinate BOD angles $(\Theta_{\bar{1}},\Theta_{\bar{2}},\Theta_{\bar{3}})$ or LAB angles $(\Theta_1,\Theta_2,\Theta_3)$ is evident. The Θ are non-integral coordinates conjugate to $(J_{\bar{1}},J_{\bar{2}},J_{\bar{3}})$ or (J_1,J_2,J_3) and unable to uniquely orient a rotor. Derivatives by Θ are found by Jacobian chain links to Euler angles $(\alpha\beta\gamma)$ as in (6.7.13) and not by simple inspection.

    Jacobian derivation of time derivatives $(\dot{J}_{\bar{1}},\dot{J}_{\bar{2}},\dot{J}_{\bar{3}})$ or $(\dot{J}_1,\dot{J}_2,\dot{J}_3)$ is reduced to a page or so by doing just symmetric tops ($I_{II} = I_{\bar{1}} = I_{\bar{2}}$) with Euler $\{J_\alpha, J_\beta, J_\gamma\}$ and $\{\dot{J}_\alpha, \dot{J}_\beta, \dot{J}_\gamma\}$ given by (6.7.34) and (6.7.36).

$J_\alpha = I_{II}(\dot{\alpha}\sin^2\beta)$ $+ I_{\bar{3}}(\dot{\alpha}\cos^2\beta + \dot{\gamma}\cos\beta)$	$J_\beta = I_{II}\dot{\beta}$	$J_\gamma =$ $I_{\bar{3}}(\dot{\alpha}\cos\beta + \dot{\gamma})$
$\dot{J}_\alpha = 0$	$\dot{J}_\beta = I_{II}\dot{\alpha}^2\sin\beta\cos\beta$ $- I_{\bar{3}}(\dot{\alpha}\cos\beta + \dot{\gamma})\dot{\alpha}\sin\beta$	$\dot{J}_\gamma = 0$

$$(6.7.44)$$

The 1st- LAB momentum component derivative has the Euler chain introduced by (6.7.12).

$$\dot{J}_1 = \frac{d}{dt}[\frac{\partial L}{\partial \dot{\alpha}}\frac{\partial \dot{\alpha}}{\partial \Theta_1} + \frac{\partial L}{\partial \dot{\beta}}\frac{\partial \dot{\beta}}{\partial \Theta_1} + \frac{\partial L}{\partial \dot{\gamma}}\frac{\partial \dot{\gamma}}{\partial \Theta_1}] = \frac{\partial L}{\partial \Theta_1} = \frac{\partial L}{\partial \alpha}\frac{\partial \alpha}{\partial \Theta_1} + \frac{\partial L}{\partial \beta}\frac{\partial \beta}{\partial \Theta_1} + \frac{\partial L}{\partial \gamma}\frac{\partial \gamma}{\partial \Theta_1} + \quad \frac{\partial L}{\partial \dot{\alpha}}\frac{d}{dt}\frac{\partial \alpha}{\partial \Theta_1} + \frac{\partial L}{\partial \dot{\beta}}\frac{d}{dt}\frac{\partial \beta}{\partial \Theta_1} + \frac{\partial L}{\partial \dot{\gamma}}\frac{d}{dt}\frac{\partial \gamma}{\partial \Theta_1}$$

$$= \frac{d}{dt}[J_\alpha\frac{\partial \alpha}{\partial \Theta_1} + J_\beta\frac{\partial \beta}{\partial \Theta_1} + J_\gamma\frac{\partial \gamma}{\partial \Theta_1}] = \frac{\partial L}{\partial \Theta_1} = \dot{J}_\alpha\frac{\partial \alpha}{\partial \Theta_1} + \dot{J}_\beta\frac{\partial \beta}{\partial \Theta_1} + \dot{J}_\gamma\frac{\partial \gamma}{\partial \Theta_1} + \quad J_\alpha\frac{d}{dt}\frac{\partial \alpha}{\partial \Theta_1} + J_\beta\frac{d}{dt}\frac{\partial \beta}{\partial \Theta_1} + J_\gamma\frac{d}{dt}\frac{\partial \gamma}{\partial \Theta_1}$$

$$(6.7.45)$$

Jacobian (6.7.14b) and Euler-J (6.7.44) are sorted by inertial parameters and powers of $\dot{\alpha}$, $\dot{\beta}$, and $\dot{\gamma}$.

$$\dot{J}_1 = \dot{J}_\alpha\frac{\partial \alpha}{\partial \Theta_1} + \dot{J}_\beta\frac{\partial \beta}{\partial \Theta_1} + \dot{J}_\gamma\frac{\partial \gamma}{\partial \Theta_1} + \qquad\qquad J_\alpha\frac{d}{dt}\frac{\partial \alpha}{\partial \Theta_1} + J_\beta\frac{d}{dt}\frac{\partial \beta}{\partial \Theta_1} + J_\gamma\frac{d}{dt}\frac{\partial \gamma}{\partial \Theta_1}$$

$$= 0 + \dot{J}_\beta(-\sin\alpha) + 0 + \qquad J_\alpha\frac{d}{dt}\left(\frac{-\cos\alpha\cos\beta}{\sin\beta}\right) + J_\beta\frac{d}{dt}(-\sin\alpha) + J_\gamma\frac{d}{dt}\left(\frac{\cos\alpha}{\sin\beta}\right)$$

$$= I_{II}\left[\dot{\alpha}^2\sin\beta\cos\beta(-\sin\alpha) + \dot{\alpha}\sin^2\beta\frac{d}{dt}\left(\frac{-\cos\alpha\cos\beta}{\sin\beta}\right) + \dot{\beta}\frac{d}{dt}(-\sin\alpha) + 0\right]$$

$$+ I_{\bar{3}}\left[-(\dot{\alpha}\cos\beta+\dot{\gamma})\dot{\alpha}\sin\beta(-\sin\alpha) + (\dot{\alpha}\cos^2\beta+\dot{\gamma}\cos\beta)\frac{d}{dt}\left(\frac{-\cos\alpha\cos\beta}{\sin\beta}\right) + (\dot{\alpha}\cos\beta+\dot{\gamma})\frac{d}{dt}\left(\frac{\cos\alpha}{\sin\beta}\right)\right]$$

$$(6.7.46)$$

$$= I_{II}\left[-\dot{\alpha}^2\sin\beta\cos\beta\sin\alpha + \dot{\alpha}\sin^2\beta\left(\frac{\dot{\alpha}\sin\alpha\cos\beta}{\sin\beta} + \frac{\dot{\beta}\cos\alpha}{\sin^2\beta}\right) - \dot{\beta}\dot{\alpha}\cos\alpha + 0\right]$$

$$+ I_{\bar{3}}\left[(\dot{\alpha}^2\sin\beta\cos\beta+\dot{\gamma}\dot{\alpha}\sin\beta)\sin\alpha + (\dot{\alpha}\cos^2\beta+\dot{\gamma}\cos\beta)\left(\frac{\dot{\alpha}\sin\alpha\cos\beta}{\sin\beta} + \frac{\dot{\beta}\cos\alpha}{\sin^2\beta}\right) - (\dot{\alpha}\cos\beta+\dot{\gamma})\left(\frac{\dot{\alpha}\sin\alpha}{\sin\beta} + \frac{\dot{\beta}\cos\alpha\cos\beta}{\sin^2\beta}\right)\right]$$

The terms add up to zero $\dot{J}_1 = 0$, and similarly $\dot{J}_2 = 0 = \dot{J}_3$. (This is explained later by symmetry.)

$$\dot{J}_1 = I_{II}\left[\dot{\alpha}^2(-\sin\beta\cos\beta\sin\alpha + \sin^2\beta\,\frac{\sin\alpha\cos\beta}{\sin\beta}) + \dot{\alpha}\dot{\beta}\left(\sin^2\beta\frac{\cos\alpha}{\sin^2\beta} - \cos\alpha\right)\right] \qquad (6.7.47)$$

$$+ I_{\bar{3}}\left[\dot{\alpha}^2(\sin\beta+\frac{\cos^2\beta-1}{\sin\beta})\cos\beta\sin\alpha + \dot{\alpha}\dot{\beta}\frac{1-1}{\sin^2\beta}\cos^2\beta\cos\alpha + \dot{\alpha}\dot{\gamma}(\sin\beta+\frac{\cos^2\beta-1}{\sin\beta})\sin\alpha + \dot{\beta}\dot{\gamma}\frac{1-1}{\sin^2\beta}\cos\alpha\cos\beta\right] = 0$$

However, the BOD momentum component derivatives $(\dot{J}_{\bar{1}},\dot{J}_{\bar{2}},\dot{J}_{\bar{3}})$ do not vanish so easily.

The 1ˢᵗ- BOD torque $\dot{J}_{\bar{1}}$ has an Euler chain similar to that of $\dot{J}_1$.

$$\dot{J}_{\bar{1}} = \frac{d}{dt} \left[\frac{\partial L}{\partial \dot{\alpha}} \frac{\partial \dot{\alpha}}{\partial \dot{\Theta}_{\bar{1}}} + \frac{\partial L}{\partial \dot{\beta}} \frac{\partial \dot{\beta}}{\partial \dot{\Theta}_{\bar{1}}} + \frac{\partial L}{\partial \dot{\gamma}} \frac{\partial \dot{\gamma}}{\partial \dot{\Theta}_{\bar{1}}} \right] = \frac{\partial L}{\partial \Theta_{\bar{1}}} = \frac{\partial L}{\partial \alpha} \frac{\partial \alpha}{\partial \Theta_{\bar{1}}} + \frac{\partial L}{\partial \beta} \frac{\partial \beta}{\partial \Theta_{\bar{1}}} + \frac{\partial L}{\partial \gamma} \frac{\partial \gamma}{\partial \Theta_{\bar{1}}} + \quad \frac{\partial L}{\partial \dot{\alpha}} \frac{d}{dt} \frac{\partial \alpha}{\partial \Theta_{\bar{1}}} + \frac{\partial L}{\partial \dot{\beta}} \frac{d}{dt} \frac{\partial \beta}{\partial \Theta_{\bar{1}}} + \frac{\partial L}{\partial \dot{\gamma}} \frac{d}{dt} \frac{\partial \gamma}{\partial \Theta_{\bar{1}}}$$

$$= \frac{d}{dt} \left[J_{\alpha} \frac{\partial \alpha}{\partial \Theta_{\bar{1}}} + J_{\beta} \frac{\partial \beta}{\partial \Theta_{\bar{1}}} + J_{\gamma} \frac{\partial \gamma}{\partial \Theta_{\bar{1}}} \right] = \frac{\partial L}{\partial \Theta_{\bar{1}}} = \dot{J}_{\alpha} \frac{\partial \alpha}{\partial \Theta_{\bar{1}}} + \dot{J}_{\beta} \frac{\partial \beta}{\partial \Theta_{\bar{1}}} + \dot{J}_{\gamma} \frac{\partial \gamma}{\partial \Theta_{\bar{1}}} + \quad J_{\alpha} \frac{d}{dt} \frac{\partial \alpha}{\partial \Theta_{\bar{1}}} + J_{\beta} \frac{d}{dt} \frac{\partial \beta}{\partial \Theta_{\bar{1}}} + J_{\gamma} \frac{d}{dt} \frac{\partial \gamma}{\partial \Theta_{\bar{1}}}$$

But, Jacobian (6.7.14d) gives non-zero combinations of quadratic powers of $\dot{\alpha}$, $\dot{\beta}$, and $\dot{\gamma}$.

$$\dot{J}_{\bar{1}} = \dot{J}_{\alpha} \frac{\partial \alpha}{\partial \Theta_{\bar{1}}} + \dot{J}_{\beta} \frac{\partial \beta}{\partial \Theta_{\bar{1}}} + \dot{J}_{\gamma} \frac{\partial \gamma}{\partial \Theta_{\bar{1}}} \qquad\qquad + J_{\alpha} \frac{d}{dt} \frac{\partial \alpha}{\partial \Theta_{\bar{1}}} \qquad\qquad + J_{\beta} \frac{d}{dt} \frac{\partial \beta}{\partial \Theta_{\bar{1}}} \qquad + J_{\gamma} \frac{d}{dt} \frac{\partial \gamma}{\partial \Theta_{\bar{1}}}$$

$$= 0 \quad + \dot{J}_{\beta}(\sin \gamma) + 0 \qquad\qquad + J_{\alpha} \frac{d}{dt}\left(\frac{-\cos \gamma}{\sin \beta} \right) \qquad + J_{\beta} \frac{d}{dt}(\sin \gamma) \quad + J_{\gamma} \frac{d}{dt}\left(\frac{\cos \gamma \cos \beta}{\sin \beta} \right)$$

$$= I_{II} \left[\dot{\alpha}^2 \sin \beta \cos \beta \sin \gamma \qquad\qquad + \dot{\alpha} \sin^2 \beta \left(\frac{\dot{\gamma} \sin \gamma}{\sin \beta} + \frac{\dot{\beta} \cos \gamma \cos \beta}{\sin^2 \beta} \right) + \dot{\beta} \dot{\gamma} \cos \gamma \qquad + 0 \right] \qquad (6.7.48)$$

$$+ I_{\bar{3}} \left[-(\dot{\alpha} \cos \beta + \dot{\gamma}) \dot{\alpha} \sin \beta \sin \gamma \quad + (\dot{\alpha} \cos^2 \beta + \dot{\gamma} \cos \beta) \left(\frac{\dot{\gamma} \sin \gamma}{\sin \beta} + \frac{\dot{\beta} \cos \gamma \cos \beta}{\sin^2 \beta} \right) \qquad - (\dot{\alpha} \cos \beta + \dot{\gamma}) \left(\frac{\dot{\gamma} \sin \gamma \cos \beta}{\sin \beta} + \frac{\dot{\beta} \cos \gamma}{\sin^2 \beta} \right) \right]$$

Torque $\dot{J}_{\bar{1}}$ reduces to a quadratic $\omega_{\bar{2}} \omega_{\bar{3}}$ of BOD velocity from (6.7.5d). (So does $\dot{J}_{\bar{2}}$, but $\dot{J}_{\bar{3}}$ is zero here.)

$$\dot{J}_{\bar{1}} = (I_{II} - I_{\bar{3}}) \left[\dot{\alpha}^2 \sin \beta \cos \beta \sin \gamma + \dot{\alpha} \dot{\beta} \cos \beta \cos \gamma + \dot{\alpha} \dot{\gamma} \sin \beta \sin \gamma + \dot{\beta} \dot{\gamma} \cos \gamma \right] = (I_{II} - I_{\bar{3}}) \omega_{\bar{2}} \omega_{\bar{3}}$$

$$\dot{J}_{\bar{2}} = (I_{II} - I_{\bar{3}}) \left[\dot{\alpha}^2 \sin \beta \cos \beta \cos \gamma - \dot{\alpha} \dot{\beta} \cos \beta \sin \gamma + \dot{\alpha} \dot{\gamma} \sin \beta \cos \gamma - \dot{\beta} \dot{\gamma} \sin \gamma \right] = -(I_{II} - I_{\bar{3}}) \omega_{\bar{1}} \omega_{\bar{3}} \quad (6.7.49)$$

$$\dot{J}_{\bar{3}} = 0$$

The zero of $\dot{J}_{\bar{3}}$ is for a special case, the *symmetric-top* Lagrangian (6.7.32a) with two equal inertia ($I_{II} = I_{\bar{1}} = I_{\bar{2}}$). For the *spherical-top* Lagrangian (6.7.32b) all three inertia are equal ($I_{\bar{1}} = I_{\bar{2}} = I_{\bar{3}}$) and that means all three BOD torques in (6.7.49) are zero. A general rigid rotor is an *asymmetric-top* that has no inertial degeneracy ($I_{\bar{1}} \neq I_{\bar{2}} \neq I_{\bar{3}} \neq I_{\bar{1}}$) and obeys *Euler-Hamilton equations* that have no zero BOD torques.

$$\dot{J}_{\bar{1}} = (I_{\bar{2}} - I_{\bar{3}}) \omega_{\bar{2}} \omega_{\bar{3}} = \frac{I_{\bar{2}} - I_{\bar{3}}}{I_{\bar{2}} I_{\bar{3}}} J_{\bar{2}} J_{\bar{3}}$$

$$\dot{J}_{\bar{2}} = (I_{\bar{3}} - I_{\bar{1}}) \omega_{\bar{3}} \omega_{\bar{1}} = \frac{I_{\bar{3}} - I_{\bar{1}}}{I_{\bar{3}} I_{\bar{1}}} J_{\bar{3}} J_{\bar{1}} \qquad\qquad (6.7.50)$$

$$\dot{J}_{\bar{3}} = (I_{\bar{1}} - I_{\bar{2}}) \omega_{\bar{1}} \omega_{\bar{2}} = \frac{I_{\bar{1}} - I_{\bar{2}}}{I_{\bar{1}} I_{\bar{2}}} J_{\bar{1}} J_{\bar{2}}$$

The Euler-Jacobian algebra of asymmetric top Lagrangians needed to prove (6.7.50) begins with a generalization of (6.7.33) and (6.7.44) and is quite a bit more formidable than the above. It becomes still worse for deformable and coupled rotors. The following Section 6.8 explores some alternative techniques for dealing with (6.7.50) as well as more advanced problems including those of quantum molecular rotors that undergo centrifugal and Coriolis distortion.

Oblate limit:
$I_{II}=(1/2) I_3$

$\dot{\gamma}=(-1/2)\dot{\alpha}\,cos\beta$

$\dot{\gamma}= -\omega_3$

$\dot{\gamma} = \omega_{\bar{3}} - \dot{\alpha}\cos\beta$
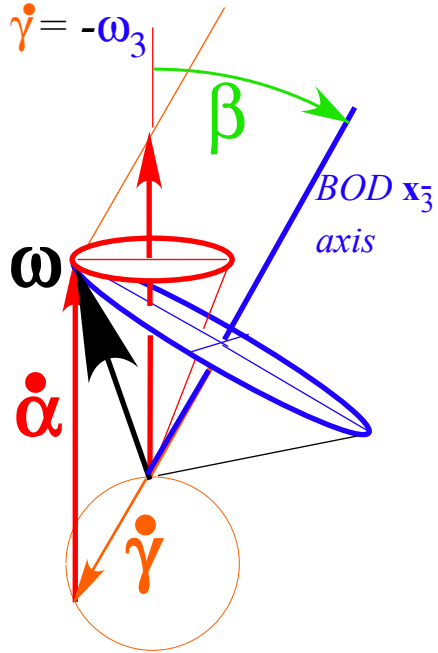
$= (\dot{\alpha}\cos\beta)(I_1-I_3)/I_3$

$= \omega_{\bar{3}}\,(I_1-I_3)/I_1$

Very prolate top: $I_{II}=9I_3$

$\dot{\gamma}=8\dot{\alpha}\,cos\beta$

$\dot{\gamma}=(8/9)\omega_{\bar{3}}$
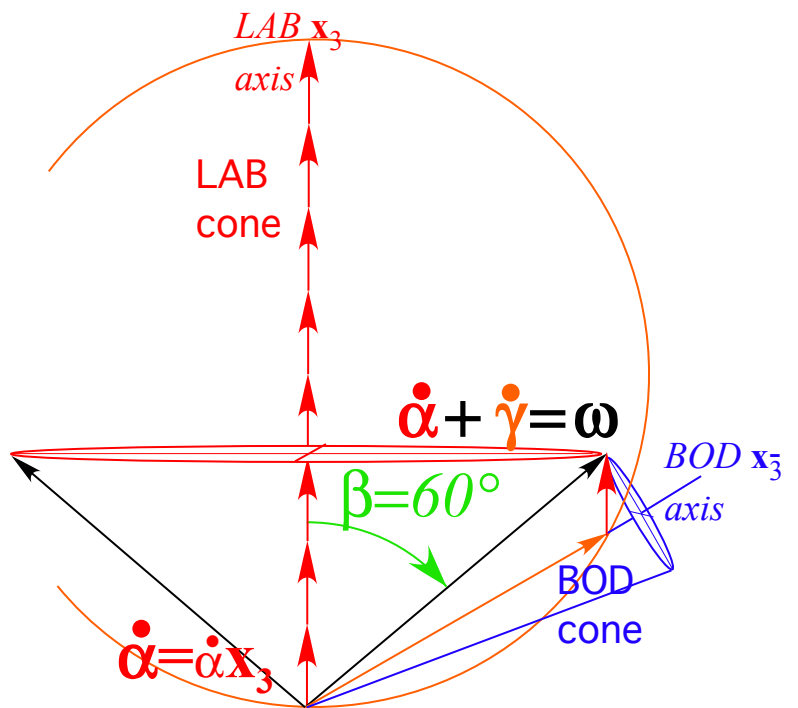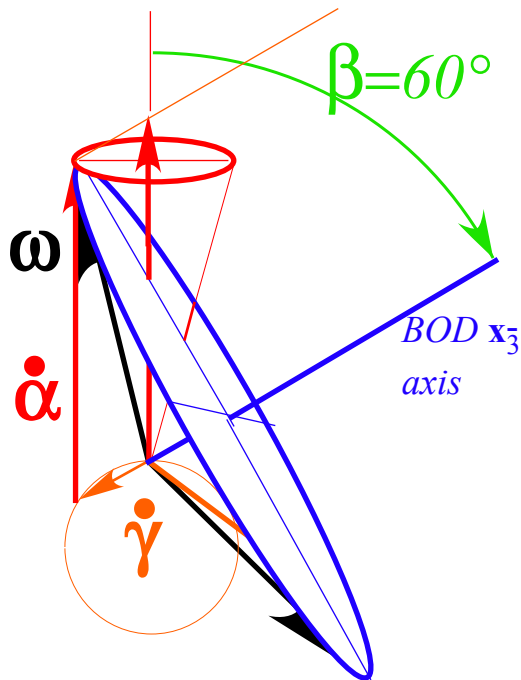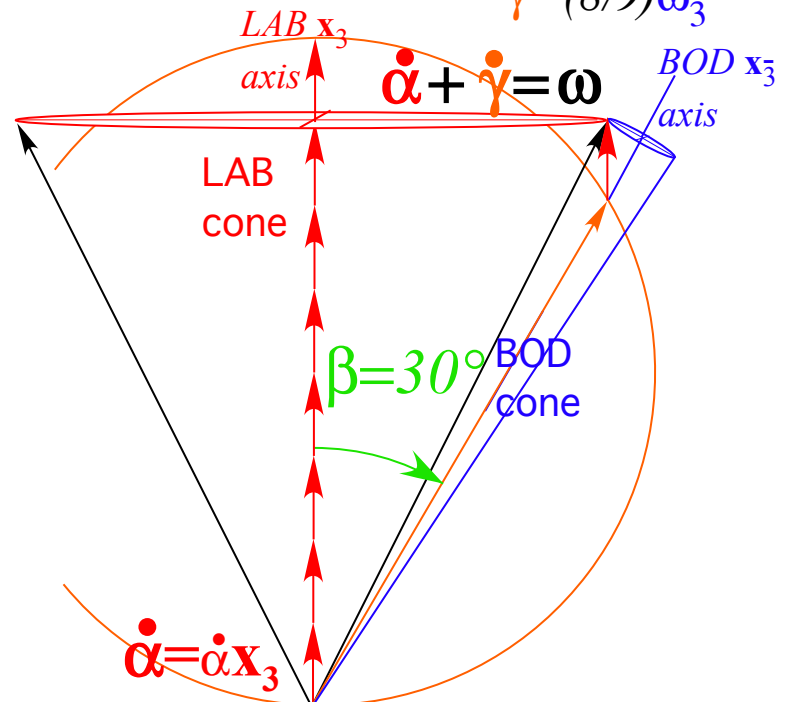
Fig. 6.7.5 Extreme cases (Oblate vs. Prolate) of symmetric-top geometry.

Chapter 6.8 Symmetry and dynamics of rotors

The Euler-Jacobian approach of preceding sections has a complexity due to mixing geometric symmetry relations such as $\mathbf{J}=\mathbf{R}\cdot\overline{\mathbf{J}}$ with physical ones like $\dot{\mathbf{j}}=\frac{\partial L}{\partial\Theta}$ or $\dot{\overline{\mathbf{J}}}=\frac{\partial L}{\partial\Theta}$ that depend on a particular Lagrangian function L. The latter grow in complexity with the internal physics of a rotor, but the former do not.

a. Asymmetic rotor equations

Euler equations (6.7.50) are mainly rotational geometry and symmetry relations of whirl vectors ω of a 3D rotation $\mathbf{R}[\omega\cdot t]=e^{\mathbf{\epsilon}\cdot\omega\cdot t}$. Levi-Civita matrix $\mathbf{\epsilon}_K$ plays the same role that Pauli $\frac{l}{2}\mathbf{\sigma}_K$ plays in 2D rotations.

$$\left(\mathbf{\epsilon}_K\right)_{JL}=\varepsilon_{JKL}=\begin{cases}+1\text{ if }\{JKL\}\text{ is EVEN permuation of }\{123\},\\ -1\text{ if }\{JKL\}\text{ is ODD permuation of }\{123\},\\ 0\qquad\qquad\text{otherwise.}\end{cases}\qquad(6.8.1)$$

Euler equations of motion arise from time derivatives of rotation relations like (6.7.25).

$$\mathbf{J}=\mathbf{R}(\alpha\beta\gamma)\cdot\overline{\mathbf{J}}\ \ represented\ by:\ \begin{pmatrix}J_1\\J_2\\J_3\end{pmatrix}=R(\alpha\beta\gamma)\cdot\begin{pmatrix}J_{\overline{1}}\\J_{\overline{2}}\\J_{\overline{3}}\end{pmatrix}\ \ example:\ \begin{pmatrix}J\cos\alpha\sin\beta\\J\sin\alpha\sin\beta\\J\cos\beta\end{pmatrix}=R(\alpha\beta\gamma)\begin{pmatrix}0\\0\\J\end{pmatrix}\qquad(6.8.2)$$

The example uses a 3D Euler R-matrix (6.6.1) that must equal the Darboux $\mathbf{R}[\omega\cdot t]$-matrix in (6.6.15).

    Time derivative of LAB $\mathbf{J}=\mathbf{R}\cdot\overline{\mathbf{J}}$ is zero by (6.7.47). (Zero LAB-based torque conserves LAB $\mathbf{J}$.)

$$\frac{d}{dt}\left(\mathbf{R}[\omega\cdot t]\cdot\overline{\mathbf{J}}\right)=\frac{d}{dt}\mathbf{J}=0=\frac{d}{dt}\left(\mathbf{R}[\omega\cdot t]\right)\cdot\overline{\mathbf{J}}+\mathbf{R}[\omega\cdot t]\cdot\frac{d}{dt}\left(\overline{\mathbf{J}}\right)\qquad(6.8.3a)$$

$$\dot{\mathbf{J}}=0=\quad\dot{\mathbf{R}}[\omega\cdot t]\cdot\overline{\mathbf{J}}+\mathbf{R}[\omega\cdot t]\cdot\dot{\overline{\mathbf{J}}}\qquad(6.8.3b)$$

Rotation operator $\mathbf{R}[\omega\cdot t]=e^{\mathbf{\epsilon}\cdot\omega\cdot t}$ has a simple time derivative of its exponential form.

$$\dot{\mathbf{R}}[\omega\cdot t]=\frac{d}{dt}e^{\mathbf{\epsilon}\cdot\omega\cdot t}=e^{\mathbf{\epsilon}\cdot\omega\cdot t}\mathbf{\epsilon}\cdot\omega=\mathbf{R}[\omega\cdot t]\mathbf{\epsilon}\cdot\omega\qquad(6.8.4a)$$

This converts the LAB $\mathbf{J}$ conservation relation (6.8.3b) into a BOD equation of motion.

$$\dot{\mathbf{J}}=\mathbf{R}[\omega\cdot t]\mathbf{\epsilon}\cdot\omega\cdot\overline{\mathbf{J}}+\mathbf{R}[\omega\cdot t]\cdot\dot{\overline{\mathbf{J}}}(=0\ for\ free\ rotor)\qquad(6.8.4b)$$

Inverse rotation $\mathbf{R}^{-1}[\omega\cdot t]$ gives equations that hold *regardless of Lagrangian L or Hamiltonian H.*

$$\dot{\overline{\mathbf{J}}}=\mathbf{R}^{-1}[\omega\cdot t]\cdot\dot{\mathbf{J}}-\mathbf{\epsilon}\cdot\omega\cdot\overline{\mathbf{J}}(=0-\mathbf{\epsilon}\cdot\omega\cdot\overline{\mathbf{J}}\ for\ free\ rotor)\qquad(6.8.5a)$$

BOD-frame components use (6.8.1). They resemble Euler equations (6.7.50) but need L or H relations.

$$\begin{aligned}\dot{J}_{\overline{1}}&=-\varepsilon_{\overline{1}KL}\omega_{\overline{K}}J_{\overline{L}}=-\varepsilon_{\overline{1}23}\omega_{\overline{2}}J_{\overline{3}}-\varepsilon_{\overline{1}32}\omega_{\overline{3}}J_{\overline{2}}\qquad&\dot{J}_{\overline{1}}&=\omega_{\overline{3}}J_{\overline{2}}-\omega_{\overline{2}}J_{\overline{3}}=-\overline{\omega}\times\overline{\mathbf{J}}\big|_{\overline{1}}\\ \dot{J}_{\overline{2}}&=-\varepsilon_{\overline{2}KL}\omega_{\overline{K}}J_{\overline{L}}=-\varepsilon_{\overline{2}31}\omega_{\overline{3}}J_{\overline{1}}-\varepsilon_{\overline{2}13}\omega_{\overline{1}}J_{\overline{3}}\qquad&\dot{J}_{\overline{2}}&=\omega_{\overline{1}}J_{\overline{3}}-\omega_{\overline{3}}J_{\overline{1}}=-\overline{\omega}\times\overline{\mathbf{J}}\big|_{\overline{2}}\\ \dot{J}_{\overline{3}}&=-\varepsilon_{\overline{3}KL}\omega_{\overline{K}}J_{\overline{L}}=-\varepsilon_{\overline{3}12}\omega_{\overline{1}}J_{\overline{2}}-\varepsilon_{\overline{3}21}\omega_{\overline{2}}J_{\overline{1}}\qquad&\dot{J}_{\overline{3}}&=\omega_{\overline{2}}J_{\overline{1}}-\omega_{\overline{1}}J_{\overline{2}}=-\overline{\omega}\times\overline{\mathbf{J}}\big|_{\overline{3}}\end{aligned}\qquad(6.8.5b)$$

Lagrangian (6.7.27) gives $J_{\overline{K}}$ in terms of $\omega_{\overline{K}}$ by $J_{\overline{K}}=\frac{\partial L}{\partial\omega_{\overline{K}}}=I_{\overline{K}}\omega_{\overline{K}}$ and the Hamiltonian gives $\omega_{\overline{K}}$ in terms of $J_{\overline{K}}$ by $\omega_{\overline{K}}=\frac{\partial H}{\partial J_{\overline{K}}}=J_{\overline{K}}/I_{\overline{K}}$, so *Euler-Lagrange* and *Euler-Hamilton* free-rigid-rotor equations(6.7.50) emerge.

$$I_{\bar{1}}\dot{\omega}_{\bar{1}} = (I_{\bar{2}} - I_{\bar{3}})\omega_{\bar{2}}\omega_{\bar{3}}$$

$$I_{\bar{2}}\dot{\omega}_{\bar{2}} = (I_{\bar{3}} - I_{\bar{1}})\omega_{\bar{3}}\omega_{\bar{1}} \quad (6.8.5c)$$

$$I_{\bar{3}}\dot{\omega}_{\bar{3}} = (I_{\bar{1}} - I_{\bar{2}})\omega_{\bar{1}}\omega_{\bar{2}}$$

$$\dot{J}_{\bar{1}} = (I_{\bar{3}}^{-1} - I_{\bar{2}}^{-1})J_{\bar{2}}J_{\bar{3}} = [(I_{\bar{2}} - I_{\bar{3}})/I_{\bar{2}}I_{\bar{3}}]J_{\bar{2}}J_{\bar{3}}$$

$$\dot{J}_{\bar{2}} = (I_{\bar{1}}^{-1} - I_{\bar{3}}^{-1})J_{\bar{3}}J_{\bar{1}} = [(I_{\bar{3}} - I_{\bar{1}})/I_{\bar{3}}I_{\bar{1}}]J_{\bar{3}}J_{\bar{1}} \quad (6.8.5d)$$

$$\dot{J}_{\bar{3}} = (I_{\bar{2}}^{-1} - I_{\bar{1}}^{-1})J_{\bar{1}}J_{\bar{2}} = [(I_{\bar{1}} - I_{\bar{2}})/I_{\bar{1}}I_{\bar{2}}]J_{\bar{1}}J_{\bar{2}}$$

(6.8.5) are non-linear with one constant, say $b = (I_{\bar{3}} - I_{\bar{1}})/I_{\bar{3}}I_{\bar{1}}$, of opposite sign if ($I_{\bar{1}} > I_{\bar{2}} > I_{\bar{3}}$).

$$\dot{x} = +|a|\, yz, \quad \dot{y} = -|b|\, zx, \quad \dot{z} = +|c|\, xy.$$

The intermediate variable $y = J_{\bar{2}}$ must blow up but the other two $x = J_{\bar{1}}$ and $z = J_{\bar{3}}$ may do small oscillation. If x and y are small compared to z then $\dot{z} \sim 0$ so $z = J$ is quasi-constant and x and y quasi-harmonic $e^{\pm i\Omega t}$.

$$\ddot{x} \simeq -|a|\,\dot{y}z \simeq -|a||b|\, z^2 x, \quad \ddot{y} \simeq -|a||b|\, z^2 y, \quad \dot{z} \simeq 0.$$

Oscillation frequency is a geometric mean of precession frequencies like (6.7.39) for symmetric tops.

$$\Omega_{x,y}^{z} = \sqrt{|a||b|\, z^2} = \frac{J}{I_{\bar{3}}}\sqrt{\frac{(I_{\bar{1}} - I_{\bar{3}})(I_{\bar{2}} - I_{\bar{3}})}{I_{\bar{1}}I_{\bar{2}}}} \left(\begin{array}{c} \uparrow clockwise \downarrow \\ \uparrow \text{around-}z \prec_{x}^{y} \downarrow \end{array} \right)_{I_{\bar{1}} > I_{\bar{2}} > I_{\bar{3}}} \quad (6.8.6a)$$

$$\Omega_{y,z}^{x} = \sqrt{|b||c|\, z^2} = \frac{J}{I_{\bar{1}}}\sqrt{\frac{(I_{\bar{1}} - I_{\bar{2}})(I_{\bar{1}} - I_{\bar{3}})}{I_{\bar{2}}I_{\bar{3}}}} \left(\begin{array}{c} \downarrow anti\text{-}clockwise \uparrow \\ \downarrow \text{around-}x \prec_{y}^{z} \uparrow \end{array} \right)_{I_{\bar{1}} > I_{\bar{2}} > I_{\bar{3}}} \quad (6.8.6b)$$

But, if x and z are small compared to y then $\dot{y} \sim 0$ so $y = J$ is quasi-constant and x and z quasi-hyperbolic $e^{\pm \Xi t}$.

$$\Xi_{x,z}^{y} = \sqrt{|a||c|\, y^2} = \frac{J}{I_{\bar{2}}}\sqrt{\frac{(I_{\bar{1}} - I_{\bar{2}})(I_{\bar{2}} - I_{\bar{3}})}{I_{\bar{1}}I_{\bar{3}}}} \left(\begin{array}{c} \leftarrow hyperbolic \rightarrow \\ \rightarrow \text{to\&from-}y \prec_{x}^{z} \leftarrow \end{array} \right)_{I_{\bar{1}} > I_{\bar{2}} > I_{\bar{3}}} \quad (6.8.6c)$$

b. Asymmetic rotor surfaces of rotational energy

To visualize nonlinear motion of asymmetric rotors and as well as non-rigid rotors we introduce methods to plot their position, velocity, momentum and energy functions. Two of these are *constant energy (CE) surfaces* that have been mentioned in regard to symmetric tops in Fig. 6.7.1 and Fig. 6.7.4 that also show a constant-energy ω-velocity-ellipsoid (6.7.27c) with a CE plot of a J-momentum-ellipsoid (6.7.27b). Also, recall earlier discussions in Fig. 6.5.2 and 6.5.3 of body coordinate or BOD-frame ellipsoid plots.

Another kind of surface used in molecular physics is a *constant-J surface* or *rotational energy (RE)* surface. To draw an RE surface (RES) one plots rotational energy *E(J)* along the BOD **J**-vector with length |**J**|=*J*=| **J**| constant. Orthogonal rotation (6.7.25a) relates LAB-**J** to BOD-**J**=**R**·**J** so length |**J**| equals length |**J**|.

$$|\,\mathbf{J}\,| = \sqrt{\mathbf{J}^T \bullet \mathbf{J}} = \sqrt{(\mathbf{R} \bullet \mathbf{J})^T \bullet \mathbf{R} \bullet \mathbf{J}} = \sqrt{\mathbf{J}^T \mathbf{R}^T \bullet \mathbf{R} \bullet \mathbf{J}} = \sqrt{\mathbf{J}^T \bullet \mathbf{J}} = |\,\mathbf{J}\,|$$

If LAB-torque is zero ($\dot{J}_a = 0$) then LAB-**J** and therefore |**J**| and |**J**| are constant even if BOD-**J** or $J_{\bar{b}}$ are not.

The RE and CE surfaces are complimentary plots of the energy function $E(\bar{\mathbf{J}})$ from (6.7.27a).

$$E(\bar{\mathbf{J}}) = \frac{J_{\bar{1}}^2}{2I_{\bar{1}}} + \frac{J_{\bar{2}}^2}{2I_{\bar{2}}} + \frac{J_{\bar{3}}^2}{2I_{\bar{3}}} \qquad (6.7.27)_{repeated}$$

An RE surface plots radii *E* for fixed *J vs* BOD-angles (β, γ) of $(\hat{J}_{\bar{1}}, \hat{J}_{\bar{2}}, \hat{J}_{\bar{3}}) = (-\cos\gamma \sin\beta, \sin\gamma \sin\beta, \cos\beta)$.

$$r_{RE} = E(J, \hat{\bar{\mathbf{J}}}) = \frac{J_{\bar{1}}^2}{2I_{\bar{1}}} + \frac{J_{\bar{2}}^2}{2I_{\bar{2}}} + \frac{J_{\bar{3}}^2}{2I_{\bar{3}}} = \frac{J^2 \cos^2 \gamma \sin^2 \beta}{2I_{\bar{1}}} + \frac{J^2 \sin^2 \gamma \sin^2 \beta}{2I_{\bar{2}}} + \frac{J^2 \cos^2 \beta}{2I_{\bar{3}}} \qquad (6.8.7)$$

A CE surface plots radii J for fixed E *vs* BOD-angles (β, γ) of $(J_{\bar{1}}, J_{\bar{2}}, J_{\bar{3}}) = (-J \cos \gamma \sin \beta, J \sin \gamma \sin \beta, J \cos \beta)$.

$$r_{CE} = J(E, \bar{\mathbf{J}}) = \sqrt{\frac{E}{\dfrac{\cos^2 \gamma \sin^2 \beta}{2I_{\bar{1}}} + \dfrac{\sin^2 \gamma \sin^2 \beta}{2I_{\bar{2}}} + \dfrac{\cos^2 \beta}{2I_{\bar{3}}}}} \qquad (6.8.8)$$

An RE surface contains a range of different E-levels for a given J-value, as is useful for molecular levels. A CE surface is *vice-versa*. It contains a range of J-values that are allowed for a given energy E.
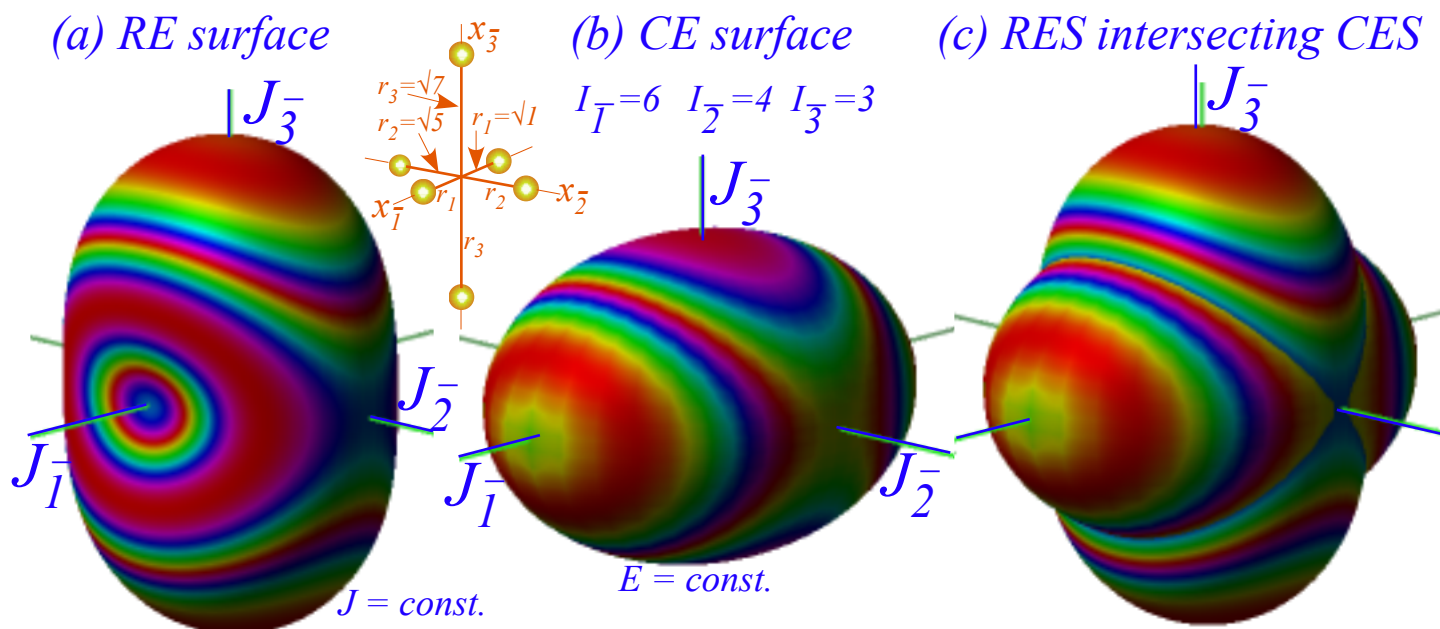

Fig. 6.8.1 Rigid rotor surfaces (a) RES polynomial, (b) CES ellipsoid, and (c) RES and CES intersected.

The CES in Fig. 6.8.1(b) is an ellipsoid though its equation (6.8.8) is not the standard form of (6.7.27b). The RES in Fig. 6.8.1(a) is not an ellipsoid but a $J_{\bar{b}}$ -polynomial whose *min*, *mid*, and *max* $(J_{\bar{1}} J_{\bar{2}} J_{\bar{3}})$ values lie on *min*, *mid*,

and *max* $(x_{\bar{1}} x_{\bar{2}} x_{\bar{3}})$ -BOD-radii *($r_1 < r_2 < r_3$)* of the rotor shown between its RES and CES plots.

$$\frac{1}{I_{\bar{1}}} : \frac{1}{I_{\bar{2}}} : \frac{1}{I_{\bar{3}}} = \frac{1}{2m(r_2^2 + r_3^2)} : \frac{1}{2m(r_1^2 + r_3^2)} : \frac{1}{2m(r_1^2 + r_2^2)} = \frac{1}{6} : \frac{1}{4} : \frac{1}{3} \qquad (6.8.8a)$$

The RES has a shape commensurate with the rotor itself. In contrast, a CES ellipsoid in Fig. 6.8.1(b) has an inverse shape with *major*, *middle*, and *minor* radii *($a < b < c$)* along *min*, *mid*, and *max* $(J_{\bar{1}} J_{\bar{2}} J_{\bar{3}})$ axes.

$$6 : 4 : 3 = I_{\bar{1}} : I_{\bar{2}} : I_{\bar{3}} = 2m(r_2^2 + r_3^2) : 2m(r_1^2 + r_3^2) : 2m(r_1^2 + r_2^2) = 2a^2 E : 2b^2 E : 2c^2 E \qquad (6.8.8b)$$

The CES aspect ratios are reciprocals of those of the RES, but both share the same level contours that are colored bands in Fig. 6.8.1. Level contours are lines of equal radius or level where the surface intersects a sphere, a constant-J sphere for a CES, but a constant-E sphere for an RES. BOD-$\hat{\bar{\mathbf{J}}}$ -paths conserve both J and E so CES and RES contours trace the same $\hat{\bar{\mathbf{J}}}$ -directions of the LAB $\mathbf{J} = J\hat{\mathbf{z}}$ axis in BOD space.

The contour being shared in Fig. 6.8.1(c) is a special one. It forms a *separatrix* that intersects the *saddle points* on the intermediate $\pm J_{\bar{2}}$ -axes. Setting $J_{\bar{1}}=0=J_{\bar{3}}$ and $J_{\bar{2}} = J$ in (6.8.7) gives the following.

$$E = 0 + \frac{J^2}{2I_{\bar{2}}} + 0 = \frac{J^2 \cos^2 \gamma_A \sin^2 \beta_A}{2I_{\bar{1}}} + \frac{J^2 \sin^2 \gamma_A \sin^2 \beta_A}{2I_{\bar{2}}} + \frac{J^2 \cos^2 \beta_A}{2I_{\bar{3}}}$$

$$= \frac{J^2 \sin^2 \gamma_B \sin^2 \beta_B}{2I_{\bar{1}}} + \frac{J^2 \cos^2 \beta_B}{2I_{\bar{2}}} + \frac{J^2 \cos^2 \gamma_B \sin^2 \beta_B}{2I_{\bar{3}}} \qquad (6.8.9)$$

Here (4.4.25b) shuffles angles so the intermediate $I_{\bar{2}}$ axis has polar angle β_B. Then, $J^2 \sin^2 \beta_B$ factors out. The separatrix is a pair of circles lying in planes of constant $I_{\bar{2}}$ -axial azimuth $\pm \gamma_B$ with $2\gamma_B$ between them.

$$\sin \gamma_B = \pm \sqrt{\frac{I_{\bar{1}}}{I_{\bar{2}}}} \sqrt{\frac{I_{\bar{3}} - I_{\bar{2}}}{I_{\bar{3}} - I_{\bar{1}}}} \qquad \cos \gamma_B = \pm \sqrt{\frac{I_{\bar{3}}}{I_{\bar{2}}}} \sqrt{\frac{I_{\bar{1}} - I_{\bar{2}}}{I_{\bar{1}} - I_{\bar{3}}}} \qquad \tan \gamma_B = \pm \sqrt{\frac{I_{\bar{1}}}{I_{\bar{3}}}} \sqrt{\frac{I_{\bar{2}} - I_{\bar{3}}}{I_{\bar{1}} - I_{\bar{2}}}} \qquad (6.8.10)$$

For inertia $(I_{\bar{1}}, I_{\bar{2}}, I_{\bar{3}}) = (6,4,3)$ used in Fig. 6.8.1, separatrix *circles* lie at right angles on $\gamma_B = \pm 45°$ planes.

The intermediate value $I_{\bar{2}} = 4$ in Fig. 6.8.1 has maximum asymmetry for $I_{\bar{1}} = 6$ and $I_{\bar{2}} = 3$. If $I_{\bar{2}}$ grows toward the high $I_{\bar{1}} = 6$ value, a more *prolate* RES emerges in Fig. 6.8.2(a-b) as shrinking separatrix-circles approach $\gamma_B = \pm 90°$ to swallow a min-energy CES. As $I_{\bar{2}}$ nears the lowest value $I_{\bar{2}} = 3$ as in Fig. 6.8.2(c), an increasingly *oblate* RES is swallowed by separatrix-circles closing on $\gamma_B = 0°$ inside a max-energy CES.
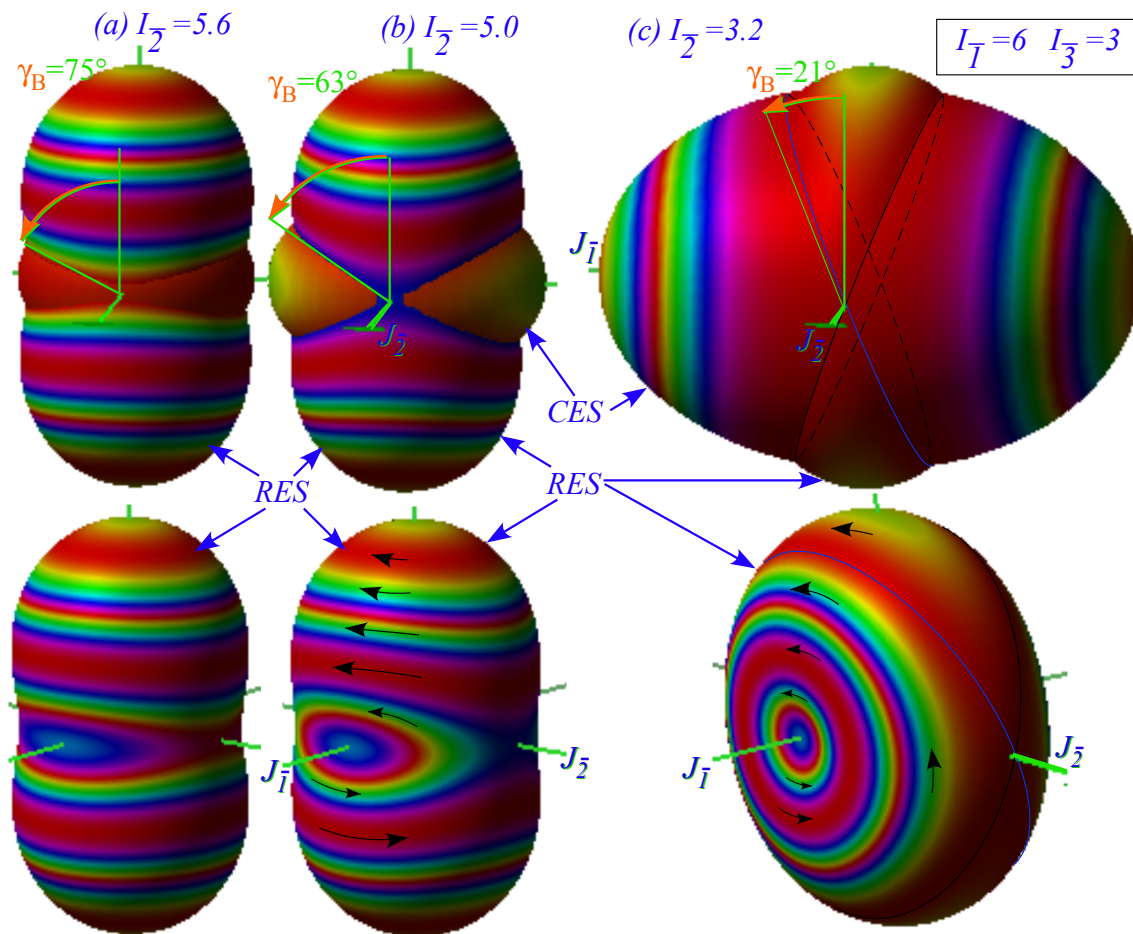

Fig. 6.8.2 Fixed-J- RES with CES at separatrix $E = J^2 / 2I_{\bar{2}}$ as $I_{\bar{2}}$ varies. (a) $I_{\bar{2}} = 5.6$ and $\gamma_B = 75.5°$ (Nearly prolate low-E CES), (b) $I_{\bar{2}} = 5.0$ and $\gamma_B = 63.4°$, (c) $I_{\bar{2}} = 3.2$ and $\gamma_B = 20.7°$ (Nearly oblate high-E CES).

J-vectors precess like a pendulum in Fig. 2.15.2 except BOD-orbits go *clockwise* by (6.8.6a) around RES *max*ima and *anti*-clockwise by (6.8.6b) around RES *min*ima. Right-hand rules of LAB frames become left-hand rules in BOD-frames. **J**-vectors arrive and depart saddle points exponentially by (6.8.6c).

c. Deformable rotors

Hamiltonians of higher-than-quadratic powers model deformable rotors that change their inertia more or less due to centrifugal force. An example in Fig. 6.8.3 is a single rotating mass m held by a spring $k = m\omega_v^2$. The rotor has vibrational kinetic and potential energy KE_v and PE_v plus rotational kinetic energy RE_J.

$$E = KE_v + \quad PE_v \quad + \quad RE_J$$
$$= \frac{m\dot{r}^2}{2} + \frac{k}{2}(r-r_0)^2 + \frac{I\dot{\theta}^2}{2} = \frac{p_v^2}{2m} + \frac{m}{2}\omega_v^2(r-r_0)^2 + \frac{\mu J^2}{2} \qquad (6.8.11)$$

Rotational inertia $I = mr^2 = 1/\mu$, angular velocity $\dot{\theta} = \omega_J$, and momentum $J = I\dot{\theta} = I\omega_J$ involve radius r that grows from rest value r_0 until spring force $F_{spring} = -m\omega_v^2(r-r_0)$ cancels centrifugal force $F_{centrif} = m\omega_J^2 r$.

$$F_{spring} + F_{centrif} = 0 = m\omega_J^2 r - m\omega_v^2(r-r_0) \quad \text{*implies:*} \quad r = r_0 \frac{\omega_v^2}{\omega_v^2 - \omega_J^2} \qquad (6.8.12)$$

Centrifugal equilibrium r blows up as rotational rate ω_J nears vibrational frequency ω_v. The derivative of effective potential $PE_v + RE_J$ in (6.8.11) is zero at equilibrium radius r or stretch distance $d = r - r_0$.

$$\frac{\partial}{\partial r}(PE_v + RE_J) = 0 = m\omega_v^2(r-r_0) + \frac{J^2}{2}\frac{\partial \mu}{\partial r} \quad \text{*implies:*} \quad d = r - r_0 = \frac{J^2}{2m\omega_v^2}\frac{\partial \mu}{\partial r} \qquad (6.8.13)$$

We assume the angular velocity ω_J varies inversely with r so that momentum J is conserved as it must be since the central spring force exerts no torque.

The inverse inertia $I = 1/\mu$ is approximated for small stretch $(d = r - r_0 \ll 1)$ and (6.8.13) is inserted.

$$\mu \cong \mu_0 + \frac{\partial \mu}{\partial r}(r-r_0) + ... = \mu_0 - \frac{\partial \mu}{\partial r}\frac{J^2}{2m\omega_v^2}\frac{\partial \mu}{\partial r} + ... \qquad (6.8.14a)$$

This with (6.8.13) is inserted into energy expression (6.8.11) to approximate the effect of momentum J.

$$E = \frac{p_v^2}{2m} + \frac{m}{2}\omega_v^2\left(r-r_0\right)^2 \qquad + \frac{\mu J^2}{2}$$
$$= \frac{p_v^2}{2m} + \frac{m}{2}\omega_v^2\left(\frac{J^2}{2m\omega_v^2}\frac{\partial \mu}{\partial r}\right)^2 + \frac{\mu_0 J^2}{2} - \frac{\partial \mu}{\partial r}\frac{J^2}{2m\omega_v^2}\frac{\partial \mu}{\partial r}\frac{J^2}{2} + ... \qquad (6.8.14b)$$
$$= \frac{p_v^2}{2m} + \qquad \frac{J^4}{8m\omega_v^2}\left(\frac{\partial \mu}{\partial r}\right)^2 + \frac{\mu_0 J^2}{2} - \frac{J^4}{4m\omega_v^2}\left(\frac{\partial \mu}{\partial r}\right)^2 + ...$$

This reduces to a simpler form that lends some insight into centrifugal distortion energy.

$$E = \frac{p_v^2}{2m} + \frac{\mu_0 J^2}{2} - \frac{J^4}{8m\omega_v^2}\left(\frac{\partial\mu}{\partial r}\right)^2 + \dots = \frac{p_v^2}{2m} + \frac{\mu_0 J^2}{2} - \frac{m}{2}\omega_v^2 d^2 + \dots \qquad (6.8.15)$$

The rigid rotor energy is perturbed by a J^4/r^6 term that reduces total energy by just the amount of work needed to stretch the spring by distance d in (6.8.13). The spring gains $PE = kd^2/2$ the whole system loses twice that in rotational kinetic energy by expanding to radius $r = r_0 + d$ for a net loss of $kd^2/2 = m\omega_v^2 d^2/2$.
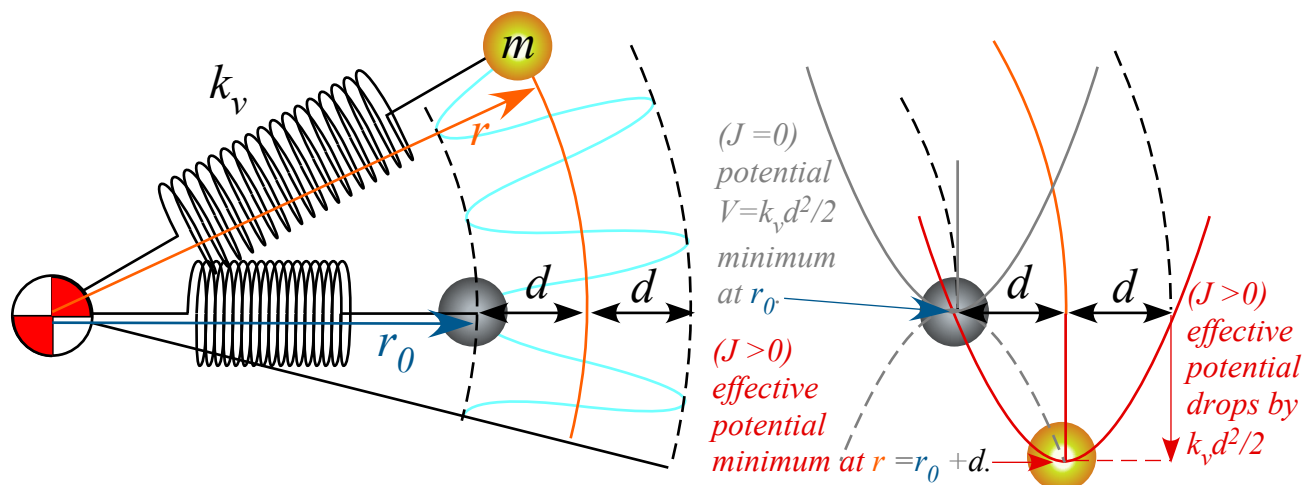

Fig. 6.8.3 Spring-mass model for centrifugal stretch of a model vib-rotor showing effective PE shift.

Imagine a rotor of energy E is held by a wire at its *(J=0)*-radius r_0 but has momentum $J>0$ tending to pull it out to radius $r = r_0 + d$. Cutting the wire changes neither energy E nor momentum J but lets mass m begin vibrating around its new equilibrium of $r = r_0 + d$ with an amplitude $\pm d$ between $r_{min} = r_0$ and $r_{max} = r_0 + 2d$.

Multi-mass molecular Hamiltonians have vibration normal coordinates q_μ and BOD momentum $J_{\bar{m}}$.

$$H = \tfrac{1}{2} p_\mu p_\mu + \tfrac{1}{2}\omega_\mu^2 q_\mu q_\mu + \tfrac{1}{2} J_{\bar{m}}\mu_{\bar{m}\bar{n}} J_{\bar{n}} \qquad (6.8.16)$$

Each normal coordinate may have an equilibrium shift δq_μ analogous to the d in (6.8.13).

$$\delta q_\mu = -\frac{J_{\bar{m}} J_{\bar{n}}}{2\omega_\mu^2}\frac{\partial\mu_{\bar{m}\bar{n}}}{\partial q_\mu} \qquad (6.8.17)$$

Here the inverse inertia is represented by a 3-by-3 matrix $\mu_{\bar{m}\bar{n}} = I_{\bar{m}\bar{n}}^{-1}$ inverse to the inertia tensor $I_{\bar{m}\bar{n}}$. The resulting effective Hamiltonian analogous to (6.8.15) involves a *4th*-degree *J*-tensor sum over all modes q_μ.

$$H = H_0 - \frac{J_{\bar{k}} J_{\bar{\ell}} J_{\bar{m}} J_{\bar{n}}}{8\omega_\mu^2}\frac{\partial\mu_{\bar{k}\bar{\ell}}}{\partial q_\mu}\frac{\partial\mu_{\bar{m}\bar{n}}}{\partial q_\mu} \quad \text{where:} \quad H_0 = \tfrac{1}{2} p_\mu p_\mu + \tfrac{1}{2} J_{\bar{m}}\mu_{\bar{m}\bar{n}}^{(0)} J_{\bar{n}} \qquad (6.8.18)$$

The sum over modes may be quite tedious, however for high symmetry molecules, the form of the possible *J*-tensors can be deduced by symmetry. For molecules that are cubic, octahedral, and tetrahedral (for example, C_8H_8, SF_6, and CF_4, respectively) there is only one linearly independent *4th*-degree *J*-tensor or *(xyz)*-polynomial. Powers J^4 or r^4 are spherical *scalars*, but expanding r^4 reveals non-scalar *tensors*.

$$r^4 = (r^2)^2 = (x^2 + y^2 + z^2)^2 = (x^4 + y^4 + z^4) + 2(x^2 y^2 + x^2 z^2 + y^2 z^2) \qquad (6.8.19)$$

An octahedral (SF$_6$-like) molecule uses the first tensor. Cubic or tetrahedral molecules use the other.

$$H^{octahedral} = H_0 + t_4(J_{\bar{1}}^4 + J_{\bar{2}}^4 + J_{\bar{3}}^4) \quad (6.8.20a) \qquad H^{cubic} = H_0 + t_{22}(J_{\bar{1}}^2 J_{\bar{2}}^2 + J_{\bar{1}}^2 J_{\bar{3}}^2 + J_{\bar{2}}^2 J_{\bar{3}}^2) \quad (6.8.20b)$$

The scalar or spherical term is $H_0 = BJ^2 + t_0 J^4$ where $BJ^2 = B(J_{\bar{1}}^2 + J_{\bar{2}}^2 + J_{\bar{3}}^2)$ is for a rigid spherical top, but total RES have octahedral and cubic shapes, respectively, as shown in Fig. 6.8.4(a) and Fig. 6.8.4(b).

$$T^{(4)}(J) = J_{\bar{1}}^4 + J_{\bar{2}}^4 + J_{\bar{3}}^4 \qquad (6.8.20c) \qquad T^{(2,2)}(J) = J_{\bar{1}}^2 J_{\bar{2}}^2 + J_{\bar{1}}^2 J_{\bar{3}}^2 + J_{\bar{2}}^2 J_{\bar{3}}^2 \qquad (6.8.20d)$$
$$= J^4[\cos^4 \gamma \sin^4 \beta + \sin^4 \gamma \sin^4 \beta + \cos^4 \beta] \qquad = J^4[\cos^2 2\gamma \sin^2 \beta + \sin^2 2\beta]$$

(a) $H^{octahedral} = BJ^2 + t_0 J^4 + t_4(J_1^4 + J_2^4 + J_3^4)$

(b) $H^{cubic} = BJ^2 + t_0 J^4 + t_{22}(J_{\bar{1}}^2 J_{\bar{2}}^2 + J_{\bar{1}}^2 J_{\bar{3}}^2 + J_{\bar{2}}^2 J_{\bar{3}}^2)$

J(100) affects centrifugal stretch of XY$_6$

J(111) affects centrifugal bend of XY$_6$

J(111) affects centrifugal stretch of XY$_4$ or XY$_8$

J(100) affects centrifugal bend of XY$_4$ or XY$_8$

Radial bonds resistant   *Bend bonds compliant*   *Radial bonds resistant*   *Bend bonds compliant*
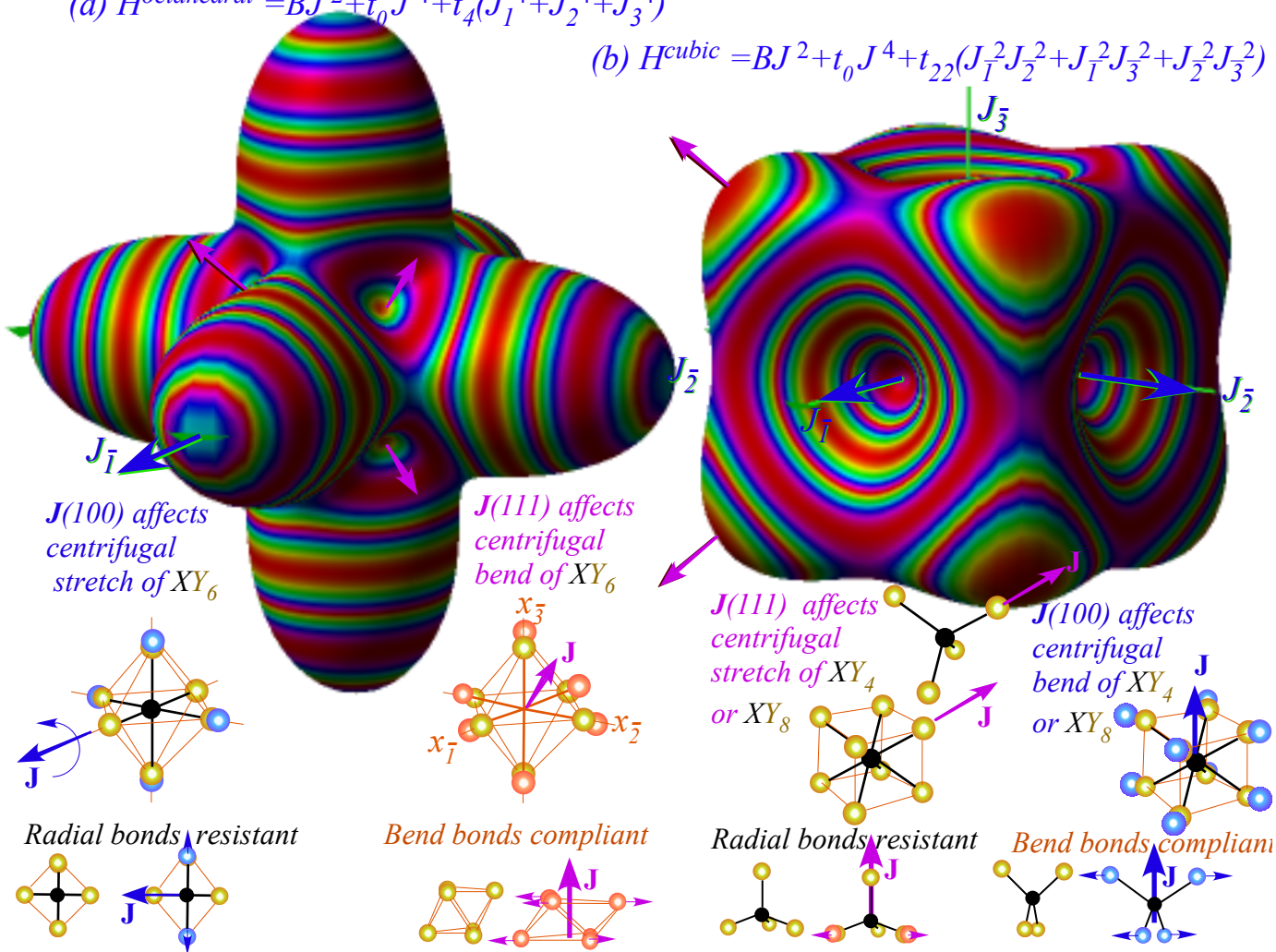
Fig. 6.8.4 Centrifugal 4th-degree sphere-top RES. (a) octahedral (SF$_6$) (b) cubic (C$_8$H$_8$) tetrahedral (CF$_4$)

The Hamiltonians (a) and (b) of (6.8.20) and RES (a) and (b) in Fig. 6.8.4 are related in (6.8.19) by a ±sign since t_{22} is just $-2t_4$ if scalar t_0 is adjusted accordingly. Nevertheless, distortion of an octahedral SF$_6$ molecule described by $T^{(4)}$ is quite different from a $T^{(2,2)}$ distortion of cubic C$_8$H$_8$ or tetrahedral CF$_4$.

The octahedral RES has a minimum when the **J** is near one of the eight (111) axes of trigonal (3-fold) symmetry. Rotation about (111) axes has maximum effect on octahedral molecules since they have relatively weak bending bonds, so centrifugal force due to (111) rotation more easily spreads the six arms of an SF$_6$ molecule and thus (111) is in a valley in Fig. 6.8.4(a). But a rotation on one of six (100) axes of tetragonal (4-

fold) symmetry can only stretch radial bonds normal to these axes and those only stretch a little due to high radial bond strength. Thus (100) is on one of six octahedral RES peaks in Fig. 6.8.4(a).

It is *vice-versa* for cubic C_8H_8 and tetrahedral CF_4 molecules. They are resistant to distortion by rotation on one of the eight (111)-axes of trigonal (3-fold) symmetry but susceptible to rotation on one of six (100), (010), or (001) tetragonal axes that bend bonds and thus lie in six RES valleys of Fig. 6.8.4(b).

Spherical top RES topography in Fig. 6.8.4 has an exaggerated scale compared to asymmetric RES topography of Fig. 6.8.1 or Fig. 6.8.2. Centrifugal $J^{(4)}$ factors t_{22} or t_4 are tiny compared to asymmetric-top factors $(A = \frac{1}{2I_{\bar{1}}}, B = \frac{1}{2I_{\bar{2}}}, C = \frac{1}{2I_{\bar{3}}})$. Thus centrifugal effects are easily washed away in low symmetry.

For a spherical top the rigid inertial components are exactly equal *(A=B=C)* and so even the tiniest anisotropy of distortion determines the RES topography lines, saddle points, and separatrices that dictate the rotational dynamics. RES paths show up like puddles on a level tennis court that might seem quite flat when it is dry, but these delicate puddles are washed away if the court experiences upheavals.

Higher-than-*4th*-degree J-tensors $T^{(6)}$, $T^{(8)}$,… may affect motion, too. All these may be organized into *multipole expansions* of cubic-symmetry *spherical harmonics* $Y_q^{(k)}(\gamma,\beta)$. Such expansions are described in the following section and include odd-degree tensors $T^{(1)}$, $T^{(3)}$,…, as well. Below are the cubic-symmetry *4th* and *6th*-degree tensors $T^{(4)}$ and $T^{(6)}$ that are linearly independent of r^2, r^4, and r^6. (Here $X_q^k = r^k Y_q^{(k)}(\gamma,\beta)$.)

$$T^{(4)} = \sqrt{\tfrac{7}{12}}X_0^4 - \sqrt{\tfrac{5}{24}}(X_4^4 + X_{-4}^4) = \tfrac{15}{8}\sqrt{\tfrac{7}{2\pi}}\left\{ x^4 + y^4 + z^4 - \tfrac{3}{5}r^6 \right\}$$

$$T^{(6)} = \sqrt{\tfrac{1}{8}}X_0^6 - \tfrac{\sqrt{7}}{4}(X_4^6 + X_{-4}^6) = \tfrac{21}{40}\sqrt{\tfrac{13}{2\pi}}\left\{ x^6 + y^6 + z^6 - 5[x^4(y^2+z^2) + y^4(x^2+z^2) + z^4((y^2+z^2))] + 70x^2y^2z^2 - \tfrac{5}{21}r^6 \right\}$$

The $T^{(6)}$ topography in Fig. 6.8.5 differs from the *4th*-degree RES above. Most remarkable is the presence of stable-loop paths around the twelve (110)-directions that only have saddle points in Fig. 6.8.4 above. Also, both (111) and (100) directions are elevated in $T^{(6)}$ while only (100) is for $T^{(4)}$ in Fig. 6.8.4(a).
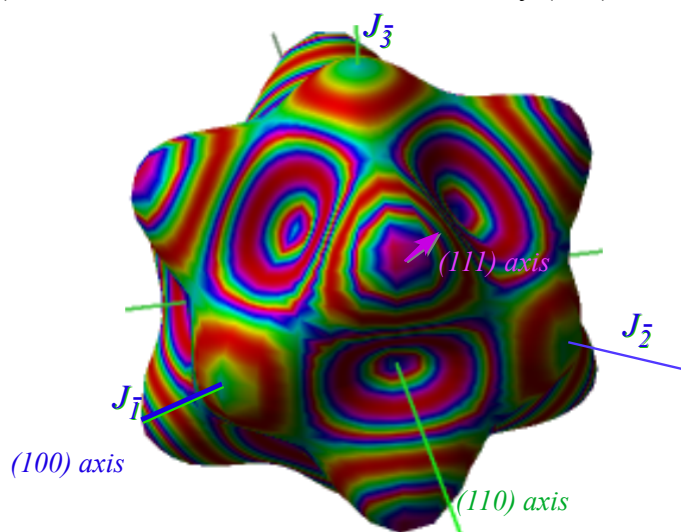

Fig. 6.8.5 Centrifugal 6th-degree sphere-top RES.

This *6th*-degree topography becomes relevant in methane CH_4 spectra. The low inertia of CH_4 means it rotates more rapidly than CCl_4, CF_4, or even CD_4. Then centrifugal effects drive its vibrational potential into anharmonic regions so higher power J-terms arise. Of course if higher-than-*4th* degree perturbations are effective, then motion may be ultra-sensitive to the relative amounts of competing multipole functions.

Chapter 6.9 Coupled rotors: multiple rotational energy surfaces MRES

The previous Sec. 6.8 introduced Hamiltonians and RE surfaces having time-reversal symmetry. Even-k multipole functions (isotropic or *monopole (k=0)*, quadratic or *quadrupole (k=2)*, quartic or *hexadecapole (k=4)*, *etc.*) have $(\mathbf{J} \rightarrow -\mathbf{J})$ symmetry but odd-k (linear-*dipole (k=1)*, cubic or *octupole (k=3)* , *etc.*) do not. However, rotors with gyros ("rotor-rotors") have Hamiltonians that may use any multipole function. The lowest anisotropic multipole is the *dipole (k=1)* and will be described first.

a. Gyro-Rotors

A coupled rotor is one composed of two or more spinning objects with more or less independent angular momentum such as a molecule with attached methyl (CH_3) "gyro" or "pinwheel" sub-rotors, a system of considerable biophysical interest. Or else a single molecule may have a vibration or "phonon" excitation that couples strongly to rotation. Nuclear or electronic spins with significant coupling may be regarded as an elementary sub-rotors. A classical analogy would be a spacecraft with gyro(s) on board.

A rotor-rotor Hamiltonian is the sum of the H_R and H_S for each and coupling Hamiltonian H_{RS}.

$$H_{rotor\ R+S} = H_{rotor_R} + H_{rotor_S} + V_{RS} \qquad (6.9.1)$$

A useful approximation attaches a rotor$_S$ "gyro-bearing" to a rotor$_R$ frame so interaction V_{RS} becomes a constraint, does no work, and is thus ignored. An asymmetric top with body-fixed spin is the following modified version of (6.7.27). Rotor momentum $\mathbf{R}$ adds to gyro spin $\mathbf{S}$ to make a total momentum $\mathbf{J}=\mathbf{R}+\mathbf{S}$.

$$H_{R+S(Body-fixed)} = A\mathbf{R}_x^2 + B\mathbf{R}_y^2 + C\mathbf{R}_z^2 + H_{rotor_S} + (\sim 0) \qquad (6.9.2a)$$

The system total angular momentum is a conserved vector $\mathbf{J}=\mathbf{R}+\mathbf{S}$ in the lab-frame and has a conserved magnitude $|\mathbf{J}|$ in the rotor$_R$ BOD frame. So we use $\mathbf{R}=\mathbf{J}-\mathbf{S}$ in place of $\mathbf{R}$.

$$
\begin{aligned}
H_{R,S(fixed)} &= A\left(\mathbf{J}_x - \mathbf{S}_x\right)^2 + B\left(\mathbf{J}_y - \mathbf{S}_y\right)^2 + C\left(\mathbf{J}_z - \mathbf{S}_z\right)^2 + H_{rotor_S} \\
&= A\mathbf{J}_x^2 + B\mathbf{J}_y^2 + C\mathbf{J}_z^2 - 2A\mathbf{J}_x\mathbf{S}_x - 2B\mathbf{J}_y\mathbf{S}_y - 2C\mathbf{J}_z\mathbf{S}_z + H'_{rotor_S}
\end{aligned}
\qquad (6.9.2b)
$$

Gyro-spin components $\mathbf{S_a}$ are constant classical parameters S_a. (Fixed bearing constraints do no work.)

$$
\begin{aligned}
H_{R,S(fixed)} &= const.\mathbf{1} - 2AS_x\mathbf{J}_x - 2BS_y\mathbf{J}_y - 2CS_z\mathbf{J}_z + A\mathbf{J}_x^2 + B\mathbf{J}_y^2 + C\mathbf{J}_z^2 \\
&= M_0\mathbf{T}_0^0 \qquad + \qquad \sum_d D_d\mathbf{T}_d^1 \qquad + \qquad \sum_q Q_q\mathbf{T}_q^2
\end{aligned}
\qquad (6.9.2c)
$$

This is a simple Hamiltonian *multipole tensor operator expansion* having here just a monopole $\mathbf{T}_0^0$ term, three dipole $\mathbf{T}_a^1$ terms, and two quadrupole $\mathbf{T}_q^2$ terms shown in Fig. 6.9.1. Each multipole graph is a radial plot of a spherical harmonic function $Y_q^k(\varphi, \vartheta)$ representing a tensor operator $\mathbf{T}_q^k$ for each polar (φ, ϑ)-coordinate direction in the BOD -frame of the $\mathbf{J}$-vector fixed on LAB $\mathbf{z}.(\varphi = -\gamma, \vartheta = -\beta)$

(a)
Monopole
$$\mathbf{T}^0_0$$

(b)
Dipole
$$\mathbf{T}^1_x$$
$$\mathbf{T}^1_y$$
$$\mathbf{T}^1_z$$

(c)
Quadrupole
$$\mathbf{T}^2_0$$
$$2z^2\text{-}x^2\text{-}y^2$$
$$\mathbf{T}^2_{+2}\text{-}\mathbf{T}^2_{-2}$$
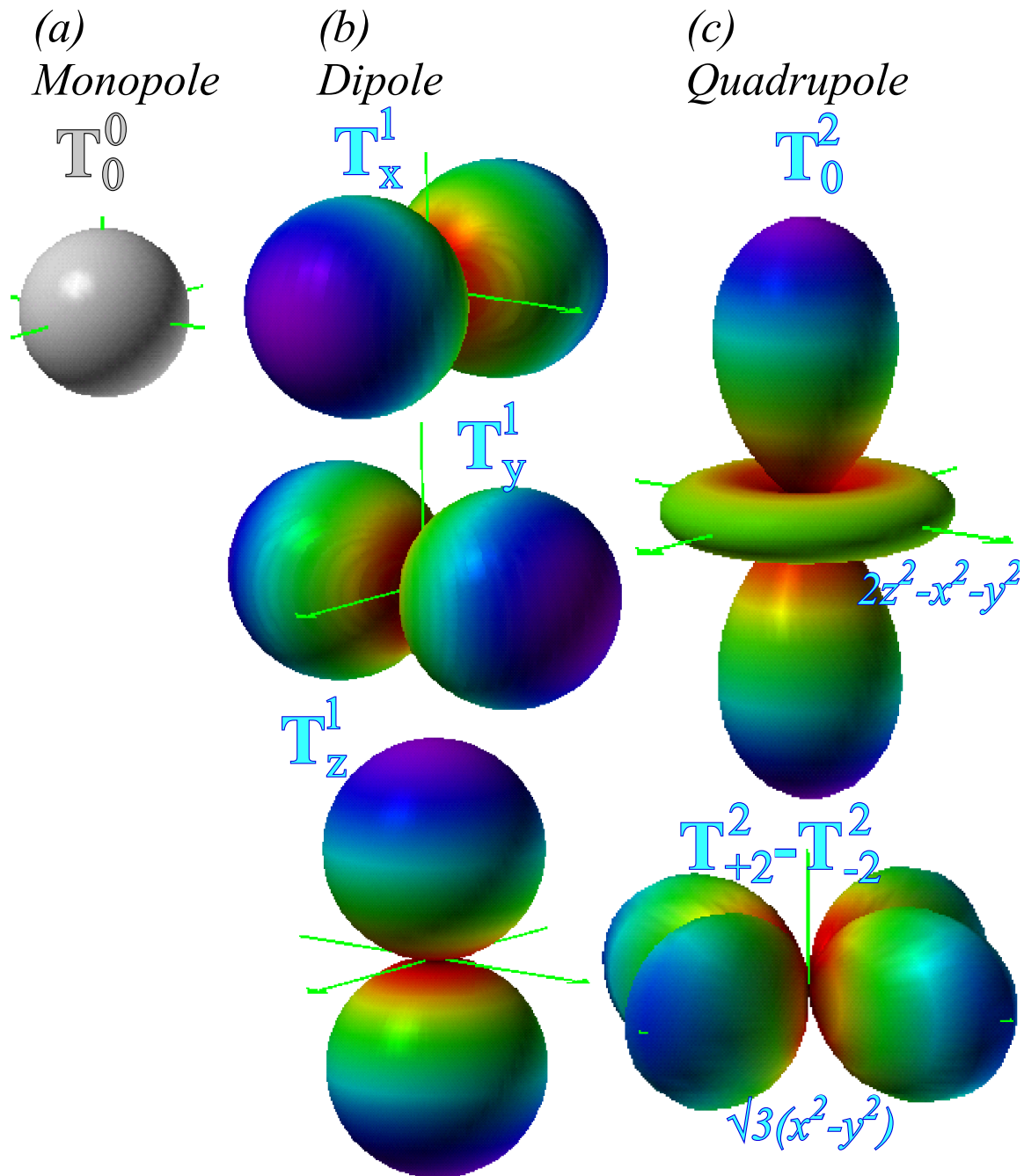$$\sqrt{3}(x^2\text{-}y^2)$$

Fig. 6.9.1 The six lowest order RES components needed to describe rigid gyro-rotors.

$$\mathbf{T}^0_0 = \frac{\mathbf{J}^2_x + \mathbf{J}^2_y + \mathbf{J}^2_z}{3} \quad (6.9.3a)$$

$$\mathbf{T}^1_x = \mathbf{J}_x = \frac{\mathbf{T}^1_{+1} + \mathbf{T}^1_{-1}}{\sqrt{2}}$$

$$\mathbf{T}^1_y = \mathbf{J}_y = \frac{\mathbf{T}^1_{+1} - \mathbf{T}^1_{-1}}{i\sqrt{2}} \quad (6.9.3b)$$

$$\mathbf{T}^1_z = \mathbf{J}_z = \mathbf{T}^1_0$$

$$\mathbf{T}^2_{zz} = \frac{2\mathbf{J}^2_z - \mathbf{J}^2_x - \mathbf{J}^2_y}{2} = \mathbf{T}^2_0$$

$$\mathbf{T}^2_{x^2-y^2} = \mathbf{J}^2_x - \mathbf{J}^2_y = \frac{2\left(\mathbf{T}^2_2 - \mathbf{T}^2_{-2}\right)}{\sqrt{6}} \quad (6.9.3c)$$

The constant coefficients or *moments* indicate strength of the respective multipole symmetry. The scalar monopole RES (a) is a sphere, while vector dipole RES (b) are bi-spheres pointing along Cartesian axes, and the RES (c) resemble quadrupole antenna patterns or *d*-wave ($\ell = 2$) functions.

$$M_0 = A + B + C + 3H'_{rotor_S} \quad (6.9.4a)$$

$$\begin{aligned} D_x &= -2AS_x \\ D_y &= -2BS_y \quad (6.9.4b) \\ D_z &= -2CS_z \end{aligned}$$

$$\begin{aligned} Q_{zz} &= \left(2C - A - B\right)/6 \\ Q_{x^2-y^2} &= \left(A - B\right)/2 \end{aligned} \quad (6.9.4c)$$

Asymmetric and symmetric rotor Hamiltonians (6.7.27) and (6.7.32) are combinations of a monopole (6.9.3a) that, by itself makes a spherical rotor, and varying amounts of the two quadrupole terms (6.9.3c) to give the rigid rotor RES pictured previously in Fig. 6.8.1 and Fig. 6.8.2. Both *Q*-coefficients (6.9.4c) are zero for a spherical top *(A=B=C)*. Only one is zero for a symmetric top *(A=B)*.

Combining monopole (6.9.3a) with dipole terms (6.9.3b) gives a gyro-rotor Hamiltonian (6.9.2b) for a spherical rotor *(A=B=C)* that has the following form. (Imagine a spherical spaceship with gyro.)

$$H= BR^2=B(\mathbf{J\text{-}S})^2=const+ BJ^2 \text{ - } g\mu\mathbf{S}\cdot\mathbf{J} \qquad \text{(where: } g\mu=2A=2B=2C) \qquad (6.9.5)$$

H resembles a dipole potential -**m·B** for a magnetic moment **m**=*g***J** that precesses clockwise around a lab-fixed magnetic field **B**=μ**S**. (The PE is least for **J** lined up along **S**.)

Here, the Hamiltonian (6.9.5) is a simple example of *Coriolis* rotational energy. It is least for **J** along **S** where |**R**|=|**J-S**| is least and rotor kinetic energy BR^2 is least. (Magnitudes |J| and |S| stay constant here.) The spherical rotor-gyro RES in Fig. 6.9.2 is minimum for **J** along body axis +**S** where BR^2 is least and maximum for **J** along –**S** where BR^2 is greatest.

As is the case for rigid solid rotors in Fig. 6.8.1 and Fig. 6.8.2, the RES energy topography lines determine the precession **J**-paths in the body frame wherein gyro-**S** is fixed in Fig. 6.9.2. The left hand rule gives **J**-precession sense in the body **S**-frame, that is, all **J** precess *anti*-clockwise relative to the "low" valley on the +**S**-axis or clockwise relative to the "high" peak on the –**S**-axis. (It is like the wind on the Northern hemisphere of Earth.) In the lab, **S** appears to precess clockwise around a fixed **J**.

Gyro-RES differ from rigid rotor RES in Fig. 6.8.2 that have pairs of ±*z*-axis peaks and/or valleys separated by saddle or separatrix points where the **J**-flow direction reverses. The gyro-RES in Fig. 6.9.2 has no separatrix with one peak and one valley on opposite ends of an axis defining direction of **J**-flow. It has the same harmonic precession frequency for all **J**-vectors no matter how close to high +**S** and low –**S**-axis. Energy of a gyro-rotor Hamiltonian (6.9.5) is *harmonic* or *linear* in the *z*-axial component $K=J_z$.

$$E_{gyro-R} = const. + BJ^2 - 2BK \quad (6.9.6b) \qquad\qquad E_{symm-top} = const. + BJ^2 + (C-B)K^2 \quad (6.9.6b)$$

In contrast, a symmetric rigid rotor energy (6.7.35) is *quadratic* in *K*. Asymmetric and deformable rotor energy shown in Fig. 6.8.2 and Fig. 6.8.4 have a higher power or transcendental dependence. Harmonic or linear energy dependence is an unusual (but welcome) rarity in rotor mechanics.
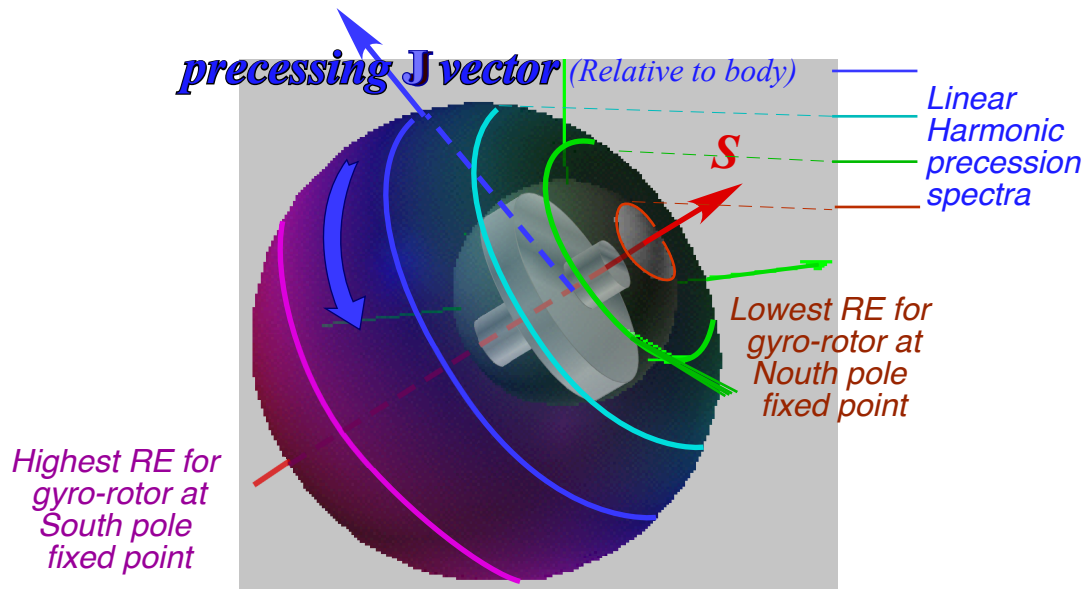
Fig. 6.9.2 The spherical gyro-rotor RES is a cardioid of revolution around gyro spin **S**

b. 3D-Rotor and 2D-Oscillator Analogy

One associates linear levels with harmonic *oscillators* not rotors. The gyro-rotor's linear spectrum reminds us of a 150-year-old analogy between motions of 3D rotors and 2D vibrations. Stokes [1863] described 2D electric vibration or *optical polarization*, by 3D vectors known as Stokes vectors and labeled by **S**. Stokes' spin uses Hamilton *quaternions*, redone 80 years later as Pauli *spinor* σ_μ components of a general 2D Hermitian operator H. This repeats some of the discussion of (4.4.9).

$$H = \begin{pmatrix} A & B - iC \\ B + iC & D \end{pmatrix} = \frac{A+D}{2}\sigma_0 + \frac{A-D}{2}\sigma_A + B\sigma_B + C\sigma_C,$$

$$\text{where: } \sigma_0 = \begin{pmatrix} 1 & 0 \\ 0 & 1 \end{pmatrix}, \ \sigma_A = \begin{pmatrix} 1 & 0 \\ 0 & -1 \end{pmatrix}, \ \sigma_B = \begin{pmatrix} 0 & 1 \\ 1 & 0 \end{pmatrix}, \ \sigma_C = \begin{pmatrix} 0 & -i \\ i & 0 \end{pmatrix}. \tag{6.9.7}$$

Labels: *A ("Asymmetric-diagonal"), B ("Bilateral-balanced"), and C("Circular-Coriolis")* are mnemonic alternatives to Pauli's dry *z*, *x*, and *y*, respectively. The 2D Hamiltonian has an **S·J=S·**σ**/2=**Ω**·**σ form of Coriolis coupling (6.9.5). (Note: Do not confuse *ABCD*'s above with our inertial labels $(A=\frac{1}{2I_1}, B=\frac{1}{2I_2}, C=\frac{1}{2I_3})$.)

$$H = S_0\mathbf{1} + S_A J_A + S_B J_B + S_C J_C = S_0 J_0 + \vec{S} \bullet \mathbf{J},$$

$$\text{where: } J_0 = \mathbf{1}, \quad J_A = \frac{\sigma_A}{2}, \quad J_B = \frac{\sigma_B}{2}, \ J_C = \frac{\sigma_C}{2},$$

$$\text{and: } S_0 = (A + D)/2, \ S_A = (A - D), \ S_B = 2B, \quad S_C = 2C. \tag{6.9.8}$$

The 2D-3D analogy writes Pauli **J**=σ/2 operators using elementary oscillator ladder operators $e_{jk}=a_j^\dagger a_k$.

$$\mathbf{J}_0 = \mathbf{N} = a_1^\dagger a_1 + a_2^\dagger a_2, \ \mathbf{J}_A = \frac{1}{2}\left(a_1^\dagger a_1 - a_2^\dagger a_2\right), \ \mathbf{J}_B = \frac{1}{2}\left(a_1^\dagger a_2 + a_2^\dagger a_1\right), \ \mathbf{J}_C = \frac{-i}{2}\left(a_1^\dagger a_2 - a_2^\dagger a_1\right).$$

$$\text{where: } a_1^\dagger a_1 = \begin{pmatrix} 1 & 0 \\ 0 & 0 \end{pmatrix}, \ a_1^\dagger a_2 = \begin{pmatrix} 0 & 1 \\ 0 & 0 \end{pmatrix}, \ a_2^\dagger a_1 = \begin{pmatrix} 0 & 0 \\ 1 & 0 \end{pmatrix}, \ a_2^\dagger a_2 = \begin{pmatrix} 0 & 0 \\ 0 & 1 \end{pmatrix}. \tag{6.9.9}$$

This notational trick is very useful for extending the classical analysis to quantum **J**-operators.

How all this gets "quantized"

Schwinger's 3D **J**-momentum raising-lowering operators $\mathbf{J}_+ = \mathbf{J}_B + i\mathbf{J}_C = a_1^\dagger a_2$ and $\mathbf{J}_- = \mathbf{J}_B - i\mathbf{J}_C = a_2^\dagger a_1$ are well known in the case that 2D dimensions *1* and *2* represent quantum *spin-up (+ħ/2)* and *spin-down (-ħ/2)* instead of the *x*-and *y*-polarized fundamental oscillator states envisioned by Stokes.

　　　Angular 3D ladder operation is simplified by far simpler 2D oscillator operations.

$$\mathbf{J}_+ \left| n_1 n_2 \right\rangle = a_1^\dagger a_2 \left| n_1 n_2 \right\rangle = \sqrt{n_1 + 1}\sqrt{n_2}\left| n_1 + 1, n_2 - 1 \right\rangle$$
$$\mathbf{J}_- \left| n_1 n_2 \right\rangle = a_2^\dagger a_1 \left| n_1 n_2 \right\rangle = \sqrt{n_1}\sqrt{n_2 + 1}\left| n_1 - 1, n_2 + 1 \right\rangle$$

(6.9.10)

2D oscillator states are labeled by *total* number $N=(n_1+n_2)$ of quanta and the *net* quantum population $\Delta N=(n_1-n_2)$. 3D angular momentum states $\left| {}^J_K \right\rangle$ are labeled by total momentum $J=N/2=(n_1+n_2)/2$ and *z*-component $K=N/2=(n_1+n_2)/2$, just half (or *ħ/2*) of *N* and *ΔN*.

$$\left| n_1, n_2 \right\rangle = \frac{\left(a_1^\dagger\right)^{n_1}\left(a_2^\dagger\right)^{n_2}}{\sqrt{n_1! n_2!}}\left| 0,0 \right\rangle = \left| {}^J_K \right\rangle = \frac{\left(a_1^\dagger\right)^{J+K}\left(a_2^\dagger\right)^{J-K}}{\sqrt{(J+K)!(J-K)!}}\left| 0,0 \right\rangle, \text{ where:}\begin{cases} n_1 = J + K \\ n_2 = J - K \end{cases}$$

(6.9.11)

This leads to Schwinger's quantum angular momentum matrices $D_{MK}^J\left(\alpha\beta\gamma\right)$ and Clebsch-Gordan Wigner-Eckart relations needed for quantum calculations and their semiclassical RE surface approximations.

$$\left\langle {}^{J'}_{K'} \left| T_q^k \right| {}^J_K \right\rangle = C_{q\,K\,K'}^{kJ\,J'}\left\langle J' \| k \| J \right\rangle \sim C_{0\,K\,K}^{kJ\,J}\left\langle J \| k \| J \right\rangle \sim D_{JK}^J\left(\Theta_K^J\right).$$

c. Gyro-rotor and anharmonic 2D-Local mode analogy

　　　Quite beyond the computational value of the 2D-3D analogy is the insight and visualization gained for fundamental processes. In a slight stretch of the 2D analogy we imagine two 1D oscillators in place of the single 2D oscillator in the Stokes model as was introduced in Unit 4 by developing the idea of *ABCD*-symmetry types of 2D harmonic oscillators. Now an anharmonic oscillator example may be considered.

　　　If the oscillators are identical they have bilateral or *B*- symmetry and a H_B Hamiltonian commutes with both σ_B (a +45° mirror reflection of +*x* and +*y* axes) and with -σ_B (a -45° mirror reflection of -*x* and +*y* axes). σ_B interchange the oscillators. This means that to first order the Hamiltonian *is* $H_B=2B\sigma_B$, that is, a gyro rotor $\mathbf{T}_x^1$ with **S** along the *B*-axis as shown in Fig. 6.9.3. (Added $\mathbf{T}_0^0$ affects eigen*values*, not states.)

　　　Eigenvectors of H_B are the symmetric and antisymmetric *normal modes* that belong to the fixed points on the **S**-vector and ±*B*-axes of the Stokes space. If instead, the **S**-vector lies on the *A*-axis, the Hamiltonian is an asymmetric diagonal $H_A= 2A\sigma_A$ matrix. From (6.9.7) we see that operator σ_A reflects *y* into –*y* but leaves *x* alone, so eigenvectors of H_A are localized on the *x*-oscillator or the *y*-oscillator but not both. Such motions are *local modes*, but are not modes of H_B, which does not commute with H_A.

　　　Hamiltonian H_B rotates a **J**-vector from the +*A*-axis (local x-mode) around to the –*C* axis to the –*A* (local y-mode), then to the +*C* axis, and then home to +*A*. The **J**-path is the largest equator of Fig. 6.9.3(a). The ±*C*-axes

belong to what Stokes would call *circular* polarization with chirality right and left, respectively. Double vibrator, $\pm C$ resonant beats have one vibrator's phase $\pm 90°$ relative to the other's.

Simple mode beat transfer dynamics is disrupted by adding an anharmonic $\mathbf{T}_0^2$ term to existing *B*-symmetry terms $\mathbf{T}_x^1$ and $\mathbf{T}_0^0$, as shown in Fig. 6.9.3(b-c). The effect of $\mathbf{T}_0^2$ in Fig. 6.9.3(c) is to replace a stable fixed point +*B* (representing the (+)-normal mode) by a saddle point as it *bifurcates* (splits) into a pair of fixed points that head toward the $\pm A$-axes. So one *normal* mode dies to begat two stable *local* modes wherein a mass may retain its energy instead of giving it to the other by a resonant beating process. Anharmonicity $\mathbf{T}_0^2$ *decouples* the masses for the symmetric +*B*-normal mode but spares the antisymmetric -*B*-mode on the backside of Fig. 6.9.3(c). Pairs of classical local modes, each localized on different sides of an RES in Fig. 6.9.3(c) are analogous to asymmetric top $\pm K$-precession pairs in Fig. 6.8.2 that share the same (degenerate) energy level in a classical RES picture but may split by tunneling in a quantum picture.
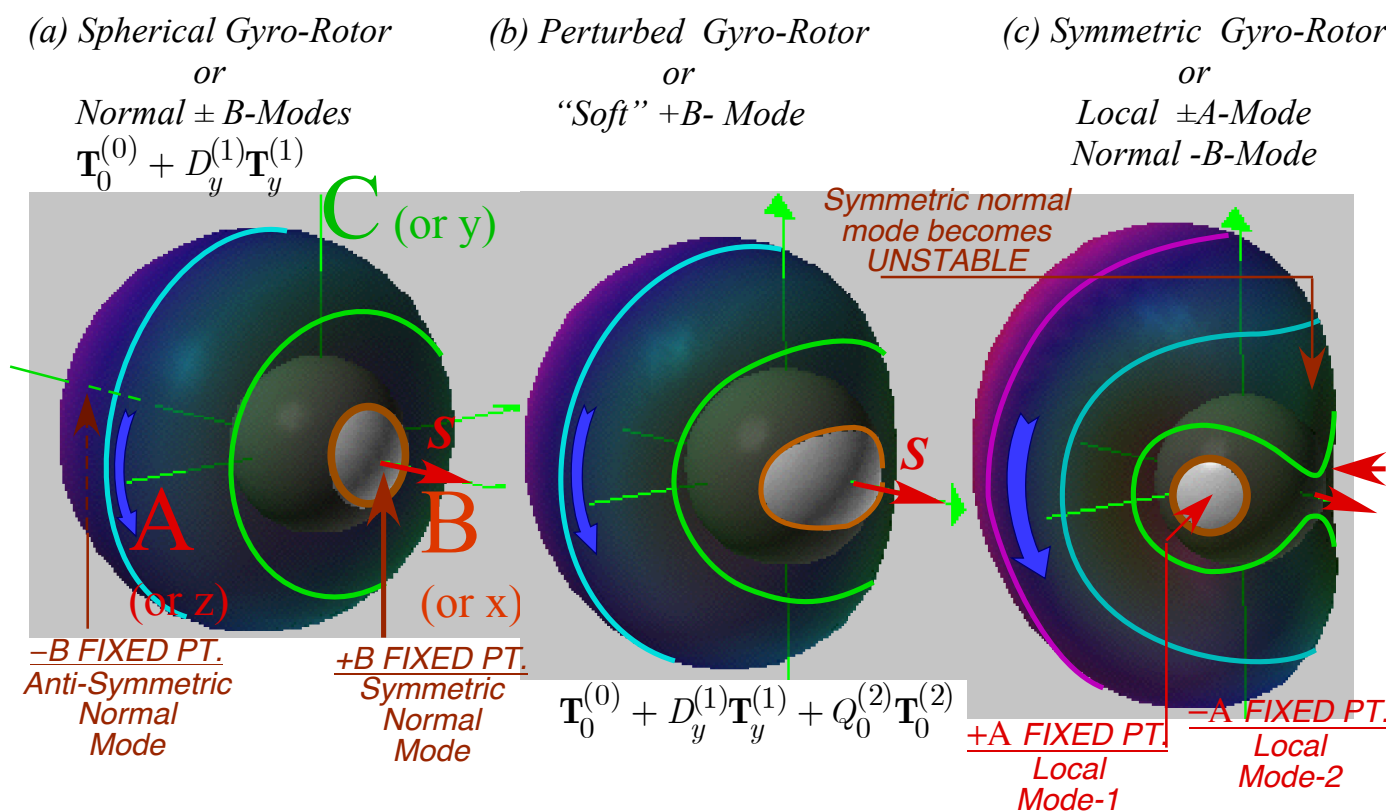

(a) Spherical Gyro-Rotor
or
Normal ± B-Modes
$\mathbf{T}_0^{(0)} + D_y^{(1)}\mathbf{T}_y^{(1)}$

(b) Perturbed Gyro-Rotor
or
"Soft" +B- Mode

(c) Symmetric Gyro-Rotor
or
Local ±A-Mode
Normal -B-Mode

$\mathbf{T}_0^{(0)} + D_y^{(1)}\mathbf{T}_y^{(1)} + Q_0^{(2)}\mathbf{T}_0^{(2)}$

Fig. 6.9.3 A spherical gyro-rotor becomes a symmetric gyro-rotor by as more of $\mathbf{T}_0^2$ is added.

In molecular rotation theory, the $\mathbf{T}_0^2$ term along with $\mathbf{T}_0^0$ comprise an unperturbed symmetric top Hamiltonian and gyro terms $\mathbf{T}_q^1$ are viewed as perturbations. For vibration theory, the latter $\mathbf{T}_q^1$ comprise a normal mode Hamiltonian and the former $\mathbf{T}_0^2$ term is viewed as an anharmonic perturbation.

d. Multiple Gyro-Rotor RES and Eigen-surfaces

A simple rotor has **J** with multiple RES paths. A *gyro-rotor* **J** may use multiple paths *and surfaces*. Gyro-rotor RES depend on **S**, and if **S** is a quantum spin, distribution over multiple RES is possible.

The simplest classical theory of **S** considers just +**S** and -**S**. The RES for each is plotted one on top of other as in Fig. 6.9.4 (a) while component RES are shown in Fig. 6.9.4(b) for +**S** and in Fig. 6.9.4(c) for -**S**. An energy sphere is shown intersecting an RES pair for an asymmetric gyro-rotor. If the spin **S** is set to zero, the pair of RES collapse to a rigid asymmetric top RES shown in Fig. 6.8.1 having angular inversion (time-reversal **J**→-**J**) and reflection symmetry. The composite RES in Fig. 6.9.4(a) has inversion symmetry but lacks reflection symmetry. Its two parts in Fig. 6.9.4 (b) and in Fig. 6.9.4 (c) have neither reflection nor inversion symmetry due to their gyro-spins ±**S**.
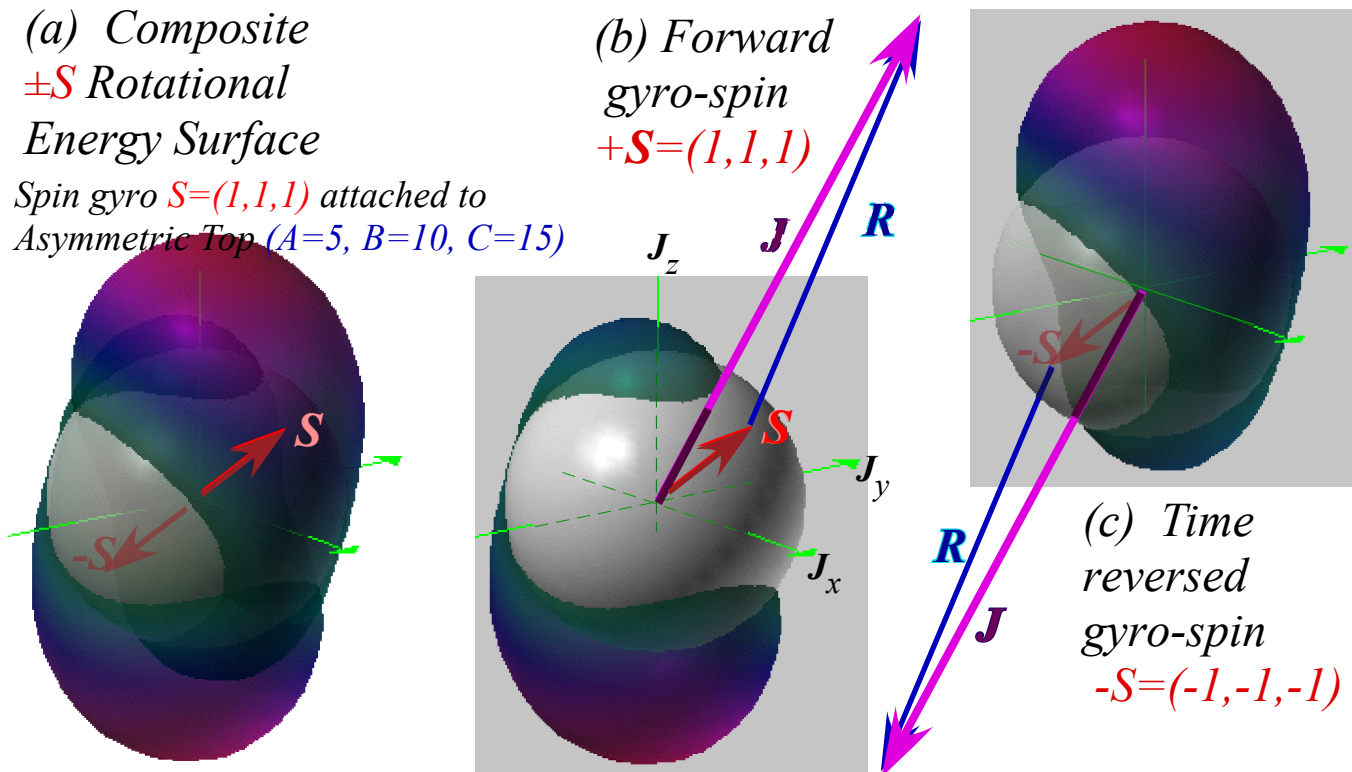

Fig. 6.9.4 Asymmetric classical gyro-rotor RES.
*(a) Composite ±**S**. (b) Forward spin +**S**. (c) Reversed spin – **S**.*

A quantum theory of multiple RES involves a tunneling or mixing between its base states. The simplest quantum gyro-spin is a two-state spin-1/2 having a 2-by-2 Hamiltonian matrix. Semi-classical gyro-rotor dynamics are approximated by a pair of RES obtained from eigensolutions of the following 2-by-2 matrix for each classical orientation (β,γ) of the **J**-vector in the body frame.

$$H_{R,S(quantized)} = A\mathbf{J}_x^2 + B\mathbf{J}_y^2 + C\mathbf{J}_z^2 - A\mathbf{J}_x\boldsymbol{\sigma}_x - B\mathbf{J}_y\boldsymbol{\sigma}_y - C\mathbf{J}_z\boldsymbol{\sigma}_z + const.$$

$$= \begin{pmatrix} RE_{atop} - JC\cos\beta & -AJ\cos\gamma\sin\beta - iBJ\sin\gamma\sin\beta \\ -AJ\cos\gamma\sin\beta + iBJ\sin\gamma\sin\beta & RE_{atop} + JC\cos\beta \end{pmatrix} \quad (6.9.12)$$

where: $RE_{atop} = J^2(A\cos^2\gamma\sin^2\beta + B\sin^2\gamma\sin^2\beta + C\cos^2\beta)$

Fig. 6.9.5 compares of views of both the classical RES of Fig. 6.9.4 (top half of Fig. 6.9.5) and the semi-classical RES (bottom half of Fig. 6.9.5) resulting from inserting quantum spin **S**=σ/*2* matrices in (6.9.2) to give (6.9.12) then diagonalizing and plotting the resulting eigenvalues. Each *sc*-RES surface is an asymmetric RES perturbed around where the *c*-RES cross. The inner surface is particularly affected by a bifurcation into an unstable saddle point and a pair of loops around fixed points.
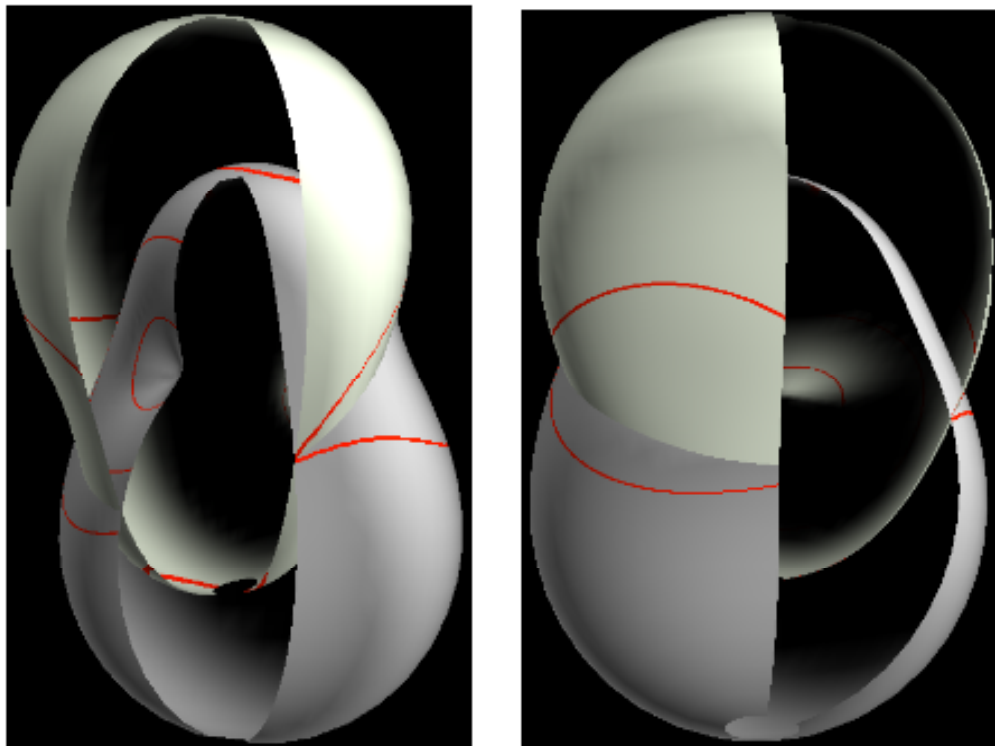

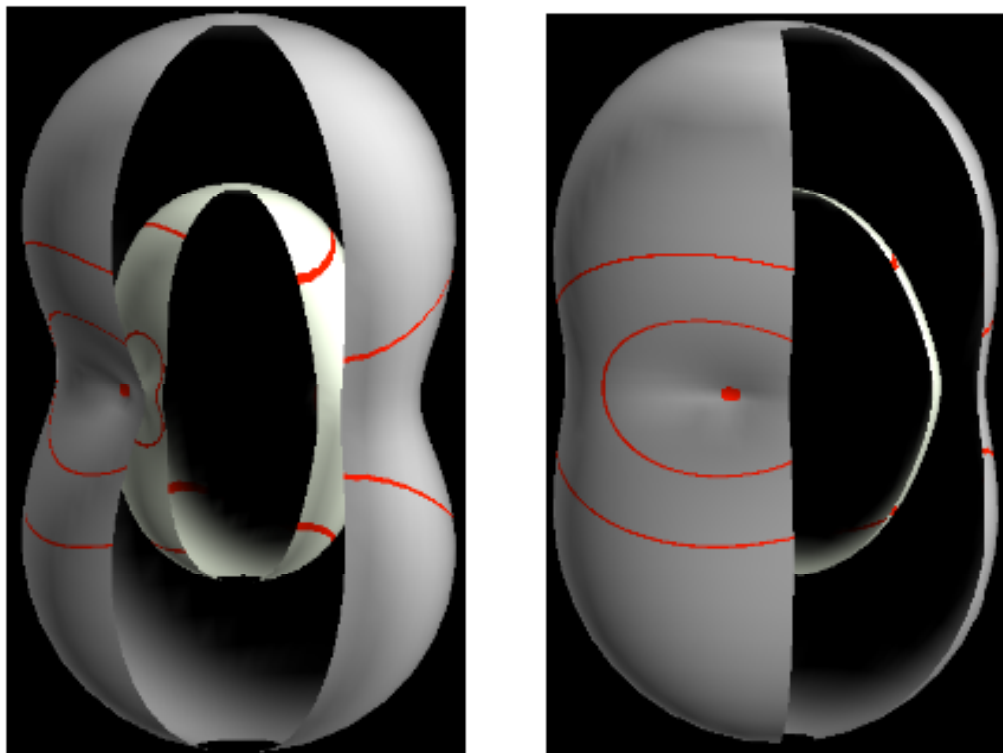*Fig. 6.9.5 (a) Views of classical gyro-rotor c-RES in Fig. 6.9.4 (a) based on (6.9.2).*

Fig. 6.9.5 (b) Views of semi-classical gyro-rotor sc-RES based on eigenvalues of (6.9.12) with **S**=σ/2.